On the analysis of minimum thickness in circular masonry arches

Giuseppe COCCHETTI [1,2], Giada COLASANTE [1], Egidio RIZZI [1]*

Submitted to Applied Mechanics Reviews: March 16, 2011
1st Revision: October 12, 2011; 2nd Revision: February 06, 2012;
Accepted: April 03, 2012; 3rd Revision: May 21, 2012

Abstract

In this paper, the so-called *Couplet-Heyman problem* of finding the minimum thickness necessary for equilibrium of a circular masonry arch, with general opening angle, subjected only to its own weight is re-examined. Classical analytical solutions provided by J. Heyman are first re-derived and explored in details. Such derivations make obviously use of equilibrium relations. These are complemented by a tangency condition of the resultant thrust force at the haunches' intrados. Later, given the same basic equilibrium conditions, the tangency condition is more correctly re-stated explicitly in terms of the true line of thrust, i.e. the locus of the centers of pressure of the resultant internal forces at each theoretical joint of the arch. Explicit solutions are obtained for the unknown position of the intrados hinge at the haunches, the minimum thickness to radius ratio and the non-dimensional horizontal thrust. As expected from quoted Coulomb's observations, only the first of these three characteristics is perceptibly influenced, in engineering terms, by the analysis. This occurs more evidently at increasing opening angle of the arch, especially for over-complete arches. On the other hand, the systematic treatment presented here reveals the implications of an important conceptual difference, which appears to be relevant in the statics of masonry arches. Finally, similar trends are confirmed as well for a Milankovitch-type solution that accounts for the true self-weight distribution along the arch.

Keywords: *masonry arches; Couplet-Heyman problem; minimum thickness; statics; limit analysis; collapse mechanism.*

---

[1] *Università degli Studi di Bergamo, Facoltà di Ingegneria (Dalmine), Dipartimento di Progettazione e Tecnologie, viale G. Marconi 5, I-24044 Dalmine (BG), Italy.*

[2] *Politecnico di Milano, Dipartimento di Ingegneria Strutturale, piazza Leonardo da Vinci 32, I-20133 Milano, Italy.*

***Lead and Corresponding Author, email:** egidio.rizzi@unibg.it, fax: +39.035.205.2310, tel: +39.035.205.2325.*

Part I:

State of the art and Heyman's solution

1 Introduction and motivation of this work

This paper addresses the classical issue of finding the minimum thickness required for equilibrium of a continuous circular masonry arch, with general half-angle of embrace ($0 < \alpha < \pi$), subjected only to its own weight (Fig. 1). The subject of this research is quite well-known and may be referred-to here as the *Couplet-Heyman problem* (for a definition see e.g. the two very valuable books by Jacques Heyman: Heyman, 1977, p. 77–78 and Heyman, 1982, p. 54). Great historical perspectives on the subject (and related issues) are provided by Heyman himself, in his often-cited works (Heyman, 1966, 1967, 1969, 1977, 1982, 1995) and e.g. by Irvine (1979), Benvenuto (1981), Sinopoli et al. (1997) and Sinopoli (2003), Huerta (2001, 2004, 2006) and Albuerne and Huerta (2010), Aita et al. (2003), Becchi (2003), Foce and Aita (2003), Foce (2005, 2007) and (specifically on stereotomy) by Aita (2003), Sakarovitch (2003), Heyman (2009).

Figure 1.

In general terms, one could say that the issue is settled: the (purely-rotational) collapse mechanism that develops when the thickness of the arch is critically small is known and displays as a symmetric five-hinge mechanism, with a hinge at the extrados at the keystone, two hinges at the extrados at the shoulders and two hinges at the intrados at the haunches (Fig. 2).

Figure 2.

Accordingly, given the value of the half-opening angle α of the arch ($\alpha = \pi/2$ for the complete semicircular arch), one attempts the determination of the following three basic characteristic parameters: the angular position of the haunches' hinges β_{cr}, given for example in terms of the inclination angle β measured from the vertical axis of symmetry at the crown; the minimum value η_{cr} of the thickness t to radius r ratio

$$\eta = \frac{t}{r} \tag{1}$$

still allowing for equilibrium; the non-dimensional horizontal thrust of the arch h_{cr} acting in such a limit state, where

$$h = \frac{H}{w\,r}\ ,\ w = \gamma\, t\, d \tag{2}$$

and H is the horizontal thrust, $w = \gamma\, t\, d$ is the specific weight per unit length of geometrical centerline of the arch, γ and d are respectively the constant specific weight per unit volume and the out-of-plane depth of the arch. An alternative way of representing the horizontal thrust in non-dimensional terms, by resorting only to known material (γ) and geometrical parameters (d, r), may also be stated as follows:

$$\hat{h} = \eta\, h = \frac{H}{\gamma d\, r^2} \tag{3}$$

As a starting point, Couplet, in 1730, is quoted by Heyman to assume, for the full semicircular arch ($\alpha = 90°$), that β_{cr} is at 45° and to obtain that η_{cr} is at around 0.101 (Heyman, 1969, p. 368; Heyman, 1982, p. 54–55; Foce, 2007, Note 8, p. 208). Furthermore, Heyman reports in Heyman (1969, p. 367–368) and Heyman (1977, p. 79) analytical formulas that can be used to determine the above-mentioned three basic characteristics β, η, h, for general angles of embrace of the arch. However, explicit analytical derivations of these formulas do not seem to have been provided in written terms in the above-quoted references. As a reference instance, for a complete semicircular arch ($\alpha = 90°$), the solution of Heyman's formulas renders the following usually-referenced values of β, η, h: $\beta_H = 58.8293° = 1.02677$ rad, $\eta_H = 0.105965$, $h_H = 0.621113$ ($\hat{h}_H = 0.0658164$)[1]. Such solution is also cited by Irvine (1979), which develops an analytical treatment of the Roman semicircular arch in the verge of collapse, including the effect of backfill weight on top of the voussoir arch, by accounting for the integration of the differential equation of the line of thrust (meant as "line of resistance" to which the thrust force is locally tangent, see later discussion on Heyman's analysis) and deriving critical thickness and relevant intrados hinge position at variable overburden depth on the arch.

[1] Throughout the paper, with the purpose of subtle academic comparisons, numerical results will be provided with 6 significative digits.

Bičanič et al. (2003), in a numerical analysis of masonry arch bridges based on the so-called Discontinuous Deformation Analysis method (DDA, belonging to the family of the Discrete Element Method, DEM, see also Thavalingam et al., 2001, a review by MacLaughlin and Doolin, 2006 and a recent DEM contribution by Tóth et al. 2009), are also referring to Heyman's results, by actually providing in their Figure 7 other slightly different values of the critical parameters as $\beta_{cr} = 56.2°$ and $\eta_{cr} = 0.10598$ and by showing that the rotational collapse mechanism really arises in the numerical solution when $\eta < \eta_{cr}$. Heyman's solution for other cut-off angles α is also often illustrated graphically in plot form, where functions $\eta_{cr}(\alpha)$, $h_{cr}(\alpha)$ are drawn, as reported e.g. for η_{cr} in Figure 10 of Heyman (1967) and in Figures 4.9–4.10 at p. 80 of Heyman (1977).

Given these available results, in trying to acquire understanding and re-derive explicitly all these outcomes, at the start of this work it was just followed literally what described in words in the above-quoted Heyman's writings. Slightly-different solutions were coming-up (labeled here *"CCR"*, for the ease of reference). Specifically, this occurred for the complete semicircular arch ($\alpha = 90°$), which was analysed first. For example, β_{cr} was found at around $\beta_{CCR} = 54.4963° = 0.951141$ rad, with η_{cr} at about $\eta_{CCR} = 0.107426$ and h_{cr} near $h_{CCR} = 0.621772$ ($\hat{h}_{CCR} = 0.0667947$). The difference appears quite marginal for the non-dimensional thrust, just a little more perceptible for the critical thickness to radius ratio (where $\eta_H < \eta_{CCR}$ appears sub-critical) and more noticeable for the inclination angle of the inner hinge, with a readable discrepancy between around 54.5° vs. about 59°. Independent sources from the literature were then accessed, which actually provided results that were rather consistent with the present.

In Sinopoli et al. (1997) the problem is stated in quite general terms by modeling the arch as a system of rigid voussoirs under unilateral constraints, by investigating the equilibrium conditions in terms of the principle of virtual work and by exploring also the role of friction on the collapse mode. Their final resolving approach is in essence numerical. As an explicit numerical outcome, that paper gives, at pages 208 and 211, for the full semicircular arch, the critical value $K_{cr} = 1.1136$ for the geometrical parameter

$$K = \frac{r_e}{r_i} = \frac{r + t/2}{r - t/2} = \frac{2 + \eta}{2 - \eta} \tag{4}$$

that represents the ratio between extrados and intrados radii r_e and r_i. Such critical value is also attached to an inclination angle of the haunches' hinge that is shown to be at around 54°. Through the inverse relation

$$\eta = 2\,\frac{K-1}{K+1} \tag{5}$$

the given K_{cr} would lead to a critical value $\eta_{cr} = 0.10749$, as compared to the value $\eta_H = 0.105965$ ($K_H = 1.11189$) put forward by Heyman and to the present resulting $\eta_{CCR} = 0.107426$ ($K_{CCR} = 1.11352$). The Authors claim good matching with a result by Petit ($K = 1.114$) and, in comparing to Heyman's result, concisely state that *"such a numerical discrepancy is not significant for practical applications"*. Lucchesi et al. (1997) also provide at p. 338 a value of η_{cr} of nearly $2 \cdot 0.0537 = 0.1074$, thus very close to Sinopoli et al. (1997)'s result and to the present CCR estimation.

Blasi and Foraboschi (1994) developed as well a treatment of equilibrium of masonry arches along Coulomb's views on the upper and lower thrusts (see e.g. Heyman, 1982, p. 56–58 and Sinopoli et al., 1997, for the role of Coulomb's contribution). The treatment is framed in an analytical setting, though results are then worked-out numerically. Their final representation depicted at p. 2302 seems rather consistent with the characteristic value η_H provided by Heyman. Indeed, there, to the critical value of thickness to span ($L=2r$) ratio of a full semicircular arch ($\alpha = 90°$)

$$\frac{t}{L} = \frac{t}{2r} = \frac{\eta}{2} \tag{6}$$

the truncated value $0.9/17 = 0.0529412$ is taken in practical terms, which would correspond to $\eta_{cr} = 0.105882 < \eta_H$. This looks more on the side of Heyman's rather than of Sinopoli et al. (1997)'s solution and constitutes a case which is slightly sub-critical.

Boothby (1996), in a discussion on the same paper by Blasi and Foraboschi (1994), formulates a numerical approach for the problem of a segmental (discretised) complete arch and plots in his Figure 12 a result in terms of the recursively-found eccentricity of the true line of thrust along the arch, obtaining a discrete approximation of the inclination of the inner hinge of about 90°–36°=54°. This result further supports the conclusion that the critical angle β_{cr} should really arise at around 54.5° and not at about 59° as calculated by Heyman.

Motivated by these further observations, the present analysis went-on by developing the final derivations that are presented in the body of this paper and by clarifying as well the differences to classical Heyman's solution. Later, it was discovered that the present independent results, based on the use of the true line of thrust, turned-out fully consistent with those provided priorly in table and plot form by Ochsendorf (2006). As stated in such paper and in Block, DeJong, Ochsendorf (2006), these results have been derived based on the concept of *"locus of pressure points"* for the true line of thrust, in the Author's Ph.D. Dissertation, Ochsendorf (2002). In that Thesis, the Author provides correct outcomes based on a "work-balance" equation (see Heyman, 1969, 2nd paragraph on top of p. 368) and discusses the difference to known results from Heyman and from other historical researchers, including those of Milankovitch (1907), as quoted below. It is also remarked that differences on the minimum thickness should appear marginal in practical terms and thus they should not worry a structural engineer. Indeed, a recent paper by Romano and Ochsendorf (2009), devoted to the analysis of pointed arches, demonstrated that arches of $\eta = 0.12$ would not stand in practice (on critical thickness criteria for stone arch bridges see also Martinez Martinez et al. 2001), which clearly makes the present discussion mainly theoretical than practical. Ochsendorf and co-workers have also provided nice valuable tools for the interactive graphical analysis of the statics of masonry arches (Block, 2005; Block, Ciblac, Ochsendorf, 2006; DeJong and Ochsendorf, 2006), which are based on funicular analyses (e.g. O'Dwyer, 1999; Andreu et al., 2007; Gilbert, 2007; Oikonomopoulou et al., 2009; Varma et al., 2010). Such tools also confirm angles of inclination of the inner hinge that, for $\alpha = 90°$, should arise at around 54.5°.

Moreover, after a main part of the present derivations, the publication of the very interesting article by F. Foce was discovered, Foce (2007), in which the Author is summarizing the earlier independent contributions to the subject by the Serbian researcher Milutin Milankovitch, Milankovitch (1904, 1907). Indeed, Milankovitch developed a quite general analysis, accounting also for the true location of the center of gravity of each ideal voussoir of the arch. In fact, in the traditional literature, the self-weight of the arch is usually assumed to be uniformly distributed along the centerline of the arch at half thickness (so is in Heyman's analysis). For the case of a full semicircular arch, Foce (2007) reports, on top of p. 197, that Milankovitch obtains

$\beta = 54°29' = 54.4833°$, together with $\eta = 0.1075$, as confirmed by the analysis that will be also derived at the end of the paper, where the values $\beta_M = 54.4840° = 0.950925$ rad, $\eta_M = 0.107478$, $h_M = 0.620881$ ($\hat{h}_M = 0.0667311$) will be obtained. Thus, the present results seem very much consistent also with the conclusions that are drawn in Foce (2007) and actually adhere to other historical contributions by Monasterio (Albuerne and Huerta, 2010), Petit, Pilgrim and Ritter, as quoted by the same F. Foce in Foce (2005, p. 132–133) and Foce (2007, Note 8, p. 208). These results basically signal overall a rupture angle β_{cr} at about 54°/55°, with a corresponding η_{cr} at around 0.114. Ochsendorf (2002, 2006)'s results on minimum thickness based on "work balance" have been quoted as well in the recent thesis by Antunes (2010) and publication by Gago et al. (2011), discovered at review stage, which make reference to the doctoral dissertation of Gago (2004). This latter thesis contains analytical derivations and results that appear rather consistent with Heyman's analysis.

Finally, in a recently-discovered publication, Heyman (2009), in discussing the methods of calculation for masonry, *"confesses to an error he made in 1969 in the determination of the minimum thickness of a circular arch (Couplet's problem)"*. He revisits Couplet's solution and states that he has *"corrected"* it in 1969 by *"using the same mechanism of collapse but (a) allowing the position of the intrados hinge to be determined by mathematics, and (b) ensuring that the thrust at these hinges was tangential to the intrados"*. Also, he claims that Ochsendorf (2006) has shown that this solution *"must itself be wrong"* and finally presents in table form a comparison of the three results by Couplet, Heyman and Ochsendorf for the two characteristics β and h (for the full semicircular arch). Later, he confirms that his *"error lies in the assumption that the direction of the thrust at the intrados hinges lies tangential to the intrados"* and presents a discussion on the difference between the "line of resistance" and the "line of pressure" and on how applying the *"(loose) label "line of thrust" to the line of resistance"* has *"led to the error in the analysis"*.

Given the framework above, it was found relevant to attempt outlining the present analytical derivations. A first part of this work was developed during the preparation of a Laurea Thesis in the years 2006–2007 (Colasante, 2007). Subsequent numerical simulations with a DDA tool within a second Laurea Thesis (Rusconi, 2008) displayed results that also adhered to the solutions derived here (see also Rizzi et al., 2010, 2011).

Now, the crucial issue in explaining the difference to classical Heyman's results turns-out to be the adoption of the true line of thrust, which should be correctly defined as the *"locus of pressure points"*, as referred-to by Ochsendorf (2002, 2006), i.e. the line that contains the centers of application of the resultant internal force at each theoretical joint of the arch. As stated by Benvenuto (1981), and by Foce (2007) in his re-reading of Milankovitch's work, this curve generally differs from the line that is locally tangent to the resultant force itself, which leads to think to the funicular polygon of a discretised segmental arch. It appears that Heyman (2009) recognizes that he was not making an explicit difference between these two curves and actually has applied the second concept, by stating the local thrust force at the haunches' intrados as normal to the rupture joint (Heyman, 1967, Figure 9, p. 232; see also Gago, 2004, p. 106–111). In this paper it is also shown that classical Heyman's analysis should be consistent with reasoning in engineering terms, leading to a sort of approximate solution. Thus, though it may be talked of an *"error"* (Heyman, 2009) in a theoretical sense, it could be referred-to as an *"approximation"* in engineering terms (actually very reasonable for η and h).

In this work, an attempt of stating clearly and in full analytical terms the different implications of adopting the tangency condition, at the haunches, of the true line of thrust, rather than of the resultant thrust is made. Results are conceived to be provided as much as possible on an explicit analytical basis (with numerical solutions that may be necessary only for the final transcendental equations in the unknown angular position of the inner hinge at the haunches). The difference to classical Heyman's results is highlighted. Such difference does not certainly appear crucial in engineering terms, with respect to main mechanical parameters η_{cr} and h_{cr}, but a bit more perceptible for the inclination angle β_{cr}, especially at increasing opening angle and for over-complete arches ($\alpha > \pi/2$), which are treated as well in the paper.

This paper deals with the solution of quite a specific problem in the statics of masonry arches. The main ideas that are adopted here belong to the general framework of Limit Analysis of masonry constructions that, after the early developed so-called pre-elastic theories, was traced-down in modern terms by Heyman himself in his above-quoted references and by many other contributions that may be referred to the reader for a throughout study (e.g. Kooharian, 1952; Livesley, 1978, 1992; Boothby and

Brown 1992; Boothby 1994, 1995, 2001; Como, 1992; Clemente et al. 1995; Del Piero, 1998; Gilbert et al., 2006; Gilbert 2007; Cavicchi and Gambarotta, 2006, 2007; Chen et al., 2007; Smars 2000, 2008, 2010, Lucchesi et al., 2012). Furthermore, in a recent review by Baratta and Corbi (2010 I,II), published on *Applied Mechanics Reviews*, masonry has been modelled in general terms as a no-tension material, with applications to portal arches in Part II. A review on experiments and modelling of arched brick structures, with citation of analytical methods, including Heyman's ones, has also appeared recently in Bednarz et al. (2011) (see also e.g. Fanning and Boothby, 2001 and Vermeltfoort, 2001). Ancient rules for masonry arches, derived from historical manuals, have been analyzed in modern mechanical terms by Brencich and Morbiducci (2007), where tables on brickwork arch thickness vs. span from different authors and other arch data have been provided. Similar tables have been also presented very recently by de Arteaga and Morer (2012), where empirical rules for the determination of the arch thickness are resumed and the effect of true read geometry (by topographic, photogrammetric, ground-penetrating radar and terrestrial laser scanner methods) on the structural capacity of masonry arch bridges is analysed by different programming tools (see also Armesto et al., 2010; Morer et al., 2011; Riveiro et al., 2011a,b and the recent review articles by Solla et al., 2012a,b). Historical empirical rules are also briefly presented and further compared against bridges' geometrical data by Oliveira et al. (2010), with parametric assessments of the load-carrying capacity of reference bridges. A recent review by Roca et al. (2010), with 140 refs, presents methods applicable to the study of masonry historical construction, including classical methods in the tone of those analysed here, Limit Analysis methods, simplified methods, FEM macro- or micro-modeling and Discrete Element Methods. Also, Atamturktur and Laman (2012) have reviewed recent developments on FEM modelling and calibration of historic masonry monuments and identified current open challenges on the use of such tools towards the structural and reliability assessment of masonry constructions (see also Lourenço, 2001; Dede and Ural, 2007; Melbourne et al., 2007; Gibbons and Fanning, 2010; Kumar, 2010; Casas, 2011). Finally, various mathematical and computational approaches have been proposed towards the modelling of masonry structures and specifically of masonry arches and arch bridges (e.g. Harvey, 1988, Smith et al., 1990, Harvey and Maunder, 2001, Harvey, 2009; Hughes and

Blackler, 1997, Hughes et al., 2002, Miri and Hughes, 2006; Molins and Roca, 1998; Ponterosso et al., 2000; Alfaiate and Gallardo, 2001; Roeder-Carbo and Ayala, 2001; Giordano et al., 2002, 2006; Ford et al., 2003; Ng and Fairfield, 2004; Toker and Ünay, 2004; Kumar and Bhandari, 2005, 2006, Kumar, 2010; Migliore et al., 2006; Audenaert et al., 2007, 2008; Betti et al., 2007, Campo et al., 2007, Drosopoulos et al., 2006, 2008; Ainsworth and Mihai, 2007, Mihai and Ainsworth, 2009; Viola et al., 2007; Oikonomopoulou 2009; Pintucchi and Zani, 2009; Vares, 2009; Grandjean, 2010; Peng et al., 2010; Tsutsui et al., 2010; Yamao et al., 2010; Manrique Hoyos, 2010, Cai, 2011 and Koltsida Spyridoula 2011; Gago et al., 2011).

The present paper is divided into three parts and organized as follows. Section 2, ending Part I, contains the definition of the Couplet-Heyman problem and provides, through a static approach in which equilibrium equations are explicitly written, a detailed derivation of classically-adopted Heyman's formulas, within the usual reasonable hypothesis that, for small thicknesses of the arch, the self-weight of the arch is distributed along its circular centerline. Within the same hypothesis and adopted static approach, Section 3, constituting Part II, develops the core of the present results (CCR solution) and furnishes detailed comparisons to Heyman's solution. Part III (Section 5) completes the study, by presenting parallel derivations for the more general case which accounts for the true location of the center of gravity of each theoretical voussoir of the arch (Milankovitch-type solution). The final closing remarks (Section 6) attempt to summarise the salient features of the obtained solutions and also highlight further possible developments of the present study.

2 Derivation of Heyman's formulas

As it is well known, and briefly resumed in the Introduction, eminent professor Jacques Heyman formulated, in a series of often-cited works (Heyman, 1966, 1967, 1969, 1977, 1982, 1995), an elegant theory for the structural analysis of masonry constructions. This is founded on the so-called pre-elastic theories in arch analysis and at the same time strictly adheres to the concepts of modern Limit Analysis. Based on fundamental observations on masonry behavior, Heyman formulated the statics of masonry arches by making the following three basic assumptions (often quoted-to as *classical three Heyman's hypotheses*, see e.g. Heyman, 1977, p. 70 and Heyman, 1982, p. 30):

1. *sliding failure does not occur;*
2. *masonry has an infinite compressive strength;*
3. *masonry has no tensile strength.*

According to that, Heyman has provided nice analytical formulas that allow to define the three basic characteristic parameters of the assumed (purely-rotational) collapse mode of circular masonry arches. *Heyman's formulas* are very often quoted and used in the literature on masonry arches. Specifically, in Heyman (1977, p. 79), the Author reports the following explicit formulas for a circular arch of angle of embrace 2α:

$$\beta \cot\beta \frac{2\beta\cos\beta + \sin\beta\cos^2\beta + \sin\beta}{2\beta\cos\beta + \sin\beta\cos^2\beta - \sin\beta\cos\beta} = \alpha \cot\frac{\alpha}{2} \tag{7}$$

$$\eta = \frac{t}{r} = 2\frac{(\beta - \sin\beta)(1-\cos\beta)}{\beta(1+\cos\beta)} \tag{8}$$

$$h = \frac{H}{wr} = \beta\cot\beta \tag{9}$$

The use of these equations should be conceived as follows. A numerical solution of Eq. (7) at given half-angle of embrace α locates first the unknown angular position β_{cr} of the haunches' hinge. For example, for the reference case of the full semicircular arch ($\alpha = \pi/2$), one gets $\beta_H = 1.02677$ rad = 58.8293°. Eq. (8), once the critical angle β_{cr} is found from Eq. (7), calculates explicitly the minimum allowable thickness to radius ratio η_{cr} that the arch must possess in order to support its own weight. Again, for $\alpha = \pi/2$ and $\beta = \beta_H$, Eq. (8) gives $\eta_H = 0.105965$ (thus, from Eqs. (6) and (4), thickness to span ratio $\eta_H/2 = 0.052983$ and extrados to intrados radius ratio $K_H = 1.11189$). Finally, Eq. (9) determines the value of the non-dimensional horizontal thrust h_{cr} acting in such a limit state. Again, for $\alpha = \pi/2$ and $\beta = \beta_H$, one gets $h_H = 0.621113$.

Now, since explicit analytical derivations of these celebrated formulas seem to be missing in the Author's classically-quoted writings (analytical derivations in line with Heyman's solution have been discovered, through Gago et al., 2001, in Gago, 2004), an attempt is made here first to provide a systematic derivation of these, by following literally Heyman's written instructions (see Heyman, 1967, paragraph right above Figure 9, p. 232 and Heyman, 1969, bottom of p. 367), with reference to Fig. 3 below. Reference is made here to cases of circular masonry arches with entirely-general half-angle of embrace, i.e. potentially $0 < \alpha < \pi$.

Figure 3.

Due to the symmetry of the problem with respect to the vertical axis of symmetry at crown *A*, only one half *AC* of the arch can be considered; also, the vertical shear force at keystone *A* is not present. Therefore, only the horizontal thrust *H* acts there, at the crown's extrados. At outward rotational collapse, a hinge forms at the haunch's intrados *B* ($\beta < \alpha$), which divides the half-arch into two portions *AB* and *BC*.

From the rotational equilibrium of upper portion *AB* around inner hinge *B* one has (Fig. 3):

$$H \cdot \left[r + \frac{t}{2} - \left(r - \frac{t}{2} \right) cos\beta \right] = W_1 \cdot \left[\left(r - \frac{t}{2} \right) sin\,\beta - x_1 \right] \tag{10}$$

where, in the hypothesis of a uniformly-distributed self-weight along the centerline of the arch, the weight W_1 of the upper portion of the half-arch is obtained as

$$W_1 = \int_0^{\beta} \underset{w}{\gamma t d}\; r\; d\varphi = w r \left[\varphi \right]_0^{\beta} = w r \beta \tag{11}$$

and the center of gravity of the upper portion of the half-arch is located at the following horizontal distance x_1 from the vertical axis of symmetry:

$$x_1 = \frac{\int_{V_1} \gamma\, x\, dV}{\int_{V_1} \gamma\, dV} = \frac{\int_0^{\beta} \gamma t d\; r\; r sin\varphi\; d\varphi}{\int_0^{\beta} \gamma t d\; r\, d\varphi} = r\, \frac{\left[cos\,\varphi \right]_{\beta}^{0}}{\left[\varphi \right]_0^{\beta}} = r\, \frac{1 - cos\beta}{\beta} \tag{12}$$

On the other hand, the vertical distance of the center of gravity from center *O* (see Fig. 4, shown later) can also be evaluated for later use as:

$$y_1 = \frac{\int_{V_1} \gamma\, y\, dV}{\int_{V_1} \gamma\, dV} = \frac{\int_0^{\beta} \gamma t d\; r\; r cos\varphi\; d\varphi}{\int_0^{\beta} \gamma t d\; r\, d\varphi} = r\, \frac{\left[sin\,\varphi \right]_0^{\beta}}{\left[\varphi \right]_0^{\beta}} = r\, \frac{sin\,\beta}{\beta} \tag{13}$$

Moreover, the following geometrical relations can be employed in terms of the non-dimensional geometrical parameter thickness to radius ratio $\eta = t/r$, which actually defines indirectly the external (extrados) and internal (intrados) radii:

$$r_e = r + \frac{t}{2} = \frac{r}{2}\left(2 + \eta \right); \quad r_i = r - \frac{t}{2} = \frac{r}{2}\left(2 - \eta \right) \tag{14}$$

By substituting Eqs. (11)–(12) and (14) into rotational equilibrium Eq. (10) one obtains a *first equilibrium relation* in terms of the non-dimensional horizontal thrust $h = H/(w\, r)$ and the non-dimensional geometrical parameter $\eta = t/r$:

$$h\cdot\left[2+\eta-(2-\eta)\cos\beta\right]=(2-\eta)\,\beta\sin\beta-2(1-\cos\beta) \tag{15}$$

which, being linear in both h and η, might be solved right-away either with respect to h or to η, by obtaining either

$$h=h_1=\frac{(2-\eta)\;\beta\;\sin\beta-2(1-\cos\beta)}{2+\eta-(2-\eta)\cos\beta} \tag{16}$$

or

$$\eta=\eta_1=2\,\frac{\beta\;\sin\beta-(1+h)(1-\cos\beta)}{\beta\;\sin\beta+h(1+\cos\beta)} \tag{17}$$

Now, from the rotational equilibrium of the total half-arch AC around hinge C at the shoulder's extrados, one gets a second equilibrium condition (Fig. 3):

$$H\cdot\left[r+\frac{t}{2}-\left(r+\frac{t}{2}\right)\cos\alpha\right]=W\cdot\left[\left(r+\frac{t}{2}\right)\sin\alpha-x_W\right] \tag{18}$$

where W ($W = W_1+W_2$) is the total weight of the half-arch, with half-angle of embrace α, acting at a horizontal distance x_W from crown A. Given Eqs. (11)–(12), one has:

$$W=w\,r\,\alpha\,,\qquad x_W=r\,\frac{1-\cos\alpha}{\alpha} \tag{19}$$

and, by substituting Eqs. (14) and (19) into rotational equilibrium Eq. (18) one gets a second equilibrium relation in terms of non-dimensional parameters h and η:

$$h\,(2+\eta-(2+\eta)\cos\alpha)=(2+\eta)\,\alpha\,\sin\alpha-2(1-\cos\alpha) \tag{20}$$

or:

$$h\,(2+\eta)(1-\cos\alpha)=(2+\eta)\,\alpha\,\sin\alpha-2(1-\cos\alpha) \tag{21}$$

Notice the similar roles that play, respectively, inner hinge angle β in Eq. (15) and half-opening angle α in Eq. (20). Notice also that the different roles taken by coefficient η in the two equations is due to the fact that hinge B is located at the intrados, while hinge C at the extrados. Obviously, Eq. (15) contains only angle β, while Eq. (20) only angle α.

Moreover, Eq. (21) might be further elaborated by dividing its both hand sides by the common factor $(1 - \cos\alpha)$, to get:

$$h(2+\eta)=(2+\eta)\;\alpha\,\frac{\sin\alpha}{1-\cos\alpha}-2 \tag{22}$$

and, since from trigonometrics

$$\alpha\frac{\sin\alpha}{1-\cos\alpha}=\alpha\frac{2\sin\frac{\alpha}{2}\cos\frac{\alpha}{2}}{1-\left(1-2\sin^2\frac{\alpha}{2}\right)}=\boxed{\alpha\cot\frac{\alpha}{2}=A}=2-\frac{\alpha^2}{6}-\frac{\alpha^4}{360}+O(\alpha^6) \tag{23}$$

one obtains the following final form of a *second equilibrium relation*:

$$\boxed{h(2+\eta)=(2+\eta)A-2} \tag{24}$$

This equilibrium relation is again linear in both h and η. It is also linear in the group $A(\alpha) = \alpha\,cot\,\alpha/2$, which inserts the explicit dependence on the half-opening angle α (in other words the final solution will depend on α always through term A). Eq. (24) might be solved again linearly with respect to either h or η, or even $A = \alpha\,cot\,\alpha/2$, by obtaining either

$$\boxed{h=h_2=A-\frac{2}{2+\eta}=\frac{(2+\eta)\,\alpha\,\sin\alpha-2(1-\cos\alpha)}{(2+\eta)\,(1-\cos\alpha)}} \tag{25}$$

or

$$\boxed{\eta=\eta_2=2\left(\frac{1}{A-h}-1\right)=2\,\frac{-\alpha\sin\alpha+(1+h)(1-\cos\alpha)}{\alpha\sin\alpha-h(1-\cos\alpha)}} \tag{26}$$

or even

$$\boxed{A=\alpha\cot\frac{\alpha}{2}=h+\frac{2}{2+\eta}} \tag{27}$$

Equilibrium Eqs. (15) and (24) must hold true at the same time to impose the equilibrium of the arch: they represent a system of two statics equations. One may want to eliminate the non-dimensional horizontal thrust h from the two equations and work with a single equilibrium relation in terms of the given angular parameter α (always through the group $A = \alpha\,cot\,\alpha/2$) and the unknown critical parameters β and η. Thus, by setting $h_1 = h_2$ one gets the following *single equilibrium equation*:

$$\boxed{\frac{(2-\eta)\,\beta\,\sin\beta-2(1-\cos\beta)}{2+\eta-(2-\eta)\cos\beta}=A-\frac{2}{2+\eta}} \tag{28}$$

which might be rewritten as well as follows, in the spirit of Heyman's Eq. (7), by isolating at the right-hand side the term $A = \alpha\,cot\,\alpha/2$:

$$\frac{(2-\eta)\beta\sin\beta-2(1-\cos\beta)}{2+\eta-(2-\eta)\cos\beta}+\frac{2}{2+\eta}=A \tag{29}$$

Notice as well that, in an equivalent approach that will not be explicitly pursued here, one might want to eliminate η, by setting $\eta_1 = \eta_2$, and get instead a single equilibrium relation in terms of β and h, leading to same results.

It should be observed at this stage that, up to now, only (two) standard equilibrium relations have been used. These equations, i.e. two Eqs. (15) and (24) or the single Eq. (28) (or (29)), must hold true to set equilibrium. Another equation is thus needed to complement single Eq. (28) and thus allow solving for the two unknowns β and η (h could be solved later by either one of relations (16) and (25)). According to Heyman's indications, such second relation should arise from the tangency condition of the line of thrust at the haunches' intrados B, but it should have been rather stated in terms of the tangency condition of the resultant thrust force itself, as follows.

First, once more from equilibrium, the polygon of forces formed by the horizontal thrust H in A, the vertical weight W_1 of the upper part and the resultant internal force acting in B on the upper portion (which should be imposed at end to be tangent to the intrados) must be close, in order to guarantee again the equilibrium of the upper portion of the half-arch (Fig. 4). This states that the angle of inclination of the thrust in B to the horizontal is such that its tangent is given by the ratio W_1/H, which, from Eqs. (2) and (11), poses

$$\frac{W_1}{H}=\frac{\beta}{h} \tag{30}$$

Indeed, due to the translational equilibrium along x and y directions, the thrust acting in B has H as its horizontal component and, given the zero shear force at crown A, due to symmetry, has W_1 as its vertical component (Fig. 4).

Figure 4.

Alternatively, one notices that the line of action of the resultant thrust, passing from B, must pass as well from point D at the intersection of the lines of application of forces H, at crown A, and W_1. This imposes the rotational equilibrium of the upper part around point D. Thus, the tangent of the angle of inclination of the thrust in B is given as well by the following ratio of difference of coordinates:

$$\frac{y_A - y_B}{x_B - x_1} = \frac{r + \frac{t}{2} - \left(r - \frac{t}{2}\right)\cos\beta}{\left(r - \frac{t}{2}\right)\sin\beta - r\,\frac{1-\cos\beta}{\beta}} = \beta\,\frac{2 + \eta - (2-\eta)\cos\beta}{(2-\eta)\beta\sin\beta - 2(1-\cos\beta)} \tag{31}$$

which has been worked-out again through the relations in Eq. (14).

Going now to Heyman's tangency condition, since the local inclination of the circular intrados in *B* is given by the angle β itself, the tangency condition might thus be stated in the following two possible equivalent ways:

$$\frac{W_1}{H} = \tan\beta \quad \text{or} \quad \frac{y_A - y_B}{x_B - x_1} = \tan\beta \tag{32}$$

Then, using relations (30) and (31), the tangency condition (32) becomes:

$$\frac{\beta}{h} = \tan\beta \quad \text{or} \quad \beta\,\frac{2 + \eta - (2-\eta)\cos\beta}{(2-\eta)\beta\sin\beta - 2(1-\cos\beta)} = \tan\beta \tag{33}$$

which leads to the following final *tangency relation:*

$$\boxed{h = h_H = \beta\cot\beta \quad \text{or} \quad \beta\cot\beta = \frac{(2-\eta)\beta\sin\beta - 2(1-\cos\beta)}{2 + \eta - (2-\eta)\cos\beta}} \tag{34}$$

Notice that tangency conditions (32)–(34) regard only the upper portion of the arch and thus they are obviously independent of the cut-off angle α. The first tangency relation in (34) is expressed in terms of *h*, the second one in terms of η; both depend on β. Notice that Eq. (34) implicitly confirms equilibrium relation $h = h_1$, Eq. (16). Finally, the sought second relation *(tangency equation)*, to be coupled to the equilibrium equation (28), might thus be stated as follows, in terms of variables β and η:

$$\boxed{\beta\cot\beta = \frac{(2-\eta)\beta\sin\beta - 2(1-\cos\beta)}{2 + \eta - (2-\eta)\cos\beta}} \tag{35}$$

Actually, by solving directly Eq. (35) with respect to η, it is possible to obtain η as a function of β, given the assumed tangency condition of the resulting thrust force to the intrados:

$$\boxed{\eta = \eta_H = 2\,\frac{(\beta - \sin\beta)(1-\cos\beta)}{\beta(1+\cos\beta)}} \tag{36}$$

This is indeed the same expression provided by Heyman, Eq. (8).

From Eq. (36) one also finds the following useful relations

$$2+\eta = 2\ \frac{2\beta - \sin\beta(1-\cos\beta)}{\beta(1+\cos\beta)} = \frac{4\beta - 2\sin\beta + \sin 2\beta}{\beta(1+\cos\beta)}$$
$$2-\eta = 2\ \frac{2\beta\cos\beta + \sin\beta(1-\cos\beta)}{\beta(1+\cos\beta)} = \frac{4\beta\cos\beta + 2\sin\beta - \sin 2\beta}{\beta(1+\cos\beta)} \tag{37}$$

so that the alternative critical geometrical parameters $\eta/2$ and K would become, in terms of β and according to Heyman's solution:

$$\boxed{\begin{aligned}&\frac{\eta_H}{2} = \frac{(\beta - \sin\beta)(1-\cos\beta)}{\beta(1+\cos\beta)}\\ &K_H = \frac{2+\eta}{2-\eta} = \frac{2\beta - \sin\beta(1-\cos\beta)}{2\beta\cos\beta + \sin\beta(1-\cos\beta)} = \frac{4\beta - 2\sin\beta + \sin 2\beta}{4\beta\cos\beta + 2\sin\beta - \sin 2\beta}\end{aligned}} \tag{38}$$

To analyze the system of two Eqs. (28) and (35), Eq. (36) could be back-substituted into equilibrium relation (28) and the latter worked-out in terms of β. Alternatively, by noticing that both right-hand side of Eq. (35) and left-hand side of Eq. (28) represent h, the system of the two equations might be simplified by the following single relation (to be coupled with Eq. (36)), which is consistent with Eqs. (34) and (25):

$$\beta\cot\beta = A - \frac{2}{2+\eta} \tag{39}$$

or, in line with Eqs. (7), (29):

$$\beta\cot\beta + \frac{2}{2+\eta} = A \tag{40}$$

Then, the expression in Eq. $(37)_a$, can be substituted into Eq. (40) to obtain the sought final equation in the unknown angular hinge position β:

$$\beta\cot\beta + \frac{\beta(1+\cos\beta)}{2\beta - \sin\beta(1-\cos\beta)} = A \tag{41}$$

Finally, after appropriate manipulations of Eq. (41), it is possible to recover the same expression provided by Heyman, Eq. (7):

$$\boxed{\beta\cot\beta\,\frac{2\beta\cos\beta + \sin\beta\cos^2\beta + \sin\beta}{2\beta\cos\beta + \sin\beta\cos^2\beta - \sin\beta\cos\beta} = A = \alpha\cot\frac{\alpha}{2}} \tag{42}$$

which may be used to solve for the critical value of β at any assigned value of α.

Last, the expression given by Heyman for the non-dimensional horizontal thrust h in terms of β, Eq. (9), can be recovered directly from tangency Eq. $(34)_a$:

$$\boxed{h = h_H = \beta\cot\beta} \tag{43}$$

2.1 Final interpretation of Heyman's formulas

In summary, the following system of three equations, in terms of *h*, formed by relations (25), (16) and (43)

$$\begin{cases} h = h_2 = A - \dfrac{2}{2+\eta} \\ h = h_1 = \dfrac{(2-\eta)\ \beta\ sin\beta - 2(1-cos\beta)}{2+\eta-(2-\eta)cos\beta} \\ h = h_H = \beta\, cot\beta \end{cases} \tag{44}$$

can be used to solve for the three unknowns β, η and *h*, as devised by here re-obtained Heyman's formulas, Eqs. (7)–(9). Eqs. $(44)_{a,b}$ represent rotational equilibrium and Eq. $(44)_c$ expresses the tangency condition of the local thrust force to the intrados *B*. It is worthwhile to remark that Eq. $(44)_c$ itself basically states the tangency condition in terms of *h*. Thus, system (44) represents, in the same order, Heyman's formulas (7)–(9), which clearly explains their physical meaning: Eq. (9) represents the tangency condition $(44)_c$; Eq. (8) is the equilibrium relation $(44)_b$ solved with respect to η and with tangency relation $(44)_c$ inserted in it for *h*; Eq. (7) is the equilibrium relation $(44)_a$ in which the obtained *h* and η are inserted. In practice, Heyman's Equations (7)–(9) are directly reproduced through the following rearrangement of system (44):

$$\begin{cases} h\left(1+\dfrac{2}{2+\eta}\ \dfrac{1}{h}\right) = A \\ \eta = \eta_1 = 2\dfrac{\beta\ sin\beta - (1+h)(1-cos\beta)}{\beta\ sin\beta + h(1+cos\beta)} \\ h = h_H = \beta\, cot\beta \end{cases} \tag{45}$$

where Eq. $(45)_c$ is then inserted into Eq. $(45)_b$ to get the final expression of η in terms of β and both Eqs. $(45)_{b,c}$ are inserted into Eq. $(45)_a$ to obtain the solving transcendental equation in β.

In conclusion, the three governing relations (15), (24) and (34) give rise to a system of three equations:

$$\begin{cases} \textit{first equilibrium relation}, \text{ Eq. (15)} \\ \textit{second equilibrium relation}, \text{ Eq. (24)} \\ \textit{tangency condition at the haunch (of the resultant thrust)}, \text{ Eq. (34)} \end{cases} \tag{46}$$

that can be manipulated in various ways to give rise to Heyman's solution. All relations, though obviously non-linear in β, are linear in h, η and, the second, the only dependent on α, is linear in the group $A = \alpha \cot \alpha/2$. Furthermore, while the first two equations contain both h and η, the third equation (tangency condition) displays a decoupled role of h and η, i.e. it can be expressed in terms of either one of them, giving rise right away to h_H and η_H. This last property, specifically, is a convenient feature of Heyman's solution, which is due to the assumption of stating the tangency condition on the thrust force itself. It is a true key factor in simplifying the solution as opposed to what is going to follow here for both CCR and Milankovitch solutions. In short, one could say that the problem is *'linear'* in h, η, A for Heyman's solution (while it will become *'quadratic'* for CCR solution (Part I) and *'cubic'* for Milankovitch solution (Part II)).

Different possible combinations of the equations in the governing system (46) could be considered and expressed directly, in each line, in terms of either h or η, giving rise to alternative forms, all equivalent, as represented in Heyman's system below:

$$\begin{cases} h = h_1 = \dfrac{(2-\eta)\beta\sin\beta - 2(1-\cos\beta)}{2+\eta-(2-\eta)\cos\beta} \quad \text{or} \quad \eta = \eta_1 = 2\,\dfrac{\beta\sin\beta-(1+h)(1-\cos\beta)}{\beta\sin\beta+h(1+\cos\beta)} \\ h = h_2 = A - \dfrac{2}{2+\eta} \quad \text{or} \quad \eta = \eta_2 = 2\left(\dfrac{1}{A-h}-1\right) \\ h = h_H = \beta\cot\beta \quad \text{or} \quad \eta = \eta_H = 2\dfrac{(\beta-\sin\beta)(1-\cos\beta)}{\beta(1+\cos\beta)} \end{cases} \quad \textit{Heyman} \tag{47}$$

The solution of this system renders Heyman's formulas (7)–(9).

2.2 Solution of Heyman's formulas

Heyman's Equations (7)–(9) or, which is equivalent, Heyman's system (47) may be conveniently solved, at given half-angle of embrace α (thus at given $A = \alpha \cot \alpha/2$), in order to obtain reference numerical results for the main characteristic parameters β, η, h involved in the collapse assessment of circular masonry arches.

Reference results can be obtained first for the case of the full semicircular arch ($\alpha = \pi/2$), which are summarized in the left column of Table 1. In the same table, the critical geometrical parameters $\eta/2$ and K are given as well, which may be used as alternative measures of the *geometrical factor of safety*, together with the values of the alternative measure of the non-dimensional horizontal thrust $\hat{h} = \eta\, h$.

Table 1.

For a complete view on the entire range of admissible angles of embrace (usually reference is made just to complete or under-complete arches with $\alpha \le 90°$) and to further appreciate the differences with respect to the solutions that are going to follow, another characteristic case, of an over-complete arch with half-angle of embrace larger than 90°, namely $\alpha = 140°$, is reported as well in the right column of Table 1. This angle is somehow representative of the opening angles in the range between 90° and the limit angle that corresponds to the limit of validity of the solution of the purely-rotational collapse mode, as obtained below.

Indeed, notice that from Eq. (43), the analytical limit of validity of Heyman's solution (since negative, i.e. tensile, thrusts are not admitted) is $\beta_l^H = \pi/2$, where the non-dimensional horizontal thrust becomes zero: $h_l = 0$. Accordingly, from Heyman's formulas one has the following limit values of the characteristic parameters:

$$h = h_l = \hat{h}_l = 0 \;\; at \;\; \beta_l^H = \pi/2 \;\; \Rightarrow$$
$$A_l^H = \frac{\pi}{2(\pi-1)} = 0.733471, \alpha_l^H = 2.58957\, rad = 148.371°; \eta_l^H = 2\frac{\pi-2}{\pi} = 0.726760 \quad (48)$$

Thus, Heyman's solution for the purely-rotational collapse mechanism holds for half-angles of embrace between 0 and α_l^H, $0 \le \alpha \le \alpha_l^H$, i.e. less than about 150°, which fixes the limit of analysis for over-complete arches.

Further numerical results for different given values of the cut-off angle α are systematically reported in Table 2, with α stepping every 10°. Notice that the resulting angular position β of the inner hinge is a monotonic increasing function of the half-angle of embrace α. Also, the hinge angle is always beyond half way of the cut-off angle, i.e. $\beta > \alpha/2$ and quite near to the 2/3 of it, especially for embrace angles α that are less than 90° (indeed $1/\sqrt{2} \cong 0.71$, see the comments below on the trends for α small). In looking at Table 2, almost round cases appear for example for $\alpha = 70°$, with $\beta \cong 47°$ and for $\alpha = 110°$, with $\beta \cong 70°$. The trends for η and h are also monotonic, increasing for η (meaning that the arch thickness necessary for equilibrium has to increase at increasing opening angle) and decreasing for h (meaning that the horizontal thrust that the arch transmits to the shoulders in the critical condition decreases at increasing angle of embrace). Notice that the functional dependence of $\hat{h} = \eta\, h$ is

instead necessarily bell-shaped, since η and h are separately zero on the two extremes $\alpha = 0$ ($\eta = 0$) and $\alpha = \alpha_l$ ($h = 0$) of the range of admissible half-angles of embrace. In fact, in Table 2 a decrease is recorded for $\hat{h}$ for the two values of $\alpha = 130°$ and $\alpha = 140°$, meaning that a stationary point should appear between $\alpha = 120°$ and $\alpha = 130°$. Indeed, from a stationary analysis of $\hat{h} = \eta\, h$ with respect to α (or actually to β, which is the same, due to the commented monotonic trend of $\beta(\alpha)$), one readily has the $\hat{h}$-stationary angular parameters

$$\beta_{s\hat{h}}{}^{H} = 1.32256\,rad = 75.7771° \Rightarrow A_{s\hat{h}}{}^{H} = 1.19602, \alpha_{s\hat{h}}{}^{H} = 2.11041\,rad = 120.918° \quad (49)$$

which lead to

$$\eta_{s\hat{h}}{}^{H} = 0.323435; \quad h_{s\hat{h}}{}^{H} = 0.335221, \ \hat{h}_{s\hat{h}}{}^{H} = 0.108422 \quad (50)$$

Thus, the maximum value of $\hat{h} = \eta\, h$ that the arch is able to transmit, according to Heyman's solution, at variable angle of embrace and in the critical condition, is obtained for a half-opening angle that is near 120°, with corresponding η and h around 1/3. Table 10 at the end of the paper will also gather these and other characteristic parameters, in view of comparing together the outcomes of the three analysed solutions.

Table 2.

In an alternative way to proceed for elucidating the outcomes of each of the three solutions, one could determine the unknown cut-off angle α (or parameter $A = \alpha \cot \alpha/2$) of an arch that would collapse with the inner hinge at a given position β. Indeed, the solution formulas may give right away the values of A (thus α), η, h (or $\hat{h}$) at given hinge angle β. Results in this sense are reported in Table 3, for β stepping each 5°, from 0° to 90° (i.e. the limit value leading to $h_l = 0$). In Table 3, the line of $\beta = 65°$ is highlighted for later comparison purposes (see Tables 6 and 9 presented later respectively for CCR and Milankovitch solutions). For example, for $\beta = 45°$, as assumed by Couplet, one may find that, according to Heyman's solution, the arch that develops an inner hinge at $\beta = 45°$ has a half-opening angle near $\alpha = 67°$, for $\beta = 50°$ near $\alpha = 75°$ or for $\beta = 60°$ near $\alpha = 92°$. Notice that, due to the characteristic *'linearity'* of Heyman's solution, these results are represented by single-valued functions of β.

Table 3.

On the trends for α small, Heyman is commenting in Heyman (1977, p. 79) that, for α small, thus β as well, the approximate root of Eq. (42) may be evaluated as $\beta \cong \alpha / \sqrt{2}$. Indeed, a second-order expansion of the two hand sides of Eq. (42) in β and α, respectively, renders precisely $\beta^2 \cong \alpha^2/2$. For such small values of β, from Eq. (36) the geometrical parameter η turns out to be proportional to β^4 ($\eta \cong \beta^4/12 \cong \alpha^4/48$), so that *"arches of small angle of embrace can, in theory, be very thin"*. Also, from Eq. (43), the non-dimensional horizontal thrust in such approximation becomes $h \cong 1 - \beta^2/3 \cong 1 - \alpha^2/6$, thus h keeps itself very much near 1 for α and β small. Notice that the alternative non-dimensional thrust $\hat{h}$ has the same trend $\hat{h} \cong \beta^4/12 \cong \alpha^4/48$ as that of η. Same considerations for α and β small apply to the characteristic parameters when A is near 2 as $A \cong 2 - \beta^2/3 \cong 2 - \alpha^2/6$, see Eq. (23), leading to the trends $\beta \cong \sqrt{3}\ \sqrt{(2 - A)}$, $\eta \cong \hat{h} \cong 3/4\ (2 - A)^2$ and $h \cong A - 1$. All these trends will also apply to CCR and Milankovitch solutions and are going be illustrated in the plots that follow.

2.3 Numerical aspects of Heyman's solution

The solution of the hinge angle β for Heyman's solution is depicted graphically in Figs. 5–6, respectively as a function of both $A = \alpha \cot \alpha / 2$ and α. Notice that the analytical plot $\beta(A)$ can be obtained directly from Eq. (42) as a parametric plot $(A(\beta),\beta)$, taking $0 \le \beta \le \beta_l^H = \pi/2$ as a variable parameter. On the other hand, the plot $\beta(\alpha)$ requires the numerical solution of either directly Eq. (42), for β at given α, or of $A(\beta) = \alpha \cot \alpha / 2$, for α at given β, with $A(\beta)$ calculated from Eq. (42). As revealed by the results reported in Tables 2–3, the trends in β, as α grows from 0 and A decreases from 2, are monotonic (increasing) and single-valued (meaning that to each value of β a single value of A and α corresponds). The plots of η and h as a function of α are reported as well in Figs. 7–8, with the typical trends displayed by Heyman's solution. Notice that h decreases from 1 to 0 as α grows from zero to the limit value α_l^H.

Figures 5–8.

All the produced plots contain as well some proposals of fitting functions, with calibrated best-fit parameters, useful to provide analytical representations of Heyman's solution. This will be done as well for both CCR and Milankovitch solutions. The fitting trends, expressed by combinations of power-law relationships, are derived based on the

expected trends for α and β small and, most of all, a posteriori, based on the experience that has been gained in fitting first CCR solution and then Milankovitch one. The fittings in terms of η and h turn-out very similar for all solutions, while the fittings for β are a bit different in this case, since Heyman's solution is monotonic and does not produce stationary points in $\beta(A)$ or $\beta(\alpha)$, a remarkable feature of the solution that will follow. Fitting functions based on both $A(\alpha)$ or directly on α are proposed. The fittings appear quite good in all reported cases, so either one of the proposals could be taken as reference. An easy-to-remember expression for $\beta(A)$, depicted in Figs. 5–6, is also reported below, in the context of a possible recursive search of the hinge position.

The numerical solution of transcendental Eq. (42) for β is quite straight-forward (especially in the form $A(\beta) = \alpha \cot \alpha/2$, at given β, as stated above). However, a recursive procedure could be devised, e.g. for further root refinement of a guess that could be taken from a root fit. Briefly, an effective recursive formula could be obtained as follows. Take Eq. (42), isolate a pivoting β term β_p and solve with respect to that. Different possibilities arise, that can be checked for recursive convergence. The chosen one has originated from the following choice (for compactness, as used also in the following, the following positions are made: $S = \sin\beta$, $C = \cos\beta$):

$$\beta \, \frac{2\beta_p C/S + C^2 + 1}{2\beta_p + S\,C - S} = A \tag{51}$$

Also, to further improve the convergence rate, additional splits of the pivoting term have been attempted and optimised through numerical trials by the following proposal:

$$\beta \, \frac{12\,\beta_p C/S - 10\beta\, C/S + C^2 + 1}{6\beta_p - 4\beta + S\,C - S} = A \tag{52}$$

which, by solving with respect to β_p, leads to the following expression useful for recursive evaluation of the root β in Heyman's solution:

$$\beta_{iter}{}^{H} = \frac{\beta\left(10\beta C - S\,(1+C^2)\right) - S\left(4\beta + S(1-C)\right)A}{6(2\beta C - S\,A)} \tag{53}$$

This expression can be used to generate recursive estimations for given values of A. Starting from the simple fitting guess:

$$\beta_0{}^{H} = \sqrt{3}\ \left(2-A\right)^{1/2}\ \left(1 - 1/6\,(2-A)^{2/3}\right) \tag{54}$$

a few iterations turn-out enough to recover the correct recursive estimate of root β.

Part II:

Present CCR solution

As re-derived in Part I of the paper, Heyman obtained his formulas for the analysis of circular masonry arches by imposing the tangency condition at the haunch intrados on the resultant thrust force itself. In this part, a similar derivation is developed (still through a static approach in which equilibrium equations are explicitly written), but by more correctly re-stating the tangency condition in terms of the true line of thrust (locus of pressure points). The differences between the two solutions are outlined.

3 Present CCR solution for the critical arch characteristics

3.1 Derivation by a static approach

Given the same adopted geometrical features and assumed collapse mode of the circular masonry arch (Figs. 1–3), to express the correct tangency condition, the expression of the line of thrust in terms of the eccentricity $e(\beta) = M/N$ of the centers of pressure P with respect to the geometrical centerline of the arch is derived first (e is taken positive from centerline towards center O of the circular arch, see Fig. 9).

Figure 9.

With reference to Fig. 9, one gets first a slightly-modified and more general version of equilibrium relation (10), by the rotational equilibrium of any upper portion of the arch with respect to the center of pressure P at eccentricity e, at a general position β along the arch:

$$H \cdot \left[r + \frac{t}{2} - (r-e)\cos\beta \right] = W_1 \cdot \left[(r-e)\sin\beta - x_1 \right] \tag{55}$$

or, given Eqs. (11)–(12) and in terms of non-dimensional parameters $\eta = t/r$ and $h = H/(wr)$:

$$wrh\ \frac{r}{2}\left[2 + \eta - \left(2 - \frac{2e}{r} \right)\cos\beta \right] = wr\beta\ \frac{r}{2}\left[\left(2 - \frac{2e}{r} \right)\sin\beta - 2\frac{1-\cos\beta}{\beta} \right] \tag{56}$$

By solving this equilibrium relation with respect to the non-dimensional horizontal thrust h one has:

$$h=\frac{\left(2-\frac{2e}{r}\right)\beta\sin\beta-2\left(1-\cos\beta\right)}{2+\eta-\left(2-\frac{2e}{r}\right)\cos\beta}=\frac{\left(2-\frac{2e}{t}\eta\right)\beta\sin\beta-2\left(1-\cos\beta\right)}{2+\eta-\left(2-\frac{2e}{t}\eta\right)\cos\beta} \tag{57}$$

Indeed, at the haunch B, where the angle β represents the position of the inner hinge of the rotational collapse mechanism, Eq. (16), namely $h = h_1$, is recovered from (57) for $e = t/2$ or $2e = t$, i.e., in non-dimensional terms, $\hat{e} = 2e/t = 1$. Similarly, Eq. (25), that is $h = h_2$, is recovered from (57) by setting $\hat{e} = 2e/t = -1$ at $\beta = \alpha$.

By solving instead with respect to the eccentricity e (or to the non-dimensional eccentricity $-1 \le \hat{e} = 2e/t \le 1$) one also gets the equation that expresses the line of thrust as the locus of the centers of pressure of the resultant thrust:

$$\hat{e}(\beta)=\frac{2e(\beta)}{t}=\frac{2\beta\sin\beta-2(1-\cos\beta)-h(2+\eta-2\cos\beta)}{\eta(\beta\sin\beta+h\cos\beta)}=\frac{num_{\hat{e}}(\beta)}{den_{\hat{e}}(\beta)} \tag{58}$$

Notice that function $\hat{e}(\beta)$ in Eq. (58), which displays built-in property $\hat{e}(0) = -1$ at the crown, depends on both parameters η and h. One of them could be inserted from either $h = h_2$, Eq. (25), or $\eta = \eta_2$, Eq. (26), which would automatically set $\hat{e}(\alpha) = -1$ also at the other extreme of the arch, i.e. at the shoulder. For example, by setting $h = h_2$ in Eq. (58) one obtains the final expression of the eccentricity of the line of thrust passing from crown A and shoulder C, at any given value of α and η:

$$\hat{e}(\beta)=\frac{2e(\beta)}{t}=\frac{2(2+\eta)\left(\beta\sin\beta-(1-\cos\beta)A\right)-\eta\left((2+\eta)A-2\cos\beta\right)}{\eta(2+\eta)\left(\beta\sin\beta-(1-\cos\beta)A\right)+\eta\left((2+\eta)A-2\cos\beta\right)} \tag{59}$$

where $A = \alpha\cot\alpha/2$. In the form of $\hat{e}(\beta)$ in Eq. (59) it is easy to appreciate, through Eq. (23), that, for $\beta = \alpha$, $\hat{e}(\alpha) = -1$.

At the condition of limit equilibrium, just a little instant before collapse, the line of thrust touches the intrados B where the hinge at the haunches forms (Fig. 10). Thus, in this cross section one has:

$$e(\beta)=\frac{t}{2} \quad or \quad \hat{e}(\beta)=1 \tag{60}$$

Figure 10.

At the same time, the line of thrust must be tangent to the intrados at the haunches when the sought critical condition of minimum thickness of the arch still allowing for

equilibrium is reached. So, the function $e(\beta)$ has to display a stationary point at the haunch section (where $e = t/2$), i.e. the first derivative of the eccentricity $e(\beta)$ with respect to the angular position β must be zero:

$$e'(\beta) = 0 \quad or \quad \hat{e}'(\beta) = 0 \tag{61}$$

Notice that Eq. (61) has to hold, at the haunches, together with Eq. (60). By expanding e.g. the derivative of the fractional non-dimensional form of e one has:

$$\hat{e}'(\beta) = \frac{num_{\hat{e}}' \, den_{\hat{e}} - num_{\hat{e}} \, den_{\hat{e}}'}{den_{\hat{e}}^{\,2}} = \frac{num_{\hat{e}}' - \hat{e} \, den_{\hat{e}}'}{den_{\hat{e}}} \tag{62}$$

Thus, the stationary condition (61) leads to:

$$\hat{e}(\beta) = \frac{num_{\hat{e}}'(\beta)}{den_{\hat{e}}'(\beta)} = \frac{2}{\eta} \, \frac{f(\beta) - (1+h)\sin\beta}{f(\beta) - h\sin\beta} \tag{63}$$

where, for the ease of notation in what is going to be reported in the sequel, the following convenient positions are made:

$$\begin{aligned} &f = f(\beta) = (\beta \sin\beta)' = \sin\beta + \beta\cos\beta = S + \beta C \,, \\ &g = g(\beta) = f(\beta)\cos\beta + \beta\sin^2\beta = \beta + \sin\beta\cos\beta = \beta + S\,C \\ &where \quad S = S(\beta) = \sin\beta \,, \; C = C(\beta) = \cos\beta, \; with \; link \; \beta S^2 + Cf - g = 0 \end{aligned} \tag{64}$$

Functions f and g, with link $\beta S^2 + C f - g = 0$, will turn-out useful to express the solution in compact form. Notice that $g \geq 0$ for $\beta \geq 0$; also, $g - f = (1 - \cos\beta)(\beta - \sin\beta) \geq 0$ and $f + g = (1 + \cos\beta)(\beta + \sin\beta) \geq 0$ for $\beta \geq 0$. Functions f and g both vanish at $\beta = 0$.

Since the tangency condition has to hold at the haunch B, where $\hat{e} = 2e/t = 1$, from Eq. (63) one has directly the *tangency condition* written in terms of either parameter η:

$$\eta = \eta_e = 2\frac{f - (1+h)\sin\beta}{f - h\sin\beta} = 2\left(1 - \frac{1}{1 + \beta\cot\beta - h}\right) = 2\left(1 - \frac{1}{1 + h_H - h}\right) \tag{65}$$

or, by solving Eq. (65) with respect to h:

$$h = h_e = \frac{(2-\eta)\, f - 2\sin\beta}{(2-\eta)\sin\beta} = \beta\cot\beta - \frac{\eta}{2-\eta} = h_H - \frac{\eta}{2-\eta} \tag{66}$$

where $h_H = \beta\cot\beta$ is the non-dimensional horizontal thrust of Heyman's solution. The stationary condition in terms of $h = h_e$ could be equivalently obtained from the

stationary condition $h'(\beta) = 0$, as applied to $h = h_1(\beta)$, Eq. (16). Indeed, similarly to steps in Eqs. (62)–(63), from the fractional form of $h_1 = num_{h_1} / den_{h_1}$ in Eq. (16) one gets $h = num_{h_1}' / den_{h_1}' = h_e$. Notice that, though being still linear in both η and h, the correct tangency condition stated in terms of the eccentricity e of the line of thrust cannot be directly solved in terms of only either one of the two characteristic parameters η and h, as instead it was possible for Heyman's solution, i.e. Eq. (65) or Eq. (66) contain *both* parameters η and h. Actually, looking at the final expression in Eq. (66), one sees that assuming $h_e = h_H$, as taken by Heyman, leads to an *approximation of the true tangency condition* $h = h_e$. This might look reasonable until η keeps small. All this makes the present solution slightly more involved than the former.

Finally, similarly to Heyman's system (46), equilibrium relations (15), (24) and tangency condition (60),(61) lead to a system of three equations in the unknowns β, η, h:

$$\begin{cases} \textit{first equilibrium relation}, \text{ Eq. (15)} \\ \textit{second equilibrium relation}, \text{ Eq. (24)} \\ \textit{tangency condition at the haunch (of the line of thrust)}, \text{ Eqs. (60), (61)} \end{cases} \tag{67}$$

Explicitly, by inserting the correct tangency condition (65) or (66), Heyman's system (47) transforms into the following CCR system:

$$\begin{cases} h = h_1 = \dfrac{(2-\eta)\beta\sin\beta - 2(1-\cos\beta)}{2+\eta-(2-\eta)\cos\beta} \quad \text{or} \quad \eta = \eta_1 = 2\,\dfrac{\beta\sin\beta-(1+h)(1-\cos\beta)}{\beta\sin\beta+h(1+\cos\beta)} \\ h = h_2 = A - \dfrac{2}{2+\eta} \quad \text{or} \quad \eta = \eta_2 = 2\left(\dfrac{1}{A-h}-1\right) \qquad CCR \\ h = h_e = \dfrac{(2-\eta)\,f - 2\sin\beta}{(2-\eta)\sin\beta} = \overbrace{\beta\cot\beta}^{h_H} - \dfrac{\eta}{2-\eta} \quad \text{or} \quad \eta = \eta_e = 2\,\dfrac{f-(1+h)\sin\beta}{f-h\sin\beta} \end{cases} \tag{68}$$

where recall that $A = \alpha\cot\alpha/2$ and $f = \sin\beta + \beta\cos\beta$.

The second equation of system (68) in Heyman's form $A = h + 2/(2+\eta)$ suggests, as an intermediate result in the process of finding β at given α, or A, to solve formally with respect to A (like if one, in an opposite way, would seek the unknown angle α, or

attached term A, that originates for a given haunch position β). This leads to the following analytical representation of CCR solution.

3.2 Analytical representation of CCR solution

The solution of CCR system (68) can then be obtained in compact closed-form, in terms of the functions reported in frame (64), by solving explicitly for the triplet (A, η, h):

$$\begin{aligned} A &= g\ \frac{f \pm \sqrt{f^2 - 2g\,S + S^2}}{S(2g - S)}\ ; \\ \eta &= 2\ \frac{g - S \mp \sqrt{f^2 - 2g\,S + S^2}}{f + g}\ ; \\ h &= \frac{f - S \pm \sqrt{f^2 - 2g\,S + S^2}}{2S}\ , \quad \hat{h} = \eta\, h = (g - f)\frac{f + S \pm \sqrt{f^2 - 2g\,S + S^2}}{S(f + g)} \end{aligned} \tag{69}$$

where the signs in front of the square root terms are sorted-out in the triplet (+,–,+) or in the triplet (–,+,–), i.e. with sorting (A^+, η^-, h^+) and (A^-, η^+, h^-). The non-dimensional horizontal thrust $\hat{h}$ can then be determined as well by the product of η and h (and sorted-out in the same way as that of h). Notice that $A(\beta)$, thus $\alpha(\beta)$, $\eta(\beta)$ and $h(\beta)$, or $\hat{h}(\beta)$, are two-valued functions of β, i.e. there are two values of A, thus of α, η and h, or $\hat{h}$, that correspond to the same inner hinge position β.

The first of Eqs. (69) expresses, through $A = \alpha \cot \alpha/2$, the relationship between the half-angle of embrace α and the hinge position β; it can be solved numerically for β at given $A(\alpha)$. For the corresponding value of β, the other expressions in Eqs. (69) render the sought parameters η, h (or $\hat{h}$). Thus, Eqs. (69) explicit the present CCR solution, as compared to classical Heyman's formulas (7)–(9).

One also notices that expressions (69) are actually coming from the solution of a *quadratic problem*, i.e. they are the roots of the following quadratic equations, respectively in A, η and h (or $\hat{h}$):

$$\begin{aligned} &S(2g - S)\ A^2 - 2fg\ A + g^2 = 0\ ; \\ &(f + g)\ \eta^2 - 4(g - S)\ \eta + 4(g - f) = 0\ ; \\ &2S\ h^2 - 2(f - S)\ h + g - f = 0, \quad (f + g)S\ \hat{h}^2 - 2(g - f)(f + S)\ \hat{h} + 2(g - f)^2 = 0 \end{aligned} \tag{70}$$

The three quadratic equations in A, η and h can be obtained directly by eliminating in turn the couples η and h, A and h, A and η, from the original CCR system (68). The same holds true by working with $\hat{h}$ instead of h. All this clearly shows that the present CCR solution turns-out *'quadratic'* in the solution parameters A, η, h (or $\hat{h}$), as opposed to *'linear'* Heyman's solution. As a consequence of that, and remarked above, parameters $A(\beta)$, $\eta(\beta)$, $h(\beta)$ (or $\hat{h}(\beta)$) are double-valued functions of the hinge position β.

Different ways to rewrite the first of Eqs. (70) similarly to Heyman's formula (7), with term A isolated on the rhs, could be the following:

$$\frac{2fg-g^2/A}{S(2g-S)}=A\,,\quad \frac{2fg}{S(2g-S)+g^2/A^2}=A$$
$$\frac{g^2}{2fg-S(2g-S)A}=A\,,\quad \frac{g^2+S(2g-S)A^2}{2fg}=A \tag{71}$$

though obviously there is now a dependence on A, thus on α, also on the lhs of the equation. Similar form expressions could be written as well, for η, h or $\hat{h}$.

In looking at the expressions in Eqs. (69), notice that the term $f^2-2gS+S^2$ that appears under the square roots in Eqs. (69) vanishes for $\beta=0$ and further becomes zero for a characteristic value of β, that can be solved numerically,

$$f^2-2gS+S^2=\beta^2\cos^2\beta-2\sin\beta(\beta-\sin\beta)(1-\cos\beta)=0$$
$$\rightarrow\quad \beta=\beta_{s\beta}{}^{CCR}=1.12909\ rad=64.6918^\circ \tag{72}$$

and represents a stationary point (local maximum) of the hinge angle in the response curves of β. Notice also that $f^2-2gS+S^2\geq 0$ for $0\leq\beta\leq\beta_{s\beta}{}^{CCR}$, assuring that the solution turns-out real-valued in that range of β. For $\beta=\beta_{s\beta}{}^{CCR}$ one also derives the following corresponding CCR, β-stationary, characteristic solution parameters:

$$A=A_{s\beta}{}^{CCR}=\left.\frac{fg}{S(2g-S)}\right|_{\beta=\beta_{s\beta}}=1.09292\ \rightarrow\ \alpha=\alpha_{s\beta}{}^{CCR}=2.23031\ rad=127.788^\circ,$$
$$\eta=\eta_{s\beta}{}^{CCR}=2\left.\frac{g-S}{f+g}\right|_{\beta=\beta_{s\beta}}=0.421414\,, \tag{73}$$
$$h=h_{s\beta}{}^{CCR}=\left.\frac{f-S}{2S}\right|_{\beta=\beta_{s\beta}}=0.266957\,,\quad \hat{h}_{s\beta}{}^{CCR}=\left.\frac{(g-f)(f+S)}{S(f+g)}\right|_{\beta=\beta_{s\beta}}=0.112499$$

where, on top/right of Eq. (73) the numerical solution of $A = \alpha \cot \alpha/2$ has been derived for $\alpha_{s\beta}^{CCR}$, which is near to 128°. The angle $\beta_{s\beta}^{CCR}$, near 65°, represents the maximum angular position that the inner hinge may reach at increasing α.

In the limit cases when $\beta \to 0$ one has, from Eqs. (69), the following extreme values of the triplet A, η, h (or $\hat{h}$), in the two solution branches:

$$\beta \to 0 \Rightarrow \begin{cases} A^{+} = 2 \ (\alpha = 0), \ \eta^{-} = 0, \ h^{+} = 1, \\ A^{-} = \dfrac{2}{3} \ (\alpha = 2.64839 \, rad = 151.742°), \ \eta^{+} = 1, \ h^{-} = 0, \end{cases} \quad \hat{h}^{\pm} = 0 \tag{74}$$

Thus, as β increases in the first branches from 0 to $\beta_{s\beta}^{CCR}$, A decreases from 2 to $A_{s\beta}^{CCR}$ (α increases from 0 to $\alpha_{s\beta}^{CCR}$), η increases from 0 to $\eta_{s\beta}^{CCR}$, h decreases from 1 to $h_{s\beta}^{CCR}$. As β decreases-back in the second branches from $\beta_{s\beta}^{CCR}$ to 0, A decreases from $A_{s\beta}^{CCR}$ to 2/3 (α increases from $\alpha_{s\beta}^{CCR}$ to α_{l}^{CCR}), η increases from $\eta_{s\beta}^{CCR}$ to 1, h decreases from $h_{s\beta}^{CCR}$ to 0. This shows that, in this last limit, the horizontal non-dimensional thrust vanishes and thus the limit of validity of CCR solution is reached. The corresponding limit values:

$$A_{l}^{CCR} = \frac{2}{3} \ (\alpha_{l}^{CCR} = 2.64839 \, rad = 151.742°), \quad \eta_{l}^{CCR} = 1, \quad h_{l} = \hat{h}_{l} = 0 \tag{75}$$

could be compared to those provided in Eq. (48) for Heyman's solution, as reported as well in resuming Table 10 at the end of Part III of the paper. In practice, this CCR solution is valid for angles of embrace α that are between 0 and around 152°. Note also that the thrust vanishes for a thickness to radius ratio that becomes 1.

Notice that, as remarked for Heyman's solution, the non-dimensional horizontal thrust parameter $\hat{h} = \eta h$ becomes zero on the two extremes of the solution branches, when $\beta \to 0$, since η and h play complementary roles in Eq. (74). This leads to bell-shaped trends in the curves $\hat{h}(A)$ or $\hat{h}(\alpha)$, as it will be illustrated in plot form in Part III of the paper, in comparing all the derived solutions. The trends go through a stationary point of $\hat{h}$ (local maximum) that occurs in the first branch $\hat{h}^{+}$, a bit earlier than $\beta_{s\beta}$ at variable β, at around 64°, as opposed to 76° for Heyman's solution. Indeed, the maximum point can be determined by a stationary analysis of $\hat{h}$ as a function of β (or as a function of A or of α) as follows:

$$\beta_{s\hat{h}}^{CCR} = 1.12394\,rad = 64.3969^\circ \;\Rightarrow$$
$$A_{s\hat{h}}^{CCR} = 1.16802 \quad (\alpha_{s\hat{h}}^{CCR} = 2.14389\,rad = 122.836^\circ); \tag{76}$$
$$\eta_{s\hat{h}}^{CCR} = 0.358644; \quad h_{s\hat{h}}^{CCR} = 0.320070, \; \hat{h}_{s\hat{h}}^{CCR} = 0.114791$$

Thus, the maximum value of $\hat{h} = \eta\, h$ that the arch can transfer in the critical condition at variable inner hinge or angle of embrace, is still obtained for a half-opening angle that is somehow near 120°, but with slightly different values of the $\hat{h}$-stationary characteristic solution parameters (see also Table 10 at the end of the paper).

All described features and functional dependencies of CCR solution are illustrated in detail in Fig. 11, where the characteristic functions $A(\beta)$, $\eta(\beta)$, $h(\beta)$ of CCR solution are plotted analytically, with a colour distinction for the two branches of solutions (69), on the two sides of the apex point attached to $\beta_{s\beta}^{CCR}$. In Fig. 11 three solution cases are systematically reported: the characteristic solution that corresponds to apex points in $\beta_{s\beta}^{CCR}$, which is produced for $\alpha = \alpha_{s\beta}^{CCR} = 127.788°$, and two reference cases on the two sides of that, namely $\alpha = 90°$ and $\alpha = 140°$, the second being an additional non-conventional case of over-complete arch with half-opening angle exceeding 90°, somehow in between $\alpha_{s\beta}^{CCR} = 127.788°$ and $\alpha_l^{CCR} = 151.742°$.

Figure 11.

The outcomes of CCR solution can be further represented in plots that report the classical triplet β, η, h as a function of driving variable $A(\alpha)$. These plots are single-valued in A and can be generated analytically from Eqs. (69) by parametric plots $(A(\beta), \beta)$, $(A(\beta), \eta(\beta))$, $(A(\beta), h(\beta))$, taking $0 \le \beta \le \beta_{s\beta}^{CCR}$ as variable parameter. Thus, they do not require an explicit numerical solution. On the other hand, similar plots of β, η, h as a function of α require either the numerical solution of CCR system (68) or Eqs. (69), at given discrete values of α (thus of A), or more simply the numerical solution of $A(\beta) = \alpha \cot \alpha/2$ for α at given discrete values of $0 \le \beta \le \beta_{s\beta}^{CCR}$, with $A(\beta)$, and $\eta(\beta)$, $h(\beta)$, coming from Eqs. (69). All these are going to be represented later at the end of this Part II (with appropriate fittings) and also at the end of Part III of the paper (to compare effectively all the derived solutions).

One may check that the solution for η and h in Eqs. (69), i.e. expressions $(69)_b$ and $(69)_c$, can be obtained from the 2×2 subsystem of CCR system (68) formed by its

first and third lines, e.g. $\{h = h_1, h = h_e\}$, in terms of h, that is the two lines that do not depend on A. This allows to get right-away expressions for η and h that are independent of A. Expression $(69)_a$ for A can then be obtained from the second line of system (68), e.g. $h = h_2$, by solving with respect to $A = h + 2/(2 + \eta)$ and by substituting in it the just-obtained expressions for η and h. The other two alternative ways to proceed by combining the first and second lines of CCR system (68), e.g. $\{h = h_1, h = h_2\}$, and the second and third lines of CCR system (68), e.g. $\{h = h_2, h = h_e\}$, would give rise to alternative representations of the solution for η and h, which however appear more involved, since they contain as well the term A. Thus, these expressions are not going to be reported here.

However, according to this path of reasoning, the following equivalent compact explicit expressions of η and h as a function of both β and A (values at the solution instance) can be derived:

$$\eta = 2\frac{g(f+g-S)-S(2g-S)A}{g(f+g)} = 2\frac{g-(f-g+S)A}{(f+g)A} = 2\frac{g-SA}{g+SA} = 2\frac{g-(f+S)A+SA^2}{(f-SA)A} \quad (77)$$

$$h = \frac{(2g-S)A-g}{2g} = \frac{(2f-S)A-g}{2SA} = \frac{(f+g-S)A-g}{g+SA} = \frac{g-f}{g-SA}A \quad (78)$$

The first two expressions of η and h in Eqs. (77) and (78) can be obtained by eliminating the square root terms in Eqs. $(69)_{a,b,c}$. This is equivalent to work first with a 2×2 subsystem with the first and third lines of system (68), to solve for η and h and then eliminate the square root terms through the use of the second line of system (68). Similarly, the third and fourth expressions in Eqs. (77) and (78) could be obtained, respectively, by working on 2×2 subsytems with the first and second lines of system (68) and with the second and third lines of system (68). Expressions (77) and (78) can be used to calculate η and h, at the solution instance, i.e. at given $A(\alpha)$ and corresponding determined β. As a difference to Heyman's solution, Eqs. (8) and (9), Eqs. (77) and (78) contain also the explicit dependence on $A(\alpha)$. Notice that relations $(77)_d$ and $(78)_d$ are self-coherent, through the second line of system (68). The same holds for relations $(77)_c$ and $(78)_a$, which are compactly expressed just in terms of function g. Self-coherent expressions $(77)_d$–$(78)_d$ and $(77)_c$–$(78)_a$ also generate the following compact representations for the non-dimensional thrust parameter $\hat{h}$ (at the solution instance):

$$\hat{h} = \eta\, h = 2\,\frac{\left(g-(f+S)A+SA^2\right)(g-f)}{(f-SA)(g-SA)} = \frac{(g-SA)\left((2g-S)A-g\right)}{(g+SA)\,g} \tag{79}$$

3.3 Solution of CCR formulas

CCR system (68) or Eqs. (69) can be used to derive numerically the final outcomes of the present CCR solution, as compared to the classical results provided by Heyman. The relations obtained above can be solved numerically, at given half-angle of embrace α (thus at given $A = \alpha\, cot\, \alpha/2$), for the usual characteristic parameters β, η, h (or $\hat{h}$).

Following the presentation that has been already outlined in Part I for Heyman's solution, Table 4 below reports first the results for the two taken reference cases of $\alpha = 90°$ and $\alpha = 140°$ (compare to Table 1). Furthermore, additional numerical results for different values of the half cut-off angle $0 < \alpha < \alpha_l^{CCR} = 151.742°$ can be derived systematically, as reported in Table 5, with α stepping every 10° (compare to Table 2).

Tables 4–5.

Notice first that, as commented above, the resulting angular position β of the inner hinge according to the present CCR solution is a non-monotonic function of the half-angle of embrace α. Also, the numerical results reported in Table 5 appear to be consistent with those provided by Ochsendorf (2006) for $\alpha \le 90°$. Moreover, the following main remarks are in order, with reference also to plots that will follow:

- The angular hinge position β is the parameter that displays a more appreciable difference for the two solutions, specifically at increasing opening angle α and especially for over-complete arches ($\alpha > 90°$). On the other hand, as expected, the estimates of η and h (or $\hat{h}$) turn-out less sensitive on the different tangency condition.
- The η values are practically the same for the two solutions for non-high values of α and deviate just a bit more for bigger values of α. Even at $\alpha = 90°$ the difference is of the order of 1/1000, thus not that significant in engineering terms. However, Heyman's estimate turns-out sub-critical ($\eta_H < \eta_{CCR}$). Also, higher differences are obtained for larger values of α approaching the α_l^{CCR} limit.
- Same considerations, in form even more important in terms of minimal difference, apply to the trends of the non-dimensional horizontal thrust h or $\hat{h}$, with some deviations on $\hat{h}$ when α is around $\alpha_{s\hat{h}}$, i.e when $\hat{h}$ is around peak $\hat{h}_{s\hat{h}}$ of the bell-shaped

curves of $\hat{h}(\alpha)$. Heyman's results over-estimate CCR outcomes in terms of h ($h_H > h_{CCR}$), while the opposite holds for $\hat{h}$ ($\hat{h}_H < \hat{h}_{CCR}$).

Further specific remarks also apply (see also plots that follow):

- The inner hinge angle β is always below the trend for α small, which is confirmed also for CCR solution as $\alpha/\sqrt{2} \cong 0.71\ \alpha$, i.e. quite near to the 2/3 of α. As α grows from 0, the trend for α small is progressively abandoned and the function $\beta^{CCR}(\alpha)$ bends-down more than $\beta^{H}(\alpha)$, especially towards peak $\beta_{s\beta}{}^{CCR}(\alpha_{s\beta}{}^{CCR})$, with a quite rapid drop to zero after that.
- Also, for α values that are less than those at around peak, the hinge angle β is always beyond $\alpha/2$. Indeed, it can be calculated that the straight line $\beta = \alpha/2$ crosses the curve $\beta^{CCR}(\alpha)$ at a point where $\alpha = 2.25701$ rad = 129.317°, with a corresponding value of inner hinge angle $\beta = \alpha/2 = 1.12850$ rad = 64.6585°; since $\alpha_{s\beta}{}^{CCR} = 2.23031$ rad = 127.788°, with $\beta_{s\beta}{}^{CCR} = 1.12909$ rad = 64.6918°, this occurs just a bit after peak $\beta_{s\beta}{}^{CCR}(\alpha_{s\beta}{}^{CCR})$ of the curve $\beta^{CCR}(\alpha)$.
- In practice, one could make it short on that by saying that, for half-opening angles α up to peak abscissa $\alpha_{s\beta}{}^{CCR}$, the inner hinge position β is always between one half and two thirds of α; after peak, β is always less than $\alpha/2$ and precipitates down to zero when α increases from $\alpha_{s\beta}{}^{CCR} = 127.788°$ to $\alpha_l{}^{CCR} = 151.742°$.
- In looking at Table 5, interesting, almost round cases, appear for: $\alpha = 70°$, with $\beta \cong 45°$; $\alpha = 80°$, with $\beta \cong 50°$; $\alpha = 120°$, with $\beta \cong 64°$; $\alpha = 150°$, with $\beta \cong 40°$.
- The monotonic trends for η (increasing) and h (decreasing) are quite similar to those displayed by Heyman's solution, with minor differences on η, more visible for over-complete arches, where the sub-critical condition $\eta_H < \eta_{CCR}$ can be appreciated, and with almost unnoticeable differences for h, except in the limit $\alpha \to \alpha_l{}^{CCR}$.
- The same holds true for the bell-shaped trend of $\hat{h} = \eta\, h$, with some differences to Heyman's solution starting to occur almost at around peak $\hat{h}_{s\hat{h}}{}^{CCR}(\alpha_{s\hat{h}}{}^{CCR})$, where Heyman's solution underestimates $\hat{h}$. Indeed, in Table 5, as in Table 2, a decrease is recorded for $\hat{h}$ after $\alpha = 120°$, which confirms the $\hat{h}$-stationary point at $\alpha_{s\hat{h}}{}^{CCR} = 122.836°$ vs. $\alpha_{s\hat{h}}{}^{H} = 120.918°$, i.e. still at around 120°; at $\alpha = 120°$ the maximum values of $\hat{h}$ are reached in Tables 5 and 2, with $\hat{h}_{CCR} = 0.114146$, while $\hat{h}_H = 0.108354$.

Again, following what already done in Table 3 for Heyman's solution, one may get conversely the value of α (or of $A = \alpha\, cot\, \alpha/2$), and relevant characteristic parameters η, h (or $\hat{h}$), corresponding to a given angular hinge position β. This is reported in Table 6, still for β stepping each 5°, first from 0° to the stationary value $\beta_{s\beta}^{CCR} = 64.6918°$ of the CCR solution (line marked with colour distinction in Table 6) and then back from $\beta_{s\beta}^{CCR}$ to 0°. Indeed, as commented earlier, α turns-out to be a double-valued function of β. For example, for $\beta = 45°$, as assumed by Couplet, one may find that, according to present CCR solution, the arch that develops an inner hinge at $\beta = 45°$ might have half-opening angles near $\alpha = 70°$ or near 149°, for $\beta = 50°$ near $\alpha = 80°$ or near $\alpha = 148°$, for $\beta = 60°$ near $\alpha = 104°$ or near $\alpha = 142°$. Also notice that, for $\beta = 60°$, h reaches exactly 1/2 on one side (pre-peak) of the solution (with α near 104°), while η reaches exactly 2/3 on the other side (post-peak, with α near 142°).

Table 6.

The same conclusions that have been outlined by reading the quantitative results reported in Tables 4–6 may be directly appreciated by looking at the plots that represent the values of the critical characteristics $\beta(A)$ and $\beta(\alpha)$, $\eta(\alpha)$, $h(\alpha)$ at variable opening angle of the arch, which are depicted in Figs. 12–15, together with the trends for α small and with appropriate fittings based on power-law relationships, that can be derived as described previously for Heyman's solution. CCR Figs. 12–15 may be compared to Heyman's Figs. 5–8. Notice that, as in Fig. 5, the plot of $\beta(A)$ can be handled analytically, while, as in Figs. 6–8, the plots of $\beta(\alpha)$, $\eta(\alpha)$, $h(\alpha)$ require a discrete representation, through a numerical solution, as briefly commented below.

Figures 12–15.

3.4 Numerical aspects of CCR solution

The numerical solution of the derived CCR formulas is quite straight forward. It follows basically the same strategies that have been already outlined for Heyman's solution (refer to Section 2.3). Also, the numerical search could act at the different levels of the governing equations or of the resulting analytical representations, with same results. In practice, one could say that, once the driving CCR system (68) has been established, the final numerical solution can be handled with standard tools of root finding.

A recursive estimate of hinge position β, working well on all sides of the solution branches, can be based on the first expression in the second line of Eq. (71), leading to:

$$\beta_{iter}^{CCR} = \frac{2 f g A - S(2g - S)A^2}{g} - S C = 2 f A - 2 S A^2 + \frac{S^2 A^2}{g} - S C \tag{80}$$

Starting from the easy-to-remember CCR fitting guess

$$\beta_0^{CCR} = 3/2 \left(A - 2/3\right)^{1/4} \left(2 - A\right)^{1/2} \tag{81}$$

that one could derive for the CCR solution based on the trends for α small (A near 2) and α near α_l^{CCR} (A near 2/3), good refinement can be achieved in not many iterations.

3.5 Analytical plots of the line of thrust

As noticed above, Heyman's solution turns-out sub-critical with respect to CCR solution, the latter being the one that correctly locates the critical condition of minimum thickness. In other words, since $\eta_H < \eta_{CCR} = \eta_{cr}$, in Heyman's solution there is not enough thickness to sustain the arch. This observation is quite apparent as well in the x–y plots of the eccentricity of the line of thurst $e(\beta)$, Eq. (58), as reported (in non-dimensional form for $\hat{e} = 2e/t$) in Figs. 16–17, again for the two reference cases of $\alpha = 90°$ and $\alpha = 140°$, and for both Heyman's and CCR solutions. These plots confirm that Heyman's solution becomes sub-critical, with a corresponding line of thrust that would go out of the intrados of the arch, for values of β within a fork of two values of β that include (almost in the middle) the true value of β coming from CCR solution. Notice also that in Figs. 16–17 Heyman's solution corresponds to the highest value of β at which the line of thrust touches the intrados.

Figures 16–17.

The true appearance of the line of thrust that develops in the arch in the critical condition of minimum thickness is represented analytically for CCR solution by the polar plots reported in Fig. 18, for the two values $\alpha = 90°$ and $\alpha = 140°$of the half-angle of embrace. The plots make apparent the increasing thickness that the arch has to display to warrant equilibrium at increasing opening angle, with a corresponding decrease in horizontal thrust.

Figure 18.

Part III:

Milankovitch-type solution

The solutions derived in Part I (Heyman) and Part II (CCR) of the paper, have been based on a static analysis, by explicitly writing equilibrium equations and tangency conditions, within the usual assumption of taking the self-weight of the arch as uniformly-distributed along its geometrical centerline. Here, an additional solution along the line of Milankovitch's work is derived as well explicitly, which accounts now for the true location of the centers of gravity of each ideal voussoir of the arch. The differences between the three obtained solutions are finally highlighted in large detail.

Notice that, in general terms, Milankovicth's role appears fundamental for the general formulation of arches and vaults equilibrium, for which solutions are identified as well as a function of boundary conditions. The elegant, mathematically-clear and appealing method of Milankovicth identifies the limit thickness of semicircular arches by a static approach in which the range of admissible thrusts is reduced to a single solution. This is basically the same approach first proposed by Coulomb, who imposed the stationary condition of the admissible thrust limits. Thus, beyond the confined scopes of the present analysis, explicit mention to outstanding Coulomb's and Milankovitch's contributions should be emphasized.

4 General derivation allowing for the true location of the centers of gravity (Milankovitch-type solution)

So far, the classical (and reasonable) hypothesis of assuming the self-weight distribution along the geometrical centerline of the arch has been made. In other words, in previous Heyman's and CCR solutions, the self-weight of the arch was not considered to act at the level of the true centers of gravity of each theoretical voussoir, but simply at half thickness. The correct location of the centers of gravity is instead taken into account here, which leads to a Milankovitch-type solution.

Due to the curvature of the circular arch and the consequent wedged shape of each ideal infinitesimal chunk of the arch (of opening $d\varphi$), it appears that its center of gravity is slightly displaced, from centerline at radial distance r, towards the extrados of the arch, at radial distance r_G a bit larger than r. Indeed, referring to polar coordinates:

$$r_G = \frac{\int_{dV} \gamma \rho \, dV}{\int_{dV} \gamma \, dV} = \frac{\int_0^{d\varphi} \int_{r-t/2}^{r+t/2} \gamma \rho \overbrace{\rho \, d\rho \, d\varphi \, d}^{dV}}{\int_0^{d\varphi} \int_{r-t/2}^{r+t/2} \gamma \underbrace{\rho d\rho d\varphi}_{dA} \, d} = \frac{\gamma d \, d\varphi \int_{r-t/2}^{r+t/2} \rho^2 d\rho}{\gamma d \, d\varphi \int_{r-t/2}^{r+t/2} \rho \, d\rho} = \frac{\gamma t d \, r d\varphi \, r\left(1+\eta^2/12\right)}{\underset{w}{\gamma t d} \; r \, d\varphi} \tag{82}$$

$$= r\left(1+\eta^2/12\right)$$

where the positive multiplicative correction factor $(1 + \eta^2/12)$ appears, which is quadratic in the thickness to radius ratio η. Similarly, re-taking Eqs. (11)–(13), one gets:

$$W_1 = w r \beta, \quad x_1 = r\left(1+\eta^2/12\right)\frac{1-\cos\beta}{\beta}, \quad y_1 = r\left(1+\eta^2/12\right)\frac{\sin\beta}{\beta} \tag{83}$$

Thus, also distances x_1 and y_1 are affected in the same way, though weight W_1 is not. It must be said that accounting for the true location of the centers of gravity should modify the final results just slightly. Indeed, based on the previous solutions, the critical thickness to radius ratio $\eta = t/r$ should keep anyway small, especially for half-angles of embrace that do not exceed much the standard upper value of 90°. Thus, in such cases, the classical assumption $r_G = r$ seems quite reasonable. However, for the sake of completeness, the previous CCR analysis is reconsidered in this section, by following again the same main steps but by taking into account the true location of the centers of gravity at $r_G = r\,(1 + \eta^2/12)$. The arising results are expected to be in line with the outcomes of Milankovitch's work and will show the differences to CCR solution, which turn-out to be quite marginal, especially for half-angles of embrace $\alpha \leq 90°$.

For instance, it is worth-while to advance that, for the reference case of the full semicircular arch ($\alpha = 90°$), the difference in terms of haunch hinge angle is of the order of 0.024%, since while $\beta_{CCR} = 54.4963°$, $\beta_M = 54.4833°$, thus both at around 54.5° (as opposed to $\beta_H = 58.8293°$, thus at around 59°). This also confirms that the found discrepancy between β_{CCR} (or β_M) and β_H was not due to the implicit approximation $r = r_G$ (see the introductory discussion in Section 1). Even less important differences are expected for the other characteristics η and h. Indeed, always for the reference case of the full semicircular arch ($\alpha = 90°$), $\eta_{CCR} = 0.107426$ and $h_{CCR} = 0.621772$

($\hat{h}_{CCR}$ = 0.0667947), while η_M = 0.107478 and h_M = 0.620881 ($\hat{h}_M$ = 0.0667311), which can all be compared to Heyman's values η_H = 0.105965, h_H = 0.621113 ($\hat{h}_H$ = 0.0658164).

Following steps undertaken at the beginning of Section 3, by re-taking (un-modified) rotational equilibrium equation (55), with respect to the center of pressure *P* at eccentricity *e* from centerline towards center *O*, and making use of the expressions of W_1 and x_1 in Eq. (83), by solving Eq. (55) with respect to *h* one rewrites Eq. (57) as follows:

$$h = \frac{\left(2 - \frac{2e}{t}\eta\right)\beta \sin\beta - 2\left(1-\cos\beta\right)\left(1+\eta^2/12\right)}{2+\eta-\left(2-\frac{2e}{t}\eta\right)\cos\beta} \tag{84}$$

with factor $(1 + \eta^2/12)$ that affects the term $(1 - \cos\beta)$. Thus, the expressions of equilibrium relations $h = h_1 = h_L$ and $h = h_2$ are re-obtained from Eq. (84), by setting respectively $\hat{e} = 2e / t = 1$ at the haunch *B*, at β, and $\hat{e} = -1$ at the shoulder *C*, at $\beta = \alpha$:

$$h = h_1 = h_L = \frac{\left(2-\eta\right)\ \beta\ \sin\beta - 2\left(1-\cos\beta\right)\left(1+\eta^2/12\right)}{2+\eta-\left(2-\eta\right)\cos\beta} \tag{85}$$

$$h = h_2 = A - \frac{2}{2+\eta}\left(1+\eta^2/12\right) = \frac{\left(2+\eta\right)\ \alpha\ \sin\alpha - 2\left(1-\cos\alpha\right)\left(1+\eta^2/12\right)}{\left(2+\eta\right)\left(1-\cos\alpha\right)} \tag{86}$$

By solving instead Eq. (55) with respect to the eccentricity *e* (or to the non-dimensional eccentricity $-1 \le \hat{e} = 2e / t \le 1$) one also gets:

$$\hat{e}(\beta) = \frac{2e(\beta)}{t} = \frac{2\beta\sin\beta - 2(1-\cos\beta)\left(1+\eta^2/12\right) - h\,(2+\eta-2\cos\beta)}{\eta\,(\beta\sin\beta + h\cos\beta)} \tag{87}$$

which provides the true position of the line of thrust in Milankovitch's sense. Similarly to what discussed for CCR solution in deriving Eq. (59), one may also set $h = h_2$ in Eq. (87), so that to impose that $\hat{e}(\alpha) = -1$ at any given value of α (thus $A = \alpha\cot\alpha/2$) and η, giving rise to:

$$\hat{e}(\beta) = \frac{2e(\beta)}{t} = \frac{2(2+\eta)\left(\beta\sin\beta - (1-\cos\beta)A\right) - \eta\left((2+\eta)A - 2\cos\beta\left(1+\eta^2/12\right)\right)}{\eta(2+\eta)\left(\beta\sin\beta - (1-\cos\beta)A\right) + \eta\left((2+\eta)A - 2\cos\beta\left(1+\eta^2/12\right)\right)} \tag{88}$$

To get the tangency condition in Milankovitch's terms one could either work on the stationary condition at the haunch as $e' = 0$ or, which is the easiest since it does not even require the definition of e, as $h_1' = 0$, with equivalent results (Section 3), leading to:

$$h = h_e = \frac{(2-\eta)\left(\beta \sin\beta\right)' - 2\sin\beta\left(1+\eta^2/12\right)}{(2-\eta)\sin\beta} = \overbrace{\beta\cot\beta}^{h_H} - \frac{\eta}{2-\eta}\left(1+\eta/6\right) \tag{89}$$

Thus, the correction term $-\eta/(2-\eta)$ to Heyman's tangency condition $h = h_H$ introduced by CCR solution is further affected by the multiplicative factor $(1+\eta/6)$ (thus with expected negligible variations, especially in terms of the predicted h).

In sum, with reference to all previous derivations, equilibrium equations and tangency conditions are all slightly modified, just by the presence of multiplicative factor $(1+\eta^2/12)$ on selected terms. The equations turn-out still linear in h, but no longer linear in η, which puts in favor the option of expressing them just in terms of h, by linear solving with respect to h, as already done above. This allows to cast Milankovitch solution system as follows:

$$\begin{cases} h = h_1 = \dfrac{\left(2-\eta\right)\beta\sin\beta - 2\left(1-\cos\beta\right)\left(1+\eta^2/12\right)}{2+\eta-\left(2-\eta\right)\cos\beta} \\ h = h_2 = A - \dfrac{2}{2+\eta}\left(1+\eta^2/12\right) \\ h = h_e = \dfrac{(2-\eta)\,f - 2\sin\beta\left(1+\eta^2/12\right)}{(2-\eta)\sin\beta} = \overbrace{\beta\cot\beta}^{h_H} - \dfrac{\eta}{2-\eta}\left(1+\eta/6\right) \end{cases} \quad \textit{Milankovitch} \tag{90}$$

where, from frame (64), function f is defined as $f = (\beta\sin\beta)' = \sin\beta + \beta\cos\beta$. By comparison to earlier-derived Heyman's system (47) and CCR system (68), it appears clear that Milankovitch system (90) contains both as particular cases.

Similarly to what derived for CCR solution, Milankovitch system (90) actually results into the solution of the following *"cubic problem"* for the triplet A, η, h (or $\hat{h}$):

$$\begin{aligned} &S^2(3g-2S)\,A^3 + 3(g-f)\,g\,S\,A^2 - 3fg^2A + 2g^3 = 0\ ; \\ &S\,\eta^3 + 3(f+g)\,\eta^2 - 12(g-S)\,\eta + 12(g-f) = 0\ ; \\ &6S^2h^3 - 3S(3f-g-2S)\,h^2 - 3(g-f)(f-2S)\,h + 2(g-f)^2 = 0\ , \\ &\quad 2S^3\hat{h}^3 - 3(g-f)(f+g+2S)\,S\,\hat{h}^2 + 6(g-f)^2(f+2S)\,\hat{h} - 8(g-f)^3 = 0 \end{aligned} \tag{91}$$

where again $f = S + \beta C$, $g = \beta + S C$, $S = \sin\beta$, $C = \cos\beta$, as defined in frame (64).

Milankovitch solution could then be represented and handled analytically by the explicit solution of Milankovitch system (90) or of cubic problem (91). However, explicit representations of such solutions are too lengthy to be reported, whereas the meaningful branches of the solution will be represented below in table and plot forms.

Quantitative numerical results, on the line of what already presented and described earlier in details for both Heyman's (Tables 1–3) and CCR (Tables 4–6) solutions, are reported in Tables 7–9 below. Only some differences to CCR solution are found, and mainly for over-complete arches. Almost round cases in the determination of β turn-out: $\alpha = 70°$ with $\beta \cong 45°$; $\alpha = 80°$ with $\beta \cong 50°$; $\alpha = 140°$ with $\beta \cong 59°$. The estimates on η are very slightly under-conservative (smaller η) for CCR solution; however, not as those of Heyman's solution. Accordingly, the values of h or $\hat{h}$ are a bit over-estimated by CCR solution. Finally, Table 10 gathers the stationary and limit parameters of Milankovitch solution, together with those found for Heyman's and CCR solutions.

Tables 7–10.

Also, as for Heyman's and CCR solutions, a recursive strategy could be devised for refining the angular hinge position β in Milankovitch solution, according to expressions

$$\begin{aligned} \beta_{iter}{}^{M} &= \frac{-2g^3 + 3fg^2A + 3fgSA^2 + S^2(2S-3g)A^3}{3gSA^2} - SC \\ &= f - SA + \frac{2S^2A}{3g} + \frac{fg}{SA} - \frac{2g^2}{3SA^2} - SC \end{aligned} \tag{92}$$

starting from an appropriate fitting guess, such as

$$\beta_0{}^{M} = 1.53 \left(A - \left(\sqrt{3} - 1\right)\right)^{1/4} (2 - A)^{1/2} \tag{93}$$

These have been derived based on the previous experience gained in treating CCR solution and on Eq. $(91)_a$.

Analytic parametric plots useful to explore the details of all three derived solutions are provided in Fig. 36 for the solution couples (β, $\eta(\beta)$), (β, $h(\beta)$), ($\eta(\beta)$, $h(\beta)$). The trends competent to α and β small (η near 0, h near 1) are reported as well. The plots are useful to read directly the link between two of the characteristic solution parameters out of the three β, η, h: the first plot allows to trace the hinge position at given least thickness of the arch; the second, the hinge position at given horizontal thrust in the

critical condition; the third, the minimum thickness corresponding to a given resulting critical thrust. In the first two plots, which involve β and the consequent non-monotonic trends for CCR and Milankovitch solutions, the apparent difference to Heyman's solution can be noticed. Much minor differences are experienced for the monotonic trends in the third plot, just when the horizontal thrust becomes small at increasing thickness.

Figure 19.

The triplet of the characteristic solution parameters β, η, h for the three solutions is then represented analytically in Fig. 20 as a function of true driving variable $A = \alpha \cot \alpha/2$, with usual trends for α small (A near 2). The plots are useful in analytic terms, in order to compare the different solutions in terms of driving variable A. In the first plot of $\beta(A)$ the expected non-monotonic trends of CCR and Milankovitch solutions differ much from Heyman's solution at increasing half-angle of embrace α (decreasing A), especially in the second branches. In the second plot of $\eta(A)$ the common monotonic trends differentiate a bit towards the solution limits with η increasing; CCR and Milankovitch trends for η are quite tight to each other and progressively detach from Heyman's one. In the third plot of $h(A)$ the monotonic trends are quite adherent to each other, with some little deviation for CCR solution towards the solution limit with $h = 0$; surprisingly, Heyman's solution, which was stating the tangency condition at the intrados on the resultant thrust force itself, is very much attached to Milankovitch solution in terms of h, which means that Heyman's solution provides a good estimate of the real horizontal thrust, despite missing the correct position of the inner hinge.

Figure 20.

Similar plots for the triplet β, η, h but as a function of true physical variable α are reported in Fig. 21, together with the usual trends for α small. These graphs summarise the main results of the present paper, since they compare together Heyman's, CCR and Milankovitch solutions in engineering terms. The most interesting newly-discovered

feature is the non-monotonic dependence of β at variable α, with Heyman's solution that over-shoots considerably at increasing cut-off angle, especially for over-complete arches. CCR and Milankovitch solutions stay very much tight to each other, at least until at around peak. Identical trends of the inner hinge position, pulling-back to zero after peak, are also experienced by CCR and Milankovitch solutions. Similar remarks as those concerning previous Fig. 20 apply to the trends of $\eta(\alpha)$ and $h(\alpha)$, with even less-noticeable discrepancies between the three solutions. CCR estimate of η, though being non-conservative with respect to Milankovitch prediction, is very attached to that.

Figure 21.

Figures 22 and 23 represent the new interesting bell-shaped plots of variable $\hat{h} = \eta\, h = H/(\gamma\, d\, r^2)$, with trends for α small (A near 2), first as a function of driving variable A and second as a function of geometrical variable α. Recall that non-dimensional variable $\hat{h}$ provides in itself a readable estimate of the horizontal thrust in terms of given material (specific weight γ) and geometrical (out-of-plane depth d, radius r) parameters. The graphs in Fig. 23 clearly show that the maximum horizontal thrust of the arch in the critical condition is obtained for an α at around 120° (see characteristic values in Table 10 for the $\hat{h}$–stationary parameters). At around peak, with respect to Milankovitch prediction, Heyman's estimate of $\hat{h}$ is a bit under-shooting while CCR estimate of $\hat{h}$ turns-out instead slightly over-shooting.

Figures 22–23.

Milankovitch solution is also singularly represented in details in the four usual plots $\beta(A)$ and $\beta(\alpha)$, $\eta(\alpha)$, $h(\alpha)$, as reported in Figs. 24–27, with customary trends for α small and with adopted analytical fitting proposals. All this could be compared to companion Figs. 5–8 (Heyman's solution) and 12–15 (CCR solution).

Figures 24–27.

5 Conclusions

This paper has presented general analytical derivations, solutions and results for the classical Couplet-Heyman problem in the statics of circular masonry arches. Specifically, the characteristic solution parameters, namely the angular position of the inner intrados hinge β (from the vertical axis of symmetry at the crown), the thickness to radius ratio $\eta = t/r$ and the non-dimensional horizontal thrust $h = H/(w\,r)$ or $\hat{h} = \eta\, h = H/(\gamma d\, r^2)$ have been determined.

The following main characteristic issues and salient conclusions may be drawn:

- A complete analytical account has been provided for general half-angles of embrace $0° < \alpha < 180°$. Reference has been made to the three classical Heyman's hypotheses and, coherently, only the purely-rotational collapse mode (which is assumed to be known from scratch) has been investigated.
- Three different solutions have been derived explicitly in full analytical terms: classical Heyman's solution, present CCR solution, both based on the hypothesis of distribution of the self-weight along the centerline of the arch and a Milankovitch-type solution, which instead accounts for the true location of the centers of gravity. The physical meaning of the various equations that rule the three solutions has been clearly highlighted.
- As a crucial condition that differentiates among the three solutions, apart from common equilibrium conditions, Heyman's classical solution considers the tangency condition of the resultant thrust force to the intrados at the location of the inner hinge, while CCR and Milankovitch solutions better state the tangency condition of the true line of thrust (locus of pressure points) to the intrados curve.
- The resulting analytical problems for the explicit solution of the collapse characteristics of the circular masonry arch are "linear", "quadratic" and "cubic", respectively for Heymans's, CCR and Milankovitch solutions.
- Heyman's derivation appears rather correct in engineering terms, especially for the estimate of the non-dimensional horizontal thrust h and also for the estimate of the thickness to radius ratio η. However, it fails at determining the correct angular

position β of the inner hinge, especially at increasing half-opening angle α of the arch and specifically for over-complete arches ($\alpha > 90°$). Despite this being a sort of internal ingredient in the determination of practical parameters like η and *h*, it is also a truly geometrical characteristic of the rotational collapse mode. Heyman's solution appears as a valuable engineering approximation of the correct solution.

- Furthermore, the outcomes of Heyman's solution turn-out sub-critical in academic terms, in the sense that the estimate of the minimum thickness is not conservative. In this academic sense, the analytical solutions reported here, provide a more consistent account for the failure characteristics of circular masonry arches.
- This has been clearly shown by different results and plots, which have highlighted that Heyman's solution displays lines of thrust that may fall-out of the intrados limit of the arch. On the other hand, CCR (and Milankovitch) solutions, based on the correct tangency condition, result in appropriate representations displaying true tangencies. Also, the line of thrust has been plotted analytically on the arch profile, for different values of the angle of embrace, showing how its geometrical shape varies, by fitting always in between the extrados and intrados bounds, even at increasing half-opening angle α and consequent required thickness increase.
- The most salient new trait displayed by the present solutions as opposed to classical Heyman's solution is the non-monotonic trend experienced by the angular hinge position β as a function of half-angle of embrace α. CCR and Milankovitch curves go through stationary points, which appear for half-opening angles at around 130°, with inner hinge located at almost half way, at around 65°, namely the widest angular position β of the inner hinge at increasing half-opening angle α. After that, still at increasing opening angle, the inner hinge rapidly pulls-back to zero, until the horizontal thrust vanishes in such limit. Towards such a limit condition the arch has to increase considerably its thickness to radius ratio η, in view of withstanding its own self-weight. At this solution limit the half-opening angle turns-out at around 150°, which fixes the limit of validity of the solutions reported here (that are endowed with a purely-rotational collapse mode).
- The difference between CCR solution and reference Heyman's solution has been extensively highlighted, specifically for two reference cases that could be quoted in this respect: $\alpha = 90°$ and $\alpha = 140°$. They lead respectively to the correct hinge

positions β at around 54.5° and 61.5°, instead at near 59° and 86°, as it would be obtained by Heyman's solution.

- The dependence on the half-angle of embrace α always goes through the root term $A = \alpha \cot \alpha/2$, as put forward already by Heyman's solution. This property holds true also for CCR and Milankovitch solutions, since the dependence on α, through variable A, is inherited by a common equilibrium condition, not by the different tangency conditions. The latter may be expressed in terms of the upper portion of the collapse mechanism of the half-arch, thus are instead independent of α.
- The new bell-shaped trends experienced by the considered non-dimensional thrust parameter $\hat{h} = \eta\, h = H/(\gamma d\, r^2)$ also show that, around their peak, Heyman's solution turns-out sub-critical, while CCR solution is over-conservative with respect to Milankovitch one. This shows that there is a well-defined value of half-opening angle, say around 120°, that leads to the maximum value of the horizontal thrust (around 0.11 in terms of $\hat{h}$) that the arch is able to transfer to the shoulders in the critical condition, at given material (specific weight γ) and geometrical parameters (radius r and out-of-plane depth d) of the arch.
- The three solutions have been explored in detail and depicted extensively in both quantitative and qualitative, table and plot forms. The trends for α small have been provided as well, together with appropriate analytical fittings of the characteristic curves, which could allow an easy, sufficiently-accurate, estimate of the three main collapse characteristics β, η, h. These approximate estimates could be easily refined, by iterative recursive numerical procedures that have been also outlined in the paper.

Concerning further possible developments of the present study, more definite conclusions should be drawn on the role of friction (see e.g. Sinopoli et al. 1997, 2007; Casapulla and Lauro, 2000; Casapulla and D'Ayala, 2001; D'Ayala and Casapulla, 2001; Foce and Aita (2003); Gilbert et al., 2006; Smars 2000, 2008; D'Ayala and Tomasoni, 2011). The earlier-quoted first Heyman hypothesis ruling-out sliding failure (thus necessarily leading to a purely-rotational collapse mode) looks fairly reasonable for masonry structures, at least under ideal conditions. However, this could be released, in view of a more comprehensive investigation (preliminary results have been outlined in Frigerio, 2010, Colasante, 2010 and Rizzi et al., 2012). Different

geometrical shapes of the arch, for example elliptic or parabolic (see e.g. the numerical study in Clemente et al., 1995 and the very recent equilibrium analysis in Aita et al., 2011), could further be analysed as well, along the line of the present derivations, to inspect how the morphology of the arch may affect the critical parameters and collapse modes. In this respect, Romano (2005) and Romano and Ochsendorf (2006, 2009) have already analysed in details the structural behaviour of circular, pointed and basket-handle masonry arches, by graphical, numerical and experimental techniques. Also, analyses on pointed arches have been presented by De Rosa and Galizia (2007), through a Limit Analysis optimisation method, and by Hejazi and Jafari (2010), through numerical FEM simulations taking into account as well the effect of different brick arrangements. Collapse performances of pointed vs. semicircular arches with vertical walls have been compared in Aita et al. (2007, 2011). Furthermore, different loading conditions could be considered, to see how these may affect the factor of safety of the arch. All this is left as well for further work.

Acknowledgements

This work has been carried-out at the University of Bergamo, Faculty of Engineering (Dalmine). The financial support by *"Fondi di Ricerca d'Ateneo ex 60%"* at the University of Bergamo is gratefully acknowledged.
At review stage, the Authors would like to thank Reviewer 1 for pointing-out reference Heyman (2009) and Reviewer 2 for clarifying the role of outstanding Coulomb's and Milankovitch's contributions.

References

[1] Ainsworth M., Mihai L.A., *"Modeling and numerical analysis of masonry structures"*, Numerical Methods for Partial Differential Equations, 23(4), 798–816, 2007.

[2] Aita D., *"Between geometry and mechanics: a re-examination of the principles of stereotomy from a statical point of view"*, Proc. of the 1st Int. Congress on Construction History, Madrid, 20-24 January 2003, S. Huerta (Ed.), Madrid: Instituto Juan de Herrera, Volume I, paper CIHC1_017, p. 161–170, 2003.

[3] Aita D., Barsotti R, Bennati S., *"Some explicit solutions for flat and depressed masonry arches"*, Proc. of the 1st Int. Congress on Construction History, Madrid, 20-24 January 2003, S. Huerta (Ed.), Madrid: Instituto Juan de Herrera, Volume I, paper CIHC1_018, p. 171–183, 2003.

[4] Aita D., Foce F., Barsotti R., Bennati S., *"Collapse of masonry arches in Romanesque and Gothic constructions"*, Proc. of 5th Int. Conference on Arch Bridges, ARCH'07, Funchal, Madeira, Portugal, September 12-14, 2007, Lourenço P.B., Oliveira D.B., Portela A. (Eds.), Multicomp, Lda Publishers, Madeira, p. 625–632, 2007.

[5] Aita D., Barsotti R, Bennati S., *"Equilibrium of pointed, circular and elliptical masonry arches bearing vertical walls*", J. of Structural Engineering, ASCE, doi:http://dx.doi.org/10.1061/(ASCE)ST.1943-541X.0000522, Preview Manuscript posted ahead of print on 18 October 2011.

[6] Albuerne A., Huerta S., *"Coulomb's theory of arches in Spain ca. 1800: the manuscript of Joaquín Monasterio"*, Proc. of 6th Int. Conference on Arch Bridges, ARCH'10, Fuzhou, China, October 11-13, 2010, Baochun Chen, Jiangang Wei (Eds.), College of Civil Engineering, Fuzhou University, Paper 46, p. 354–362, 2010.

[7] Alfaiate J., Gallardo A., *"Numerical simulations of a full scale load test on a stone masonry arch bridge"*, in Historical Constructions 2001 – Possibilities of Numerical and Experimental Techniques, Proc. of the 3rd Int. Seminar, Edited by Lourenço P.B. and Roca P., Guimarães, Portugal, University of Minho, 7-8-9 November 2001, Art. 068, p. 739–748, 2001.

[8] Andreu A., Gil L., Roca P., *"Computational analysis of masonry structures with a funicular model"*, J. of Engineering Mechanics, ASCE, 133(4), 473–480, 2007.

[9] Antunes G.J.J., "Comportamento Estrutural de Edifícios Antigos. Estruturas Arqueadas Planas", Dissertação para obtenção do Grau de Mestre em Engenharia Civil, Orientador: Gago A.S., Instituto Superior Técnico, Universidade Técnica de Lisboa, Dezembro de 2010.

[10] Audenaert A., Peremans H., Reniers G., *"An analytical model to determine the ultimate load on masonry arch bridges"*, J. of Engineering Mathematics, 59(3), 323–336, 2007.

[11] Audenaert A., Fanning P., Sobczak L., Peremans H., *"2-D analysis of arch bridges using an elasto-plastic material model"*, Engineering Structures, 30(3), 845–855, 2008.

[12] Armesto J., Roca-Pardiñas J., Lorenzo H., Arias P., *"Modelling masonry arches shape using terrestrial laser scanning data and nonparametric methods"*, Engineering Structures, 32(2), 607–615, 2010.

[13] Atamturktur S., Laman J.A., *"Finite element model correlation and calibration of historic masonry monuments: review"*, The Structural Design of Tall and Special Buildings, 21(2), 96–113, 2012.

[14] Baratta A., Corbi O., *"An approach to masonry structural analysis by the no-tension assumption – Part I: Material modeling, theoretical setup, and closed form solutions"*, Applied Mechanics Reviews, 63(4), 040802 (17 pages), 2010.

[15] Baratta A., Corbi O., *"An approach to masonry structural analysis by the no-tension assumption – Part II: Load singularities, numerical implementation and applications"*, Applied Mechanics Reviews, 63(4), 040803 (21 pages), 2010.

[16] Becchi A., *"The statics of arches between France and Italy"*, Proc. of the 1st Int. Congress on Construction History, Madrid, 20-24 January 2003, S. Huerta (Ed.), Madrid: Instituto Juan de Herrera, Volume I, paper CIHC1_034, p. 353–364, 2003.

[17] Bednarz L., Górski A., Jasienko J., Rusinski E., *"Simulations and analyses of arched brick structures"*, Automation in Construction, 20(7), 741–754, 2011.

[18] Benvenuto E., "La Scienza delle Costruzioni e il suo Sviluppo Storico", Sansoni, Firenze, 1981; ristampa Edizioni di Storia e Letteratura, Roma, 2006.

[19] Betti M., Drosopoulos G.A., Stavroulakis G.E., *"On the collapse analysis of single span masonry/stone arch bridges with fill interaction"*, Proc. of 5th Int. Conference on Arch Bridges, ARCH'07, Funchal, Madeira, Portugal, September 12-14, 2007, Lourenço P.B., Oliveira D.B., Portela A. (Eds.), Multicomp, Lda Publishers, Madeira, p. 617–624, 2007.

[20] Bičanič N., Stirling C., Pearce C.J., *"Discontinuous modelling of masonry bridges"*, Computational Mechanics, 31(1-2), 60–68, 2003.

[21] Blasi C., Foraboschi P., *"Analytical approach to collapse mechanisms of circular masonry arch"*, J. of Structural Engineering, ASCE, 120(8), 2288–2309, 1994.

[22] Block P., "Equilibrium System. Studies in Masonry Structures", Master Thesis, Supervisor: J.A. Ochsendorf, Massachusetts Institute of Technology, Department of Architecture, 2005.

[23] Block P., DeJong M., Ochsendorf J., *"As hangs the flexible line: equilibrium of masonry arches"*, Nexus Network Journal, 8(2), 13–24, 2006.

[24] Block P., Ciblac T., Ochsendorf J., *"Real-time limit analysis of vaulted masonry buildings"*, Computers and Structures, 84(29-30), 1841–1852, 2006.

[25] Boothby T.E., Brown C.B., *"Stability of masonry piers and arches"*, J. of Engineering Mechanics, ASCE, 118(2), 367–383, 1992.

[26] Boothby T.E., *"Stability of masonry piers and arches including sliding"*, J. of Engineering Mechanics, ASCE, 120(2), 304–319, 1994.

[27] Boothby T.E., *"Collapse modes of masonry arch bridges"*, Masonry International, 9(2), 62–69, 1995.

[28] Boothby T.E., "Analytical approach to collapse mechanisms of circular masonry arch", *Discussion on the paper by Blasi and Foraboschi (1994), with Closure by P. Foraboschi and C. Blasi*, J. of Structural Engineering, , 122(8), 978–980, 1996.

[29] Boothby T.E., *"Analysis of masonry arches and vaults"*, Progress in Structural Engineering and Materials, 3(3), 246–256, 2001.

[30] Brencich A., Morbiducci R., *"Masonry arches: historical rules and modern mechanics"*, Int. J. of Architectural Heritage, 1(2), 165–189, 2007.

[31] Cai Y., "Detailed Numerical Simulation of Experiments on Masonry Arch Bridges by Using 3D FE", Master's Thesis, Advisor: Molins C., Advanced Masters in Structural Analysis of Monuments and Historical Constructions, UPC Barcelona, July 2011.

[32] Campo M., Drosopoulos G.A., Fernández J.R., Stavroulakis G.E., *"Unilateral contact and damage analysis in masonry arches*", P Wriggers and U. Nackenhorst (Eds.), IUTAM Symposium on Computational Contact Mechanics, Springer, p. 357–363, 2007.

[33] Casapulla C., Lauro F., *"A simple computation tool for the limit-state analysis of masonry arches"*, Proc. of 5th Int. Congress on Restoration of Architectural Heritage, Firenze2000, Università di Firenze, 17-24 September 2000, CDROM Proc., p. 2056–2064, 9 pages, 2000.

[34] Casapulla C., D'Ayala D., *"Lower bound approach to the limit analysis of 3D vaulted block masonry structures"*, in Proc. of the 5th Int. Symposium on Computer Methods in Structural Masonry, STRUMAS V, Roma, p. 28–36, Swansea, Computer and Geotechnics Ltd., 2001.

[35] Casas J.R., *"Reliability-based assessment of masonry arch bridges"*, Construction and Building Materials, 25(4), 1621–1631, 2011.

[36] Cavicchi A, Gambarotta L., *"Two-dimensional finite element upper bound limit analysis of masonry bridges"*, Computers and Structures, 84(31-32), 2316–2328, 2006.

[37] Cavicchi A, Gambarotta L., *"Lower bound limit analysis of masonry bridges including arch–fill interaction"*, Engineering Structures, 29(11), 3002–3014, 2007.

[38] Chen Y., Ashour A.F., Garrity S.W., *"Modified four-hinge mechanism analysis for masonry arches strengthened with near-surface reinforcement"*, Engineering Structures, 29(8), 1864–1871, 2007.

[39] Clemente P., Occhiuzzi A., Raihtel A., *"Limit behaviour of stone arch bridges"*, J. of Structural Engineering, ASCE, 121(7), 1045–1050, 1995.

[40] Colasante G., "Sui meccanismi di collasso degli archi in muratura secondo l'analisi limite", Laurea Thesis in Building Engineering, Advisor E. Rizzi, Co-Advisor G. Cocchetti, Università di Bergamo, Facoltà di Ingegneria, Italy, 175 pages, December 2007.

[41] Colasante G., "Sul ruolo dell'attrito nei meccanismi di collasso degli archi circolari in muratura", Laurea (Master) Thesis, Advisor E. Rizzi, Co-Advisor G. Cocchetti, Università di Bergamo, Facoltà di Ingegneria, Italy, 213 pages, September 2010.

[42] Como M., *"Equilibrium and collapse analysis of masonry bodies"*, Meccanica, 27(3), 185–194, 1992.

[43] D'Ayala D., Casapulla C., *"Limit state analysis of hemisferical domes with finite friction"*, in Historical Constructions 2001 – Possibilities of Numerical and Experimental Techniques, Proc. of the 3rd Int. Seminar, Edited by Lourenço P.B. and Roca P., Guimarães, Portugal, University of Minho, 7-8-9 November 2001, Art. 056, p. 617–626, 2001.

[44] D'Ayala D., Tomasoni E., *"Three-dimensional analysis of masonry vaults using limit state analysis with finite friction"*, Int. J. of Architectural Heritage, 5(2), 140–171, 2011.

[45] de Arteaga I., Morer P., *"The effect of geometry on the structural capacity of masonry arch bridges"*, Construction and Building Materials, 34(InProgress), 97–106, 2012.

[46] Dede T., Ural A., *"A finite element program for historical stone arch bridges"*, Proc. of 5th Int. Conference on Arch Bridges, ARCH'07, Funchal, Madeira, Portugal, September 12-14, 2007, Lourenço P.B., Oliveira D.B., Portela A. (Eds.), Multicomp, Lda Publishers, Madeira, p. 533–541, 2007.

[47] Del Piero G., *"Limit Analysis and no-tension materials"*, Int. J. of Plasticity, 14(1-3), 259–271, 1998.

[48] De Rosa E., Galizia F., *"Evaluation of safety of pointed masonry arches through the Static Theorem of Limit Analysis"*, Proc. of 5th Int. Conference on Arch Bridges, ARCH'07, Funchal, Madeira, Portugal, September 12-14, 2007, Lourenço P.B., Oliveira D.B., Portela A. (Eds.), Multicomp, Lda Publishers, Madeira, p. 659–668, 2007.

[49] DeJong M., Ochsendorf J.A., *"Analysis of vaulted masonry structures subjected to horizontal ground motion"*, Proc. of 5th Int. Conference on Structural Analysis of Historical Constructions - Possibilities of Numerical and Experimental Techniques,

SAHC06, New Delhi, India, 6-8 November 2006, Lourenço P.B., Roca P., Modena C., Agrawal S. (Eds.), MACMILLAN Advanced Research Series, p. 973–980, 2006.

[50] Drosopoulos G.A., Stavroulakis G.E., Massalas C.V., *"Limit analysis of a single span masonry bridge with unilateral frictional contact interfaces"*, Engineering Structures, 28(13), 1864–1873, 2006.

[51] Drosopoulos G.A., Stavroulakis G.E., Massalas C.V., *"Influence of the geometry and the abutments movement on the collapse of stone arch bridges"*, Construction and Building Materials, 22(3), 200–210, 2008.

[52] Fanning P.J., Boothby T.E., *"Three-dimensional modelling and full-scale testing of stone arch bridges"*, Computers and Structures, 79(29-30), 2645–2662, 2001.

[53] Foce F., Aita D., *"The masonry arch between «limit» and «elastic» analysis. A critical re-examination of Durand-Claye's method"*, Proc. of the 1st Int. Congress on Construction History, Madrid, 20-24 January 2003, S. Huerta (Ed.), Madrid: Instituto Juan de Herrera, Volume I, paper CIHC1_088, p. 895–908, 2003.

[54] Foce F., *"On the safety of the masonry arch. Different formulations from the history of structural mechanics",* in Essays in the History of the Theory of Structures, S. Huerta (Ed.), Instituto Juan de Herrera, Madrid, p. 117–142, 2005.

[55] Foce F., *"Milankovitch's Theorie der Druckkurven: Good mechanics for masonry architecture"*, Nexus Network Journal, 9(2), 185–210, 2007.

[56] Ford T.E., Augarde C.E., Tuxford S.S., *"Modelling masonry arch bridges using commercial finite element software"*, Proc. of the 9th Int. Conf. on Civil and Structural Engineering Computing, Egmond aan Zee, The Netherlands, 2-4 September 2003, B.H.V. Topping (Ed.), Civil-Comp Press, Stirlingshire, UK, Paper 101, 20 pages, 2003.

[57] Frigerio A., "Sul meccanismo di collasso misto negli archi semicircolari in muratura", Laurea Thesis in Building Engineering, Advisor E. Rizzi, Co-Advisor G. Colasante, Università di Bergamo, Facoltà di Ingegneria, Italy, 130 pages, March 2010.

[58] Gago A.S., "Análise Estrutural de Arcos, Abóbadas e Cúpulas – Contributo para o Estudo do Património Construído", Dissertação, Doutoramento em Engenharia Civil, Orientador: Lamas A., Universidade Técnica de Lisboa, Instituto Superior Técnico, IST-UTL, Dezembro de 2004.

[59] Gago A.S., Alfaiate J., Lamas A., *"The effect of the infill in arched structures: Analytical and numerical modelling"*, Engineering Structures, 33(5), 1450–1458, 2011.

[60] Gibbons N., Fanning P.J., *"Ten stone masonry arch bridges and five different assessment approaches"*, Proc. of 6th Int. Conference on Arch Bridges, ARCH'10,

Fuzhou, China, October 11-13, 2010, Baochun Chen, Jiangang Wei (Eds.), College of Civil Engineering, Fuzhou University, Paper 63, p. 482–489, 2010.

[61] Gilbert M., Casapulla C., Ahmed H.M., *"Limit analysis of masonry block structures with non-associative frictional joints using linear programming"*, Computers and Structures, 84(13-14), 873–887, 2006.

[62] Gilbert M., *"Limit analysis applied to masonry arch bridges: state-of-the-art and recent developments"*, Proc. of 5th Int. Conference on Arch Bridges, ARCH'07, Funchal, Madeira, Portugal, September 12-14, 2007, Lourenço P.B., Oliveira D.B., Portela A. (Eds.), Multicomp, Lda Publishers, Madeira, p. 13–28, 2007.

[63] Giordano A., Mele E., De Luca A., *"Modelling of historical masonry structures: comparison of different approaches through a case study"*, Engineering Structures, 24(8), 1057–1069, 2002.

[64] Giordano A., De Luca A., Mele E., Romano A., *"Simplified evaluation of the horizontal capacity of masonry arches"*, Proc. of 5th Int. Conference on Structural Analysis of Historical Constructions - Possibilities of Numerical and Experimental Techniques, SAHC06, New Delhi, India, 6-8 November 2006, Lourenço P.B., Roca P., Modena C., Agrawal S. (Eds.), MACMILLAN Advanced Research Series, p. 1221–1229, 2006.

[65] Grandjean A., "Capacité Portante de Ponts en Arc en Maçonnerie de Pierre Naturelle - Modèle d'Évaluation Intégrant le Niveau d'Endommagement", Thèse No. 4596 (2009), Doctorat ès Sciences, Directeur de Thèse E. Brühwiler, École Polytechnique Fédérale de Lausanne (EPFL), Suisse, Février 2010.

[66] Harvey W.J.(Bill), *"Application of the mechanism analysis to masonry arches"*, The Structural Engineer, 66(5), 77–84, 1988.

[67] Harvey B., *"Interactive analysis of arching masonry structures"*, Prof. of 3rd Australasian Engineering Heritage Conference, Engineering in the Development of a Region – Heritage and History, Salmond College, University of Otago, Dunedin, New Zealand, 22–25 November 2009, 7 pages, 2009.

[68] Harvey B., Maunder E., *"Thrust line analysis of complex masonry structures using spreadsheets"*, in Historical Constructions 2001 – Possibilities of Numerical and Experimental Techniques, Proc. of the 3rd Int. Seminar, Edited by Lourenço P.B. and Roca P., Guimarães, Portugal, University of Minho, 7-8-9 November 2001, Art. 045, p. 521–528, 2001.

[69] Hejazi M., Jafari F., *"Structural effects of brick arrangement and span length on mid-pointed arches"*, Proc. of 7th Int. Conf. SAHC 2010, Shanghai, China, Oct. 6-8, 2010, Advanced Materials Research, Trans Tech Publications, Vols. 133-134, p. 411–416, 2010.

[70] Heyman J., *"The stone skeleton"*, Int. J. of Solids and Structures, 2(2), 249–279, 1966.

[71] Heyman J., *"On shell solutions for masonry domes"*, Int. J. of Solids and Structures, 3(2), 227–241, 1967.

[72] Heyman J., *"The safety of masonry arches"*, Int. J. of Mechanical Sciences, 11(4), 363–385, 1969.

[73] Heyman J., "Equilibrium of Shell Structures", Oxford Univ. Press, Oxford, 1977.

[74] Heyman J., "The Masonry Arch", Ellis Horwood Ltd., Chichester, 1982.

[75] Heyman J., "The Stone Skeleton – Structural Engineering of Masonry Architecture", Cambridge University Press, Cambridge, 1995.

[76] Heyman J., *"La coupe des pierres"*, Proc. of the Third Int. Congress on Construction History, Brandenburg University of Technology, Cottbus, Germany, 20–24 May 2009, Vol. 2, p. 807–812, 2009.

[77] Huerta S., *"Mechanics of masonry vaults: the equilibrium approach"*, in Historical Constructions 2001 – Possibilities of Numerical and Experimental Techniques, Proc. of the 3rd Int. Seminar, Edited by Lourenço P.B. and Roca P., Guimarães, Portugal, University of Minho, 7-8-9 November 2001, Art. 004, p. 47–70, 2001.

[78] Huerta S., *"Arcos, bóvedas y cúpulas. Geometría y equilibrio en el cálculo tradicional de estructuras de fábrica"*, Instituto Juan de Herrera, Madrid, 2004.

[79] Huerta S., *"Galileo was wrong: the geometrical design of masonry arches"*, Nexus Network Journal, 8(2), 25–52, 2006.

[80] Hughes T.G., Blackler M., *"A review of the UK masonry arch assessment methods"*, Proceedings of the Institution of Civil Engineers - Structures and Buildings, 122(3), 305–315, Paper 11302, 1997.

[81] Hughes T.G., Hee S.C., Soms E., *"Mechanism analysis of single span masonry arch bridges using a spreadsheet"*, Proceedings of the Institution of Civil Engineers - Structures and Buildings, 152(4), 341–350, Paper 12710, 2002.

[82] Koltsida Spyridoula I., "Detailed numerical simulation of experiments on masonry arch bridges by using 3D FE", Master's Thesis, Advisor: Molins C., Advanced Masters in Structural Analysis of Monuments and Historical Constructions, UPC Barcelona, July 2011.

[83] Kooharian A., *"Limit analysis of voussoir (segmental) and concrete arches"*, Journal Proceedings of the American Concrete Institute, 49(12), 317–328, 1952.

[84] Kumar P., Bhandari N.M., *"Non-linear finite element analysis of masonry arches for prediction of collapse load"*, Structural Engineering International, IABSE, 15(3), 166–174, 2005.

[85] Kumar P., Bhandari N.M., *"Mechanism based assessment of masonry arch bridges"*, Structural Engineering International, IABSE, 16(3), 226–234, 2006.

[86] Kumar P., *"Performance Assessment and Maintenance of Masonry Arch Bridges",* 34th IABSE Symposium on Large Structures and Infrastructures for Environmentally Constrained and Urbanised Areas, Venice, 22-24 Sept. 2010,

International Association for Bridge and Structural Engineering, p. 818, 8 pages, 2010.

[87] Livesley R.K., *"Limit analysis of structures formed from rigid blocks"*, Int. J. for Numerical and Analytical Methods in Engineering, 12(12), 1853–1871, 1978.

[88] Livesley R.K., *"A computational model for the limit analysis of three-dimensional masonry structures"*, Meccanica, 27(3), 161–172, 1992.

[89] Lourenço P.B., *"Analysis of historical constructions: From thrust-lines to advanced simulations"*, in Historical Constructions 2001 – Possibilities of Numerical and Experimental Techniques, Proc. of the 3rd Int. Seminar, Edited by Lourenço P.B. and Roca P., Guimarães, Portugal, University of Minho, 7-8-9 November 2001, Art. 006, p. 91–116, 2001.

[90] Lucchesi M., Padovani C., Pasquinelli G., Zani N., *"On the collapse of masonry arches"*, Meccanica, 32(4), 327–346, 1997.

[91] Lucchesi M, Šilhavý M., Zani N, *"Equilibrium problems and Limit Analysis of masonry beams"*, J. of Elasticity, 106(2), 165–188, 2012.

[92] MacLaughlin M.M., Doolin D.M., *''Review of validation of the discontinuous deformation analysis (DDA) method''*, Int. J. for Numerical and Analytical Methods in Geomechanics, 30(4), 271–305, 2006.

[93] Manrique Hoyos C., "Limit Analysis: Collection of Examples of Applications", Master's Thesis, Advisor: Molins C., Advanced Masters in Structural Analysis of Monuments and Historical Constructions, UPC Barcelona, July 2010.

[94] Martinez Martinez J.A., Moreno Revilla J., Aragon Torre A., *"Critical thickness criteria on stone arch bridges with low rise/span ratio and current traffic loads"*, in Historical Constructions 2001 – Possibilities of Numerical and Experimental Techniques, Proc. of the 3rd Int. Seminar, Edited by Lourenço P.B. and Roca P., Guimarães, Portugal, University of Minho, 7-8-9 November 2001, Art. 055, p. 609–616, 2001.

[95] Melbourne C., Wang J., Tomor A., *"A new masonry arch bridge assessment strategy (SMART)"*, Proc. of 5th Int. Conference on Arch Bridges, ARCH'07, Funchal, Madeira, Portugal, September 12-14, 2007, Lourenço P.B., Oliveira D.B., Portela A. (Eds.), Multicomp, Lda Publishers, Madeira, p. 227–236, 2007.

[96] Migliore M.R., Letizia F.S., Ruocco E., *"On the stability of masonry arches"*, Proc. of 5th Int. Conference on Structural Analysis of Historical Constructions - Possibilities of Numerical and Experimental Techniques, SAHC06, New Delhi, India, 6-8 November 2006, Lourenço P.B., Roca P., Modena C., Agrawal S. (Eds.), MACMILLAN Advanced Research Series, p. 965–972, 2006.

[97] Mihai L.A., Ainsworth M., *"An adaptive multi-scale computational modelling of Clare College Bridge"*, Computer Methods in Applied Mechanics and Engineering, 198(21-26), 1839–1847, 2009.

[98] Milankovitch M., "Beitrag zur Theorie der Druckkurven". Dissertation zur Erlangung der Doctorwürde, K. K. Technische Hochschule, Wien, 1904.

[99] Milankovitch M., *"Theorie der Druckkurven"*, Zeitschrift für Mathematik und Physik, 55, 1–27, 1907.

[100] Miri M., Hughes T.G., *"The physical and numerical modelling of a repaired masonry arch bridge"*, Proc. of 5th Int. Conference on Structural Analysis of Historical Constructions - Possibilities of Numerical and Experimental Techniques, SAHC06, New Delhi, India, 6-8 November 2006, Lourenço P.B., Roca P., Modena C., Agrawal S. (Eds.), MACMILLAN Advanced Research Series, p. 1255–1262, 2006.

[101] Molins C., Roca P., *"Capacity of masonry arches and spatial frames"*, J. of Structural Engineering, ASCE, 124(6), 653–663, 1998.

[102] Morer P., de Arteaga I., Armesto J., Arias P., *"Comparative structural analyses of masonry bridges: An application to the Cernadela Bridge"*, J. of Cultural Heritage, 12(3), 300–309, 2011.

[103] Ng K.-H., Fairfield C.A., *"Modifying the mechanism method of masonry arch bridge analysis"*, Construction and Building Materials, 18(2), 91–97, 2004.

[104] Ochsendorf J., "Collapse of Masonry Structures", Doctoral Dissertation, Supervisors: Heyman J. and Calladine C.R., University of Cambridge, King's College, UK, 2002.

[105] Ochsendorf J., *"The masonry arch on spreading supports"*, The Structural Engineer, 84(2), 29–36, 2006.

[106] O'Dwyer D., *"Funicular analysis of masonry vaults"*, Computers and Structures, 73(1-5), 187–197, 1999.

[107] Oikonomopoulou A., "Approches Numériques pour l'Étude du Comportement des Structures Maçonnées Anciennes: un Outil Basé sur le Calcul à la Rupture et la Visualisation Graphique", Thèse de Doctorat de l'Université Paris Est et de l'Ecole Nationale Supérieure d'Architecture de Paris la Villette, Directeur de Thèse: Guéna F., Paris, December 2009.

[108] Oikonomopoulou A., Ciblac T., Guéna F., *"Modelling tools for the mechanical behaviour of historic masonry structures"*, Proc. of the Third Int. Congress on Construction History, Brandenburg University of Technology, Cottbus, Germany, 20–24 May 2009, Vol. 3, p. 1097–1104, 2009.

[109] Oliveira D.V., Lourenço P.B., Lemos C., *"Geometric issues and ultimate load capacity of masonry arch bridges from the northwest Iberian Peninsula"*, Engineering Structures, 32(12), 3955–3965, 2010.

[110] Peng D.M., Chen Y.Y., Jiang R.J., Fairfield C.A., *"Optimal design of masonry arch bridges"*, Proc. of 6th Int. Conference on Arch Bridges, ARCH'10, Fuzhou,

China, October 11-13, 2010, Baochun Chen, Jiangang Wei (Eds.), College of Civil Engineering, Fuzhou University, Paper 87, p. 674–682, 2010.

[111] Pintucchi B., Zani N., *"Effects of material and geometric non-linearities on the collapse load of masonry arches"*, European J. of Mechanics A/Solids, 28(1), 45–61, 2009.

[112] Ponterosso P., Fishwick R.J., Fox D.St.J., Liu X.L., Begg D.W., *"Masonry arch collapse loads and mechanisms by heuristically seeded genetic algorithm"*, Computer Methods in Applied Mechanics and Engineering, 190(8-10), 1233–1243, 2000.

[113] Riveiro B., Morer P., Arias P., de Arteaga I., *"Terrestrial laser scanning and limit analysis of masonry arch bridges"*, Construction and Building Materials, 25(4), 1726–1735, 2011.

[114] Riveiro B., Caamaño J.C., Arias P., Sanz E., *"Photogrammetric 3D modelling and mechanical analysis of masonry arches: An approach based on a discontinuous model of voussoirs"*, Automation in Construction, 20(4), 380-388, 2011.

[115] Rizzi E., Cocchetti G., Colasante G., Rusconi F., *"Analytical and numerical analysis on the collapse mode of circular masonry arches"*, Proc. of 7th Int. Conf. SAHC 2010, Shanghai, China, Oct. 6-8, 2010, Advanced Materials Research, Trans Tech Publications, Vols. 133-134, p. 467–472, 2010.

[116] Rizzi E., Rusconi F., Cocchetti G., *"Numerical DEM (DDA) analysis on the collapse mode of circular masonry arches"*, Technical Report SdC2011/02, University of Bergamo, 46 pages, March 2011.

[117] Rizzi E., Colasante G., Frigerio A., Cocchetti G., *"On the mixed collapse mechanism of semi-circular masonry arches"*, Proc. of 8th Int. Conference on Structural Analysis of Historical Constructions, SAHC 2012, October 15-17, 2012, Wroclaw, Poland, 10 pages, submitted, 2012.

[118] Roca P., Cervera M., Gariup G., Pelá L., *"Structural analysis of masonry historical constructions. Classical and advanced approaches"*, Archives of Computational Methods in Engineering, 17(3), 299–325, 2010.

[119] Roeder-Carbo G.M., Ayala A.G., *"An evaluation of methods for the determination of the structural stability of historic masonry arches"*, in Historical Constructions 2001 – Possibilities of Numerical and Experimental Techniques, Proc. of the 3rd Int. Seminar, Edited by Lourenço P.B. and Roca P., Guimarães, Portugal, University of Minho, 7-8-9 November 2001, Art. 049, p. 557–566, 2001.

[120] Romano A., "Modelling, Analysis and Testing of Masonry Structures", Doctoral Thesis, Tutors: De Luca A., Mele E, Ochsendorf J., Dottorato di Ricerca in Ingegneria delle Costruzioni, XVIII Ciclo, Università degli Studi di Napoli Federico II, Facoltà di Ingegneria, November 2005.

[121] Romano A., Ochsendorf J., *"Circular, pointed and basket-handle arches: a comparison of structural behavior of masonry spans"*, Proc. of 5th Int. Conference on Structural Analysis of Historical Constructions - Possibilities of Numerical and Experimental Techniques, SAHC06, New Delhi, India, 6-8 November 2006, Lourenço P.B., Roca P., Modena C., Agrawal S. (Eds.), MACMILLAN Advanced Research Series, p. 1205–1212, 2006.

[122] Romano A., Ochsendorf J., *"The mechanics of Gothic masonry arches"*, Int. J. of Architectural Heritage, 4(1), 59–82, 2009.

[123] Rusconi F., "Analisi numerica per elementi discreti dei meccanismi di collasso degli archi in muratura", Laurea Thesis in Building Engineering, Advisor E. Rizzi, Università di Bergamo, Facoltà di Ingegneria, Italy, 126 pages, February 2008.

[124] Sakarovitch J., *"Stereotomy, a multifaceted technique"*, Proc. of the 1st Int. Congress on Construction History, Madrid, 20-24 January 2003, S. Huerta (Ed.), Madrid: Instituto Juan de Herrera, Volume I, paper CIHC1_008, p. 69–79, 2003.

[125] Sinopoli A., Corradi M., Foce F., *"Modern formulation for preelastic theories on masonry arches"*, J. of Engineering Mechanics, ASCE, 123(3), 204–213, 1997.

[126] Sinopoli A., *"The role of geometry in the theories on vaulted structures by Lorenzo Mascheroni (1785)"*, Proc. of the 1st Int. Congress on Construction History, Madrid, 20-24 January 2003, S. Huerta (Ed.), Madrid: Instituto Juan de Herrera, Volume I, paper CIHC1_175, p. 1865–1873, 2003.

[127] Sinopoli A., Aita D., Foce F., *"Further remarks on the collapse mode of masonry arches with Coulomb friction"*, Proc. of 5th Int. Conference on Arch Bridges, ARCH'07, Funchal, Madeira, Portugal, September 12-14, 2007, Lourenço P.B., Oliveira D.B., Portela A. (Eds.), Multicomp, Lda Publishers, Madeira, p. 649–657, 2007.

[128] Smars P., "Etudes sur la Stabilité des Arcs et Voûtes, Confrontation des Méthodes de l'Analyse Limite aux Voûtes Gothiques en Brabant", Thése de Docteur en Sciences Appliquées, Promoteurs: Di Pasquale S., De Roeck G., K.U. Leuven, Mars 2000.

[129] Smars P., *"Influence of friction and tensile resistance on the stability of masonry arches"*, Proc. of the 6th Int. Conference on Structural Analysis of Historic Construction, D'Ayala D. and Fodde E. (Eds.), 2-4 July 2008, Bath (UK), Taylor & Francis Group, London, p. 1199–1206, 2008.

[130] Smars P., *"Kinematic stability of masonry arches"*, Proc. of 7th Int. Conf. SAHC 2010, Shanghai, China, Oct. 6-8, 2010, Advanced Materials Research, Trans Tech Publications, Vols. 133-134, p. 429–434, 2010.

[131] Smith F.W., Harvey W.J., Vardy A.E., *"Three-hinge analysis of masonry arches"*, The Structural Engineer, 68(11), 203–213, 1990.

[132] Solla M., Caamaño J.C., Riveiro B., Arias P., *"A novel methodology for the structural assessment of stone arches based on geometric data by integration of photogrammetry and ground-penetrating radar"*, Engineering Structures, 35, 296–306, 2012.

[133] Solla M., Lorenzo H.. Rial F.I., Novo A., *"Ground-penetrating radar for the structural evaluation of masonry bridges: Results and interpretational tools"*, Construction and Building Materials, 29, 458–465, 2012.

[134] Thavalingam A., Bičanič N., Robinson J.I., Ponniah D.A., *"Computational framework for discontinuous modelling of masonry arch bridges"*, Computers and Structures, 79(19), 1821−1830, 2001.

[135] Toker S., Ünay A.İ., *"Mathematical modeling and finite element analysis of masonry arch bridges"*, G.U. Journal of Science, 17(2), 129−139, 2004.

[136] Tóth A.R., Orbán Z., Bagi K., *"Discrete element analysis of a stone masonry arch"*, Mechanics Research Communications, 36(4), 469−480, 2009.

[137] Tsutsui M., Mizuta Y., Sakata T., *"Line of thrust and theoretical load of masonry arch bridge"*, Proc. of 6th Int. Conference on Arch Bridges, ARCH'10, Fuzhou, China, October 11-13, 2010, Baochun Chen, Jiangang Wei (Eds.), College of Civil Engineering, Fuzhou University, Paper 43, p. 332–337, 2010.

[138] Vares R.J., "Avaliação de Segurança de Pontes Existentes de Alvenaria de Pedra com Recurso a Métodos Simplificados", Dissertação de Mestre em Engenharia Civil, Orientador: Arêde A., Faculdade de Engenharia, Universidade do Porto, Junho de 2009.

[139] Varma M., Jangid R.S., Ghosh S., *"Thrust line using linear elastic finite element analysis for masonry structures"*, Proc. of 7th Int. Conf. SAHC 2010, Shanghai, China, Oct. 6-8, 2010, Advanced Materials Research, Trans Tech Publications, Vols. 133-134, p. 503–508, 2010.

[140] Vermeltfoort A.T., *"Analysis and experiments of masonry arches"*, in Historical Constructions 2001 – Possibilities of Numerical and Experimental Techniques, Proc. of the 3rd Int. Seminar, Edited by Lourenço P.B. and Roca P., Guimarães, Portugal, University of Minho, 7-8-9 November 2001, Art. 042, p. 489–498, 2001.

[141] Viola E., Panzacchi L., Tornabene F., *"General analysis and application to redundant arches under static loading"*, Construction and Building Materials, 21(5), 1129–1143, 2007.

[142] Yamao T., Yamamoto K., Kudo T., Ogami K., Nakamura H., *"Development of static analytical method for mechanical behavior of stone arch bridges"*, Proc. of 6th Int. Conference on Arch Bridges, ARCH'10, Fuzhou, China, October 11-13, 2010, Baochun Chen, Jiangang Wei (Eds.), College of Civil Engineering, Fuzhou University, Paper 48, p. 370–378, 2010.

Tables – Part I

HEYMAN SOLUTION	
$\alpha = \pi/2 = 90°$ ($A = \pi/2 = 1.57080$)	**$\alpha = 7\pi/9 = 140°$ ($A = 0.889347$)**
β_H = 1.02677 rad = 58.8293° = 58°49'45.61"	β_H = 1.49586 rad = 85.7066° = 85°42'23.60"
η_H = 0.105965, $\eta_H/2$ = 0.0529826 K_H = 1.11189	η_H = 0.573854, $\eta_H/2$ = 0.286927 K_H = 1.80476
h_H = 0.621113 $\hat{h}_H = \eta_H h_H$ = 0.0658164	h_H = 0.112302 $\hat{h}_H = \eta_H h_H$ = 0.0644451

Table 1: Numerical results of classical Heyman solution for two characteristic values of arch opening.

Arch opening			HEYMAN SOLUTION				
α		A	β		η	h	$\hat{h} = \eta h$
[deg]	[rad]	[1]	[rad]	[deg]	[1]	[1]	[1]
10	0.174533	1.99492	0.123265	7.06257	0.0000192730	0.994930	0.0000191753
20	0.349066	1.97965	0.245652	14.0748	0.000305615	0.979804	0.000299443
30	0.523599	1.95410	0.366342	20.9898	0.00152490	0.954859	0.00145606
40	0.698132	1.91810	0.484625	27.7670	0.00472692	0.920459	0.00435093
50	0.872665	1.87144	0.599945	34.3743	0.0112735	0.877041	0.00988736
60	1.04720	1.81380	0.711924	40.7902	0.0227694	0.825056	0.0187860
70	1.22173	1.74481	0.820369	47.0037	0.0410159	0.764908	0.0313734
80	1.39626	1.66400	0.925268	53.0139	0.0680052	0.696886	0.0473919
90	1.57080	1.57080	1.02677	58.8293	0.105965	0.621113	0.0658164
100	1.74533	1.46451	1.12514	64.4657	0.157463	0.537491	0.0846350
110	1.91986	1.34430	1.22077	69.9447	0.225573	0.445657	0.100528
120	2.09440	1.20920	1.31409	75.2920	0.314124	0.344942	0.108354
130	2.26893	1.05802	1.40562	80.5361	0.428043	0.234310	0.100295
140	2.44346	0.889347	1.49586	85.7066	0.573854	0.112302	0.0644451
150	2.61799	0.701489	–	–	–	–	–

Table 2: Classical Heyman solution at variable angle of embrace.

Hinge position		**HEYMAN SOLUTION**					
β		α		A	η	h	$\hat{h} = \eta\, h$
[deg]	[rad]	[rad]	[deg]	[1]	[1]	[1]	[1]
0	0	0	0	2	0	1	0
5	0.0872665	0.123488	7.07530	1.99746	0.00000483720	0.997460	0.00000482492
10	0.174533	0.247422	14.1763	1.98979	0.0000776025	0.989825	0.0000768129
15	0.261799	0.372251	21.3284	1.97685	0.000394626	0.977049	0.000385569
20	0.349066	0.498423	28.5575	1.95842	0.00125512	0.959051	0.00120372
25	0.436332	0.626385	35.8892	1.93418	0.00308950	0.935718	0.00289090
30	0.523599	0.756583	43.3490	1.90367	0.00647181	0.906900	0.00586928
35	0.610865	0.889451	50.9618	1.86637	0.0121369	0.872406	0.0105883
40	0.698132	1.02540	58.7513	1.82161	0.0210037	0.832001	0.0174751
45	0.785398	1.16482	66.7390	1.76858	0.0342060	0.785398	0.0268654
50	0.872665	1.30801	74.9436	1.70637	0.0531333	0.732253	0.0389070
55	0.959931	1.45523	83.3788	1.63393	0.0794843	0.672151	0.0534254
60	1.04720	1.60661	92.0522	1.55008	0.115338	0.604600	0.0697332
65	1.13446	1.76214	100.963	1.45355	0.163247	0.529009	0.0863594
70	1.22173	1.92165	110.102	1.34300	0.226368	0.444674	0.100660
75	1.30900	2.08477	119.448	1.21706	0.308629	0.350745	0.108250
80	1.39626	2.25096	128.970	1.07437	0.414966	0.246199	0.102164
85	1.48353	2.41950	138.627	0.913598	0.551653	0.129792	0.0716002
90	1.57080	2.58957	148.371	0.733471	0.726760	0	0

Table 3: Classical Heyman solution at variable inner hinge position.

Tables – Part II

CCR SOLUTION	
$\alpha = \pi/2 = 90°$ ($A = \pi/2 = 1.57080$)	**$\alpha = 7\pi/9 = 140°$ ($A = 0.889347$)**
β_{CCR} = 0.951141 rad = 54.4963° = 54°29'46.83"	β_{CCR} = 1.07392 rad = 61.5313° = 61°31'52.73"
η_{CCR} = 0.107426, $\eta_{CCR}/2$ = 0.0537132 K_{CCR} = 1.11352	η_{CCR} = 0.625256, $\eta_{CCR}/2$ = 0.312628 K_{CCR} = 1.90963
h_{CCR} = 0.621772 $\hat{h}_{CCR} = \eta_{CCR}\, h_{CCR}$ = 0.0667947	h_{CCR} = 0.127517 $\hat{h}_{CCR} = \eta_{CCR}\, h_{CCR}$ = 0.0797306

Table 4: Numerical results of present CCR solution for two characteristic values of arch opening.

Arch opening			CCR SOLUTION				
α		A	β		η	h	$\hat{h} = \eta\, h$
[deg]	[rad]	[1]	[rad]	[deg]	[1]	[1]	[1]
10	0.174533	1.99492	0.123148	7.05586	0.0000192731	0.994930	0.0000191754
20	0.349066	1.97965	0.244725	14.0217	0.000305632	0.979804	0.000299459
30	0.523599	1.95410	0.363259	20.8132	0.00152531	0.954859	0.00145646
40	0.698132	1.91810	0.477455	27.3561	0.00473069	0.920461	0.00435442
50	0.872665	1.87144	0.586234	33.5887	0.0112940	0.877051	0.00990537
60	1.04720	1.81380	0.688721	39.4608	0.0228482	0.825094	0.0188519
70	1.22173	1.74481	0.784190	44.9308	0.0412576	0.765024	0.0315630
80	1.39626	1.66400	0.871946	49.9588	0.0686352	0.697181	0.0478512
90	1.57080	1.57080	0.951141	54.4963	0.107426	0.621772	0.0667947
100	1.74533	1.46451	1.02045	58.4674	0.160584	0.538829	0.0865271
110	1.91986	1.34430	1.07744	61.7328	0.231885	0.448199	0.103931
120	2.09440	1.20920	1.11714	64.0072	0.326547	0.349556	0.114146
130	2.26893	1.05802	1.12784	64.6207	0.452593	0.242555	0.109779
140	2.44346	0.889347	1.07392	61.5313	0.625256	0.127517	0.0797306
150	2.61799	0.701489	0.696697	39.9178	0.901426	0.0121731	0.0109731

Table 5: Present CCR solution at variable angle of embrace.

Hinge position		CCR SOLUTION					
β		α		A	η	h	$\hat{h} = \eta\, h$
[deg]	[rad]	[rad]	[deg]	[1]	[1]	[1]	[1]
0	0	0	0	2	0	1	0
5	0.0872665	0.123547	7.07871	1.99746	0.00000484644	0.997458	0.00000483412
10	0.174533	0.247899	14.2035	1.98975	0.0000782011	0.989786	0.0000774024
15	0.261799	0.373886	21.4221	1.97665	0.000401588	0.976848	0.000392291
20	0.349066	0.502395	28.7851	1.95776	0.00129543	0.958402	0.00124154
25	0.436332	0.634402	36.3485	1.93247	0.00324957	0.934090	0.00303539
30	0.523599	0.771024	44.1764	1.89992	0.00697501	0.903400	0.00630122
35	0.610865	0.913600	52.3454	1.85891	0.0134908	0.865615	0.0116778
40	0.698132	1.06383	60.9529	1.80772	0.0242757	0.819714	0.0198991
45	0.785398	1.22403	70.1318	1.74383	0.0415551	0.764180	0.0317556
50	0.872665	1.39776	80.0860	1.66325	0.0689162	0.696565	0.0480046
55	0.959931	1.59154	91.1887	1.55886	0.112928	0.612308	0.0691470
60	1.04720	1.82196	104.391	1.41350	0.189389	1/2 = 0.500000	0.0946947
64.6918	1.12909	2.23031	127.788	1.09292	0.421414	0.266957	0.112499
60	1.04720	2.47719	141.932	0.854600	2/3 = 0.666667	0.104600	0.0697332
55	0.959931	2.54307	145.707	0.784601	0.759542	0.0598432	0.0454534
50	0.872665	2.57955	147.797	0.744619	0.821147	0.0356879	0.0293050
45	0.785398	2.60252	149.113	0.718975	0.866329	0.0212184	0.0183821
40	0.698132	2.61779	149.988	0.701722	0.900926	0.0122870	0.0110697
35	0.610865	2.62821	150.585	0.689859	0.927967	0.00679119	0.00630201
30	0.523599	2.63539	150.997	0.681639	0.949249	0.00349971	0.00332209
25	0.436332	2.64034	151.280	0.675954	0.965922	0.00162743	0.00157197
20	0.349066	2.64371	151.473	0.672069	0.978759	0.000648135	0.000634368
15	0.261799	2.64595	151.602	0.669480	0.988288	0.000200835	0.000198482
10	0.174533	2.64737	151.683	0.667848	0.994867	0.0000391021	0.0000389014
5	0.0872665	2.64814	151.727	0.666952	0.998727	0.00000242323	0.00000242014
0	0	2.64839	151.742	2/3	1	0	0

Table 6: Present CCR solution at variable inner hinge position.

Tables – Part III

MILANKOVITCH SOLUTION	
$\alpha = \pi/2 = 90°$ ($A = \pi/2 = 1.57080$)	**$\alpha = 7\pi/9 = 140°$ ($A = 0.889347$)**
$\beta_M = 0.950925$ rad = 54.4840° = 54°29'02.31"	$\beta_M = 1.02933$ rad = 58.9760° = 58°58'33.62"
$\eta_M = 0.107478$, $\eta_M/2 = 0.0537390$ $K_M = 1.11358$	$\eta_M = 0.634867$, $\eta_M/2 = 0.317434$ $K_M = 1.93012$
$h_M = 0.620881$ $\hat{h}_M = \eta_M h_M = 0.0667311$	$h_M = 0.104800$ $\hat{h}_M = \eta_M h_M = 0.0665344$

Table 7: Numerical results of Milankovitch solution for two characteristic values of arch opening.

Arch opening			MILANKOVITCH SOLUTION				
α		A	β		η	h	$\hat{h} = \eta h$
[deg]	[rad]	[1]	[rad]	[deg]	[1]	[1]	[1]
10	0.174533	1.99492	0.123148	7.05586	0.0000192731	0.994930	0.0000191754
20	0.349066	1.97965	0.244725	14.0217	0.000305632	0.979804	0.000299459
30	0.523599	1.95410	0.363259	20.8132	0.00152531	0.954859	0.00145646
40	0.698132	1.91810	0.477455	27.3561	0.0047307	0.920459	0.00435441
50	0.872665	1.87144	0.586233	33.5887	0.0112941	0.877040	0.00990534
60	1.04720	1.81380	0.688718	39.4606	0.0228489	0.825052	0.0188515
70	1.22173	1.74481	0.784173	44.9298	0.0412613	0.764887	0.0315602
80	1.39626	1.66400	0.871881	49.9551	0.0686505	0.696808	0.0478362
90	1.57080	1.57080	0.950925	54.4840	0.107478	0.620881	0.0667311
100	1.74533	1.46451	1.01981	58.4309	0.160736	0.536902	0.0862992
110	1.91986	1.34430	1.07569	61.6327	0.232295	0.444334	0.103217
120	2.09440	1.20920	1.11248	63.7402	0.327607	0.342263	0.112128
130	2.26893	1.05802	1.11491	63.8795	0.455450	0.229424	0.104491
140	2.44346	0.889347	1.02933	58.9760	0.634867	0.104800	0.0665344
150	2.61799	0.701489	–	–	–	–	–

Table 8: Milankovitch solution at variable angle of embrace.

Hinge position		MILANKOVITCH SOLUTION					
β		α		A	η	h	$\hat{h} = \eta\, h$
[deg]	[rad]	[rad]	[deg]	[1]	[1]	[1]	[1]
0	0	0	0	2	0	1	0
5	0.0872665	0.123547	7.07871	1.99746	0.00000484644	0.997458	0.00000483412
10	0.174533	0.247899	14.2035	1.98975	0.0000782011	0.989786	0.0000774024
15	0.261799	0.373886	21.4221	1.97665	0.000401588	0.976848	0.000392291
20	0.349066	0.502395	28.7851	1.95776	0.00129543	0.958402	0.00124154
25	0.436332	0.634402	36.3486	1.93247	0.00324957	0.934089	0.00303539
30	0.523599	0.771024	44.1764	1.89992	0.00697504	0.903396	0.00630122
35	0.610865	0.913602	52.3455	1.85891	0.0134910	0.865599	0.0116778
40	0.698132	1.06384	60.9533	1.80772	0.0242771	0.819664	0.0198991
45	0.785398	1.22406	70.1336	1.74381	0.0415631	0.764029	0.0317554
50	0.872665	1.39790	80.0939	1.66319	0.0689576	0.696132	0.0480036
55	0.959931	1.59213	91.2225	1.55852	0.113147	0.611054	0.0691389
60	1.04720	1.82502	104.566	1.41140	0.190859	0.495747	0.0946179
64.1635	1.11986	2.19640	125.845	1.12288	0.397561	0.277708	0.110406
60	1.04720	2.42490	138.937	0.908163	0.612095	0.118588	0.0725873
55	0.959931	2.49281	142.827	0.838263	0.702228	0.0677181	0.0475536
50	0.872665	2.52893	144.897	0.799866	0.760779	0.0404922	0.0308057
45	0.785398	2.55103	146.164	0.775951	0.803366	0.0241522	0.0194030
40	0.698132	2.56529	146.981	0.760348	0.835827	0.0140284	0.0117253
35	0.610865	2.57469	147.519	0.749997	0.861122	0.00777470	0.00669496
30	0.523599	2.58089	147.874	0.743123	0.880985	0.00401587	0.00353792
25	0.436332	2.58496	148.108	0.738603	0.896521	0.00187109	0.00167747
20	0.349066	2.58758	148.258	0.735687	0.908468	0.000746346	0.000678032
15	0.261799	2.58922	148.351	0.733865	0.917326	0.000231547	0.000212404
10	0.174533	2.59018	148.407	0.732786	0.923438	0.0000451204	0.0000416659
5	0.0872665	2.59069	148.435	0.732224	0.927022	0.00000279763	0.00000259346
0	0	2.59084	148.444	0.732051	0.928203	0	0

Table 9: Milankovitch solution at variable inner hinge position.

Parameters	HEYMAN	CCR	MILANKOVITCH
$\alpha_{s\hat{h}}$	2.11041 rad = 120.918°	2.14389 rad = 122.836°	2.11928 rad = 121.426°
$A_{s\hat{h}}$	1.19602	1.16802	1.18865
$\beta_{s\hat{h}}$	1.32256 rad = 75.7771°	1.12394 rad = 64.3969°	1.11549 rad = 63.9130°
$\eta_{s\hat{h}}$	0.323435	0.358644	0.343576
$h_{s\hat{h}}$	0.335221	0.320070	0.326862
$\hat{h}_{s\hat{h}}$	0.108422	0.114791	0.112302
$\alpha_{s\beta}$	–	2.23031 rad = 127.788°	2.19640 rad = 125.845°
$A_{s\beta}$	–	1.09292	1.12288
$\beta_{s\beta}$	–	1.12909 rad = 64.6918°	1.11986 rad = 64.1635°
$\eta_{s\beta}$	–	0.421414	0.397561
$h_{s\beta}$	–	0.266957	0.277708
$\hat{h}_{s\beta}$	–	0.112499	0.110406
α_l	2.58957 rad = 148.371°	2.64839 rad = 151.742°	2.59084 rad = 148.444°
A_l	$\pi/2/(\pi-1) = 0.733471$	$2/3 = 0.666667$	$\sqrt{3}-1 = 0.732051$
β_l	$\pi/2$ = 1.57080 rad = 90°	0	0
η_l	$2(1-2/\pi) = 0.726760$	1	$2(2\sqrt{3}-3) = 0.928203$
h_l	0	0	0
$\hat{h}_l$	0	0	0

Table 10: Characteristic stationary and limit parameters for the three solutions.

Figures – Part I

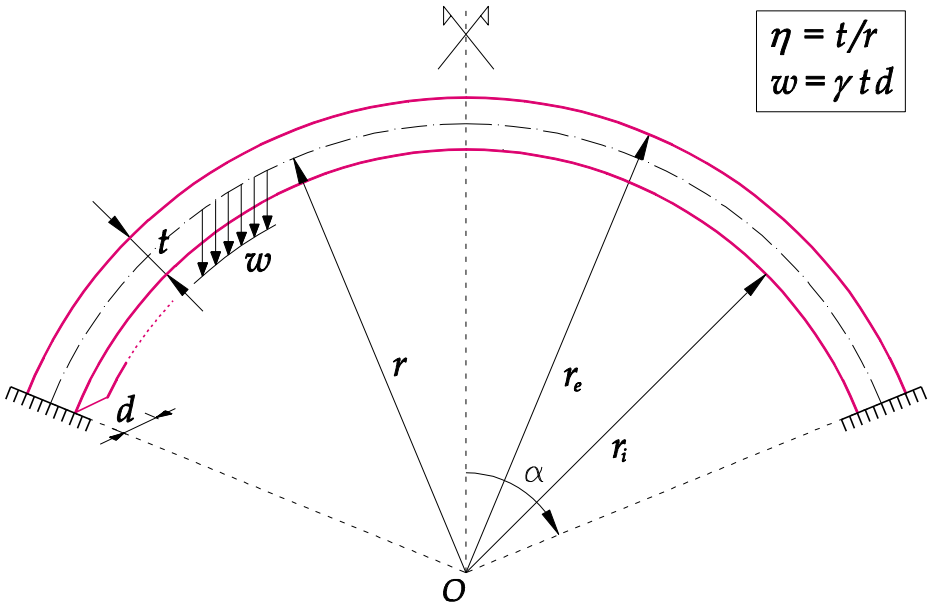

Figure 1: Sketch of a symmetric circular arch subjected only to its own weight (of specific weight γ) with all characteristic parameters involved (d: out-of-plane depth).

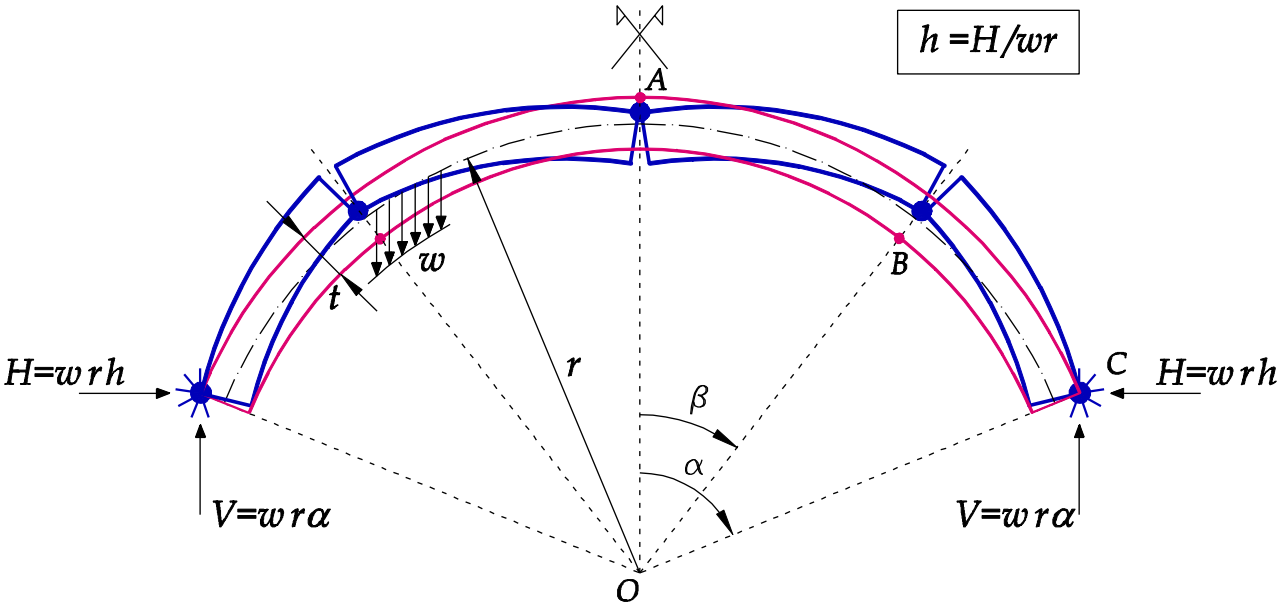

Figure 2: Five-hinge rotational collapse mechanism of a symmetric circular arch.

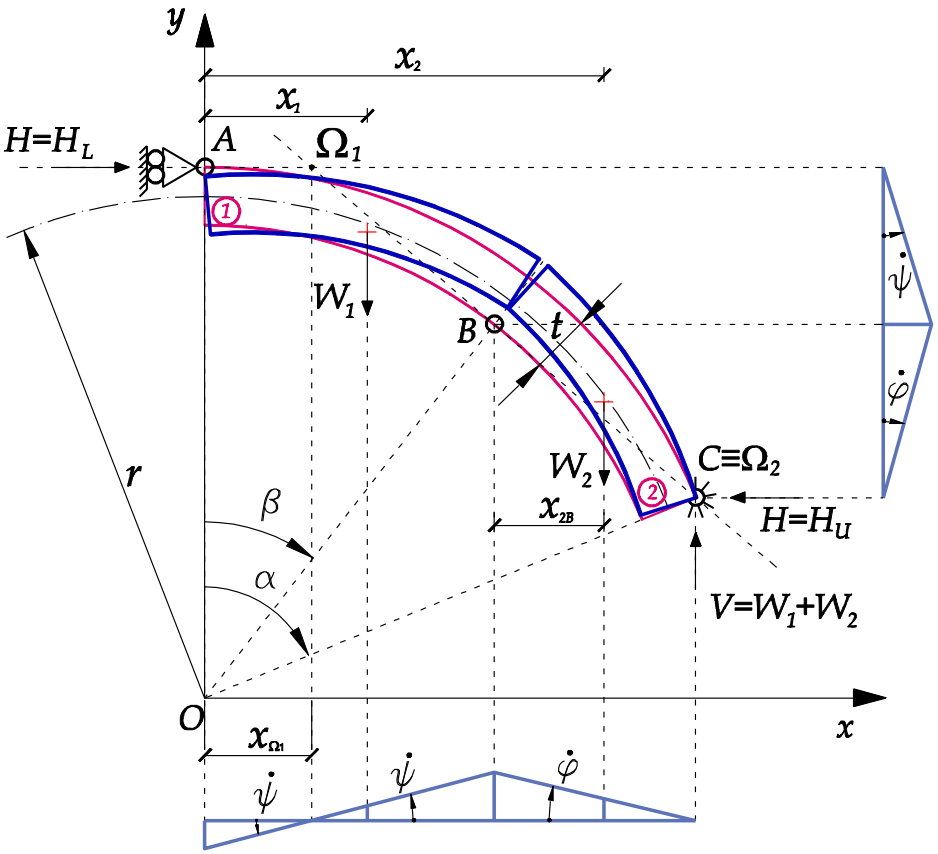

Figure 3: Statics and kinematics of a symmetric rotational collapse mechanism of a circular arch supporting only its own weight.

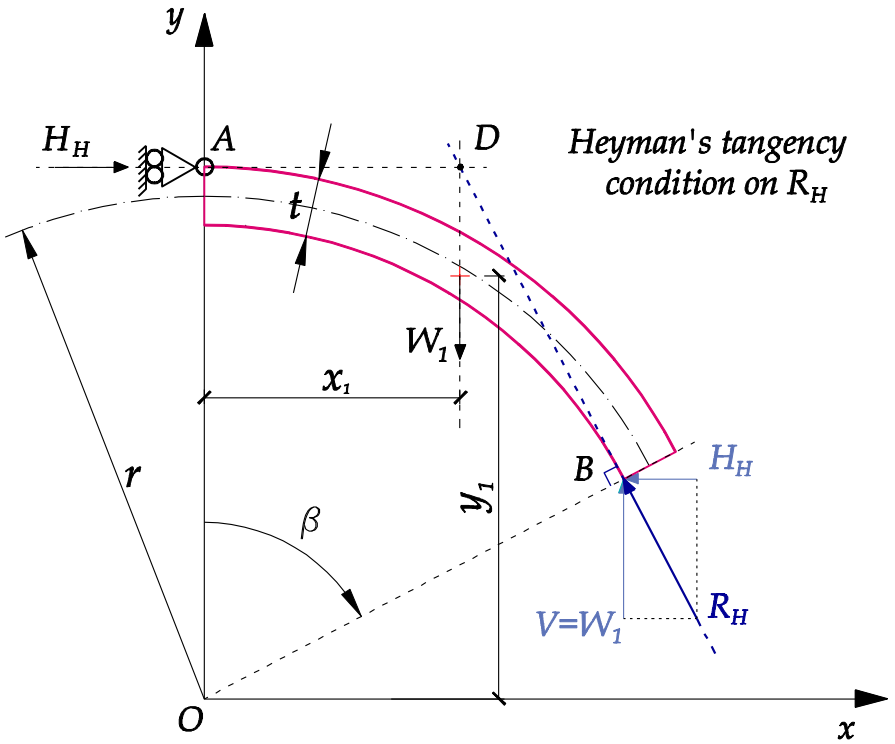

Figure 4: Equilibrium of the upper portion of the arch and Heyman's tangency condition of the resultant thrust at the haunches.

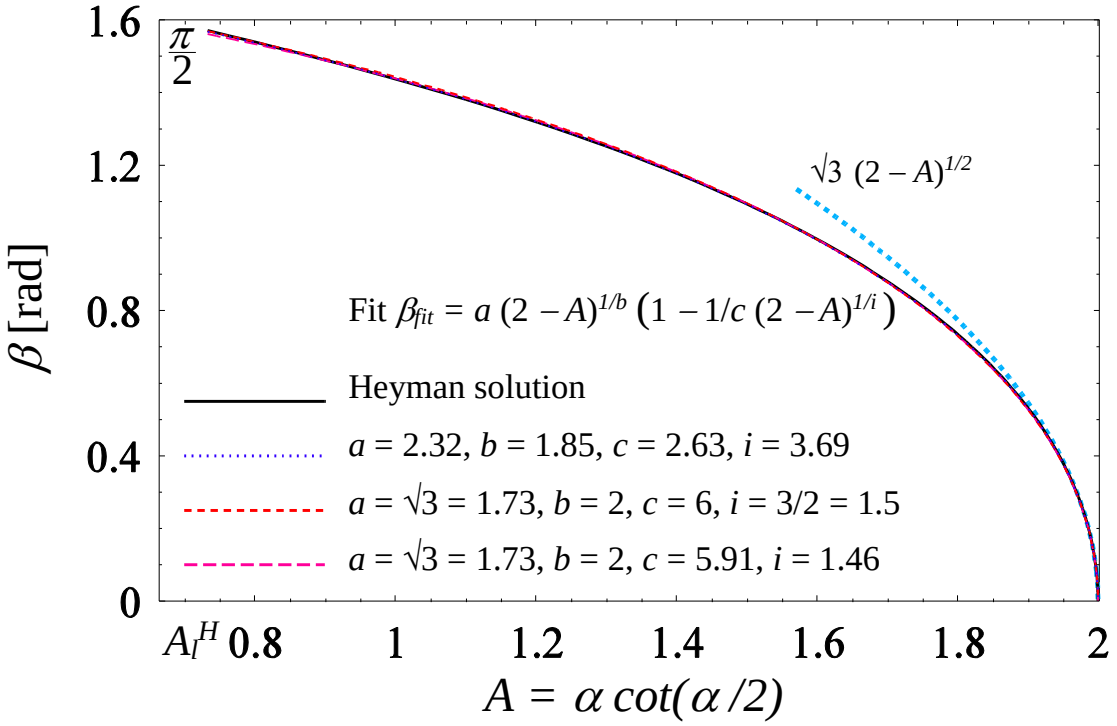

Figure 5: Heyman solution. Fit β_{fit} of β as a function of A.

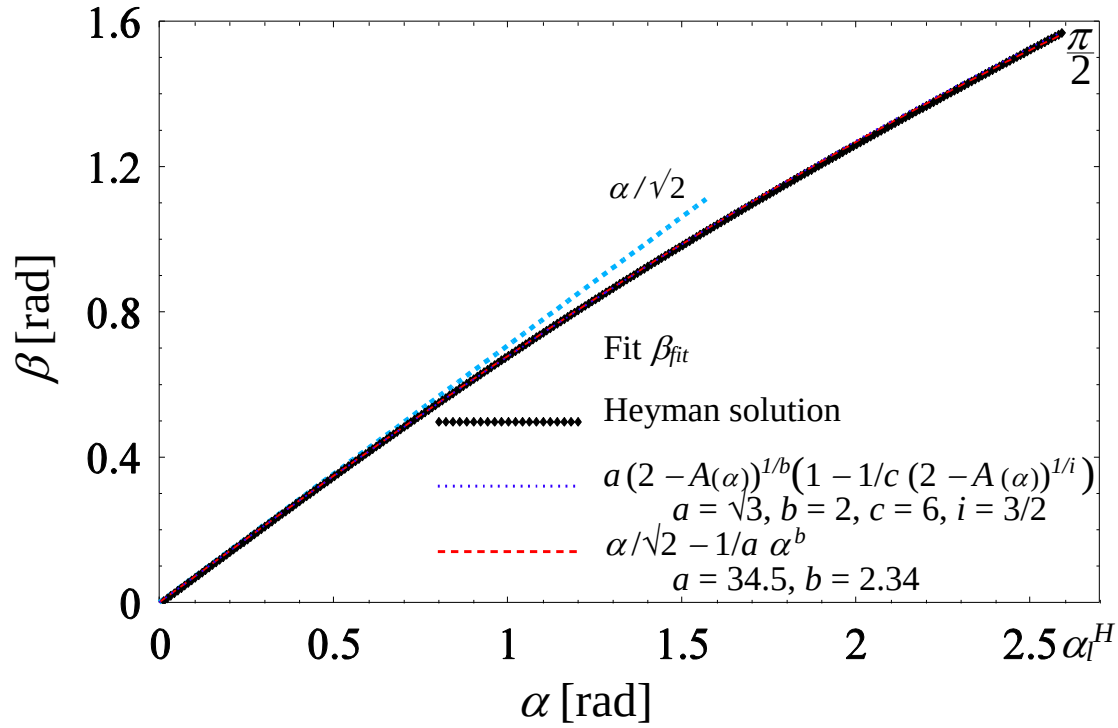

Figure 6: Heyman solution. Fit β_{fit} of β as a function of α.

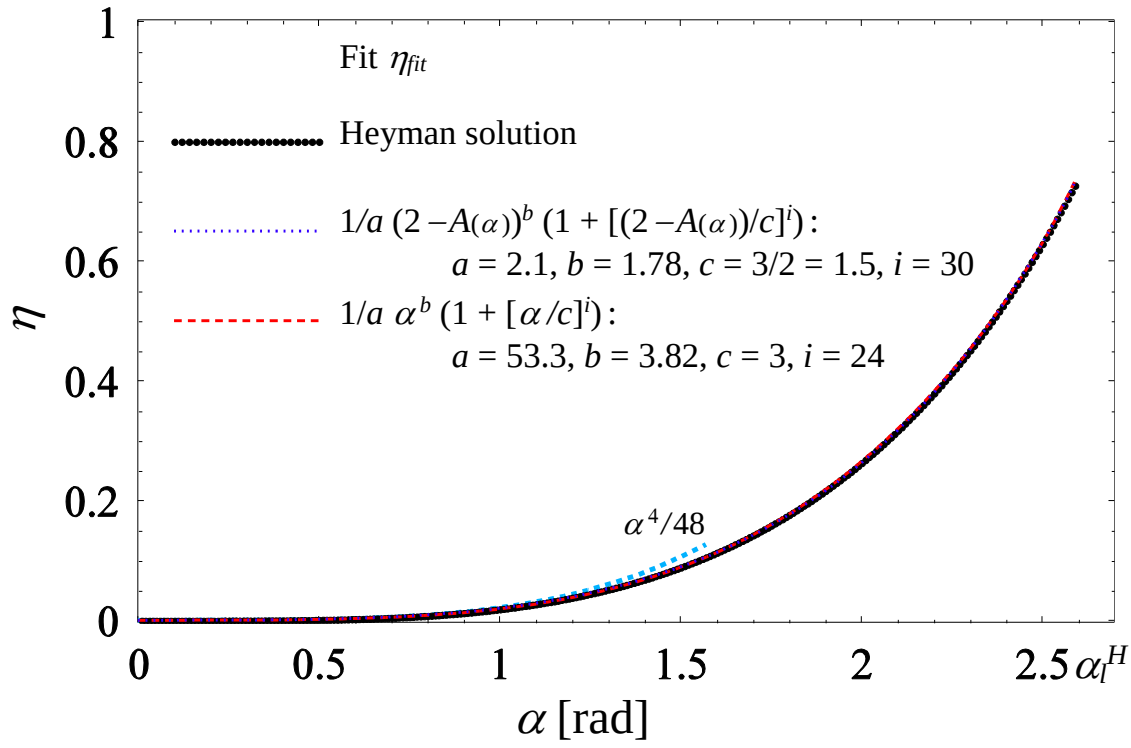

Figure 7: Heyman solution. Fit η_{fit} of η as a function of α.

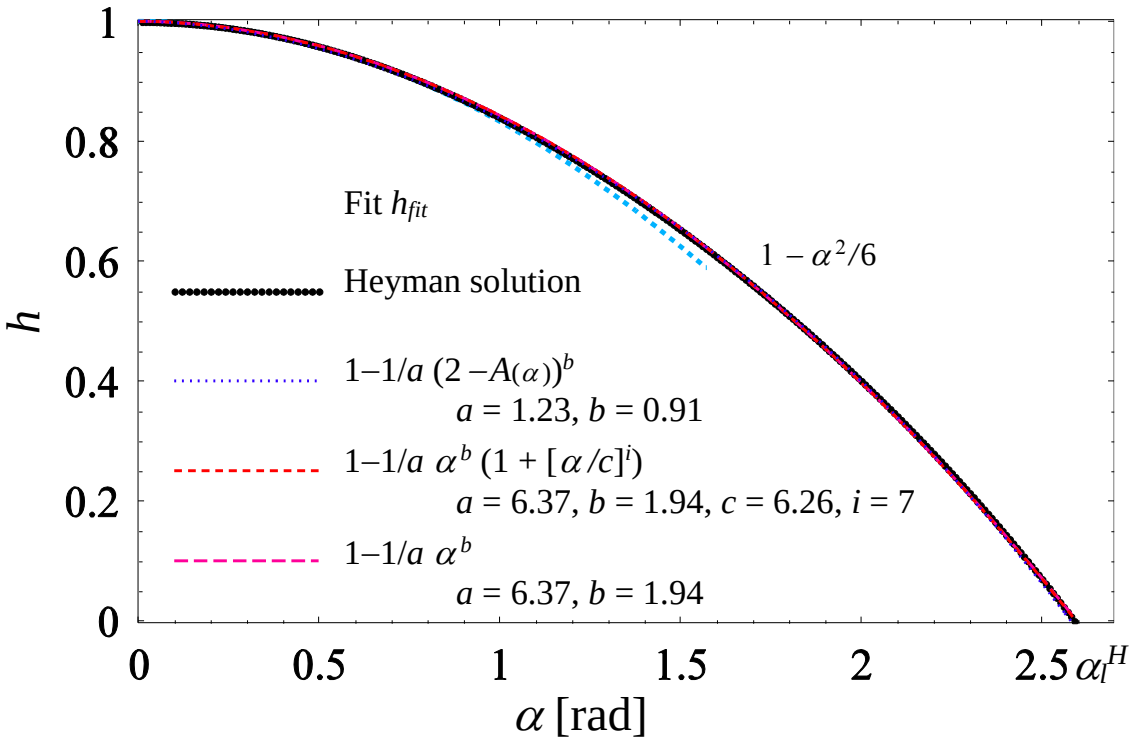

Figure 8: Heyman solution. Fit h_{fit} of h as a function of α.

Figures – Part II

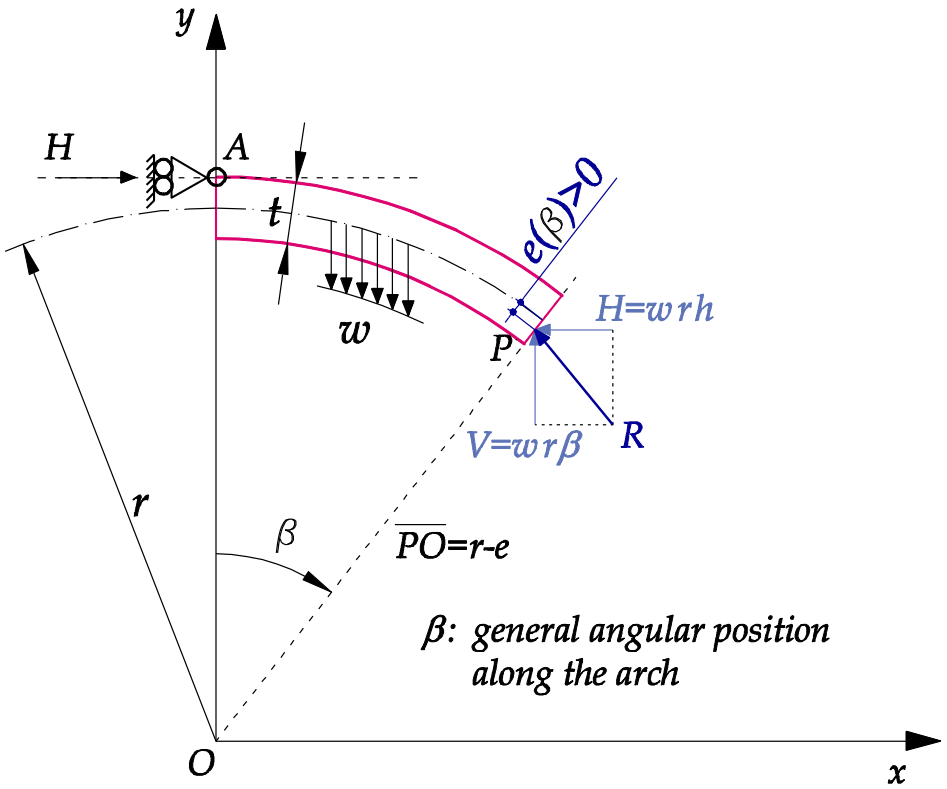

Figure 9: Eccentricity of the line of thrust with respect to the geometrical centerline of the arch.

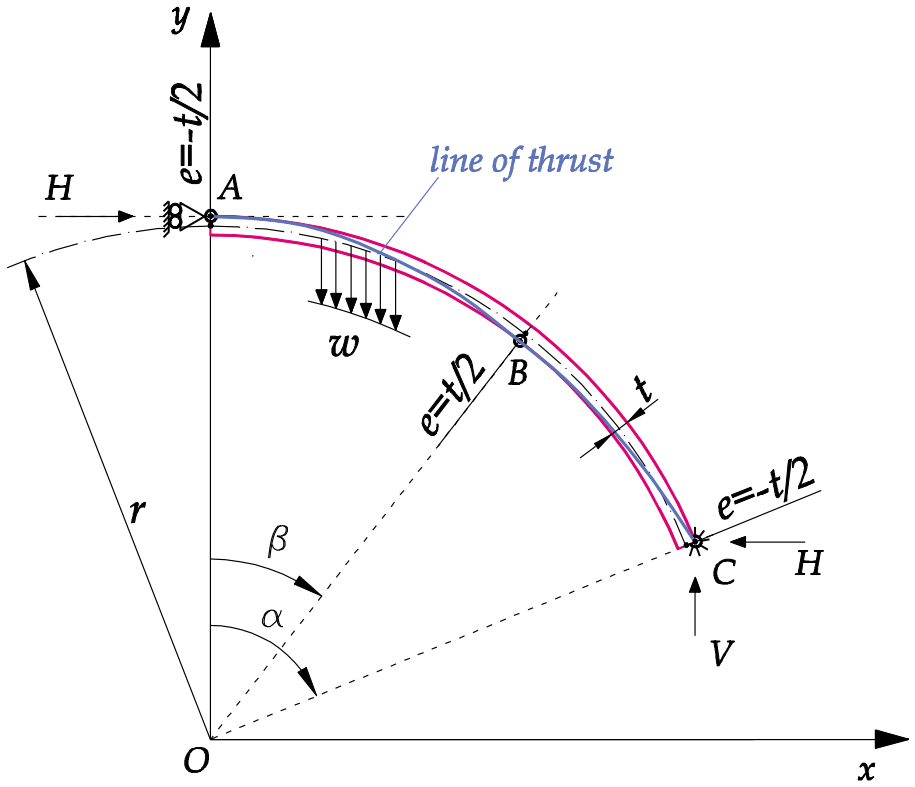

Figure 10: Qualitative representation of the line of thrust at the critical condition of minimum arch thickness.

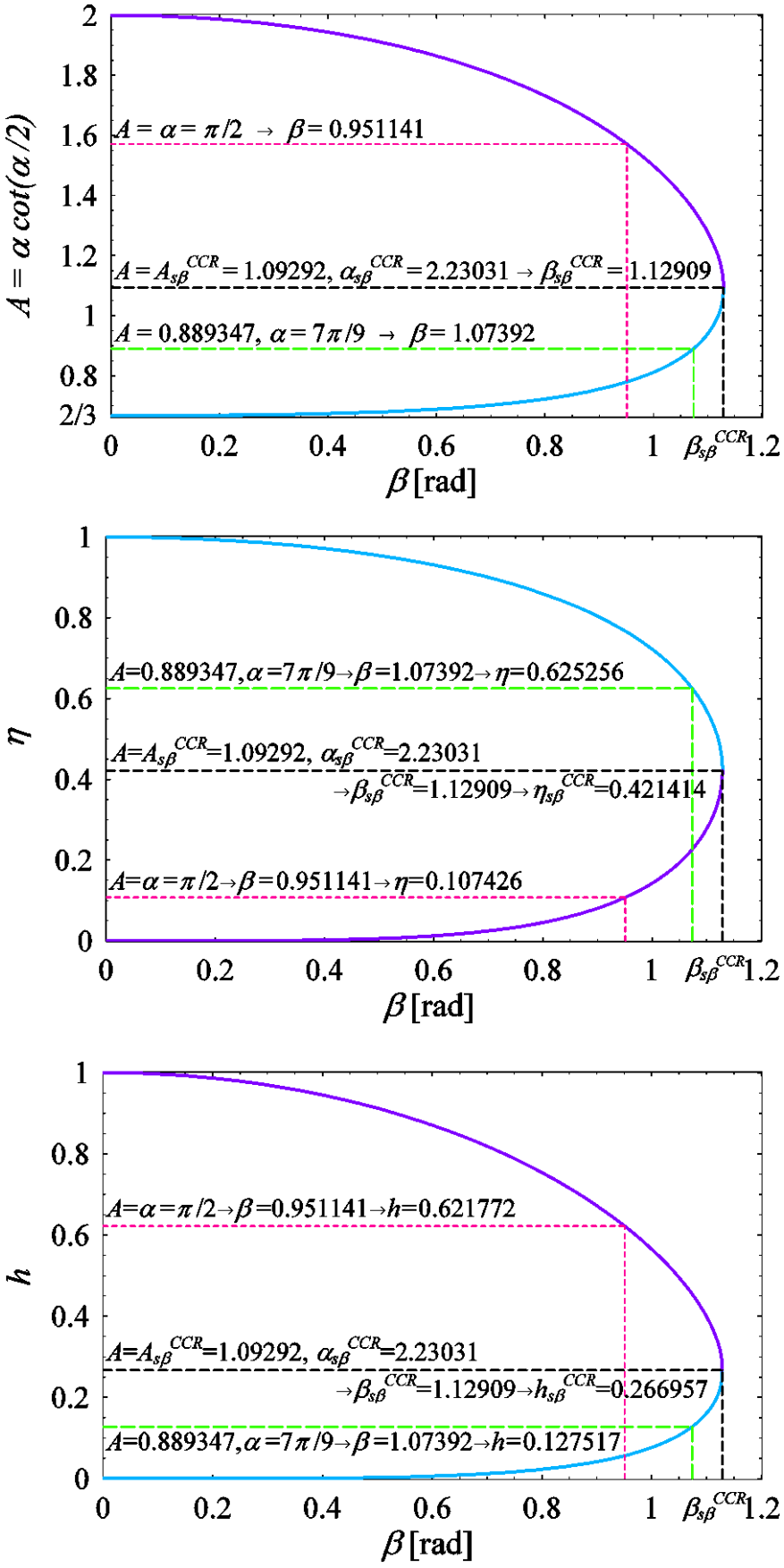

Figure 11: CCR solution. Functional dependence of A, η, h on β.

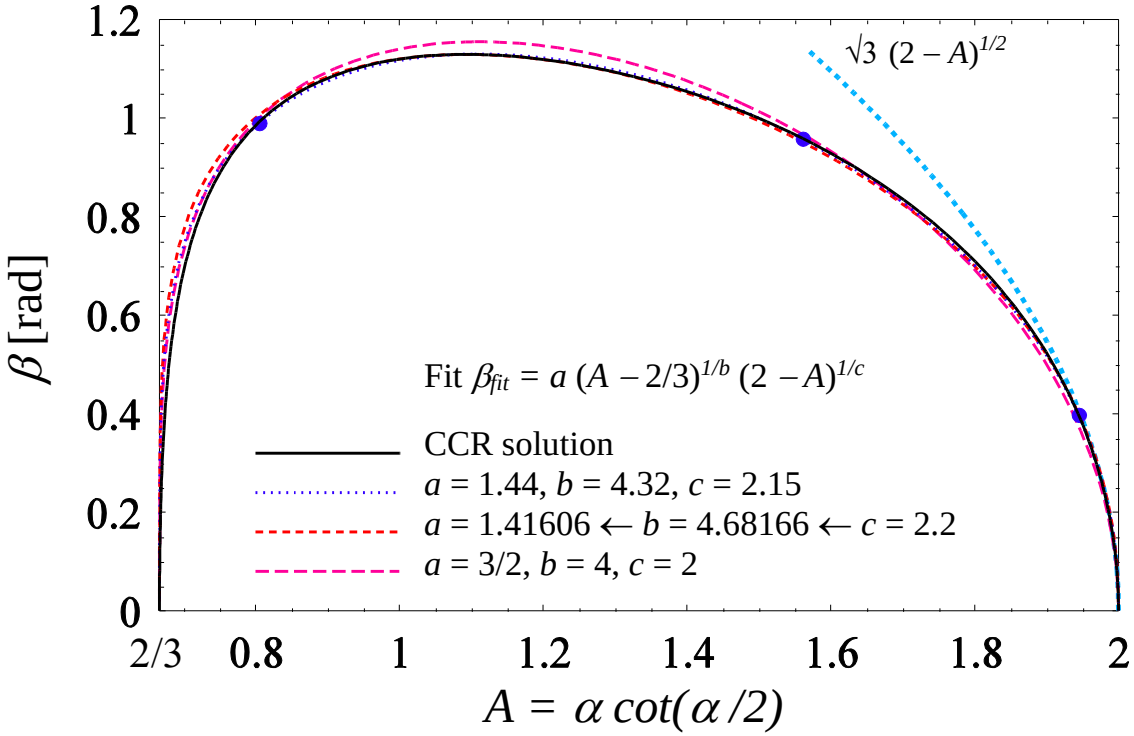

Figure 12: CCR solution. Fit $\beta_{fit} = a\,(A-2/3)^{1/b}\,(2-A)^{1/c}$ of β as a function of A.

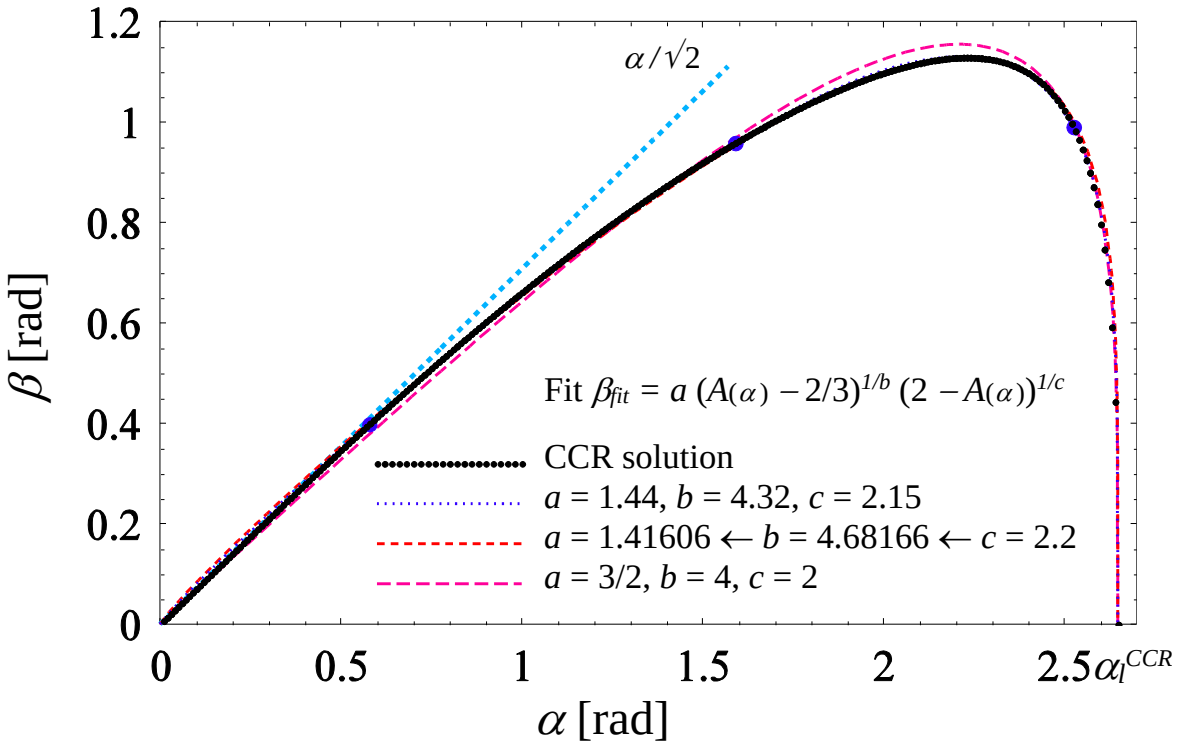

Figure 13: CCR solution. Fit $\beta_{fit} = a\,(A(\alpha)-2/3)^{1/b}\,(2-A(\alpha))^{1/c}$ of β as a function of α.

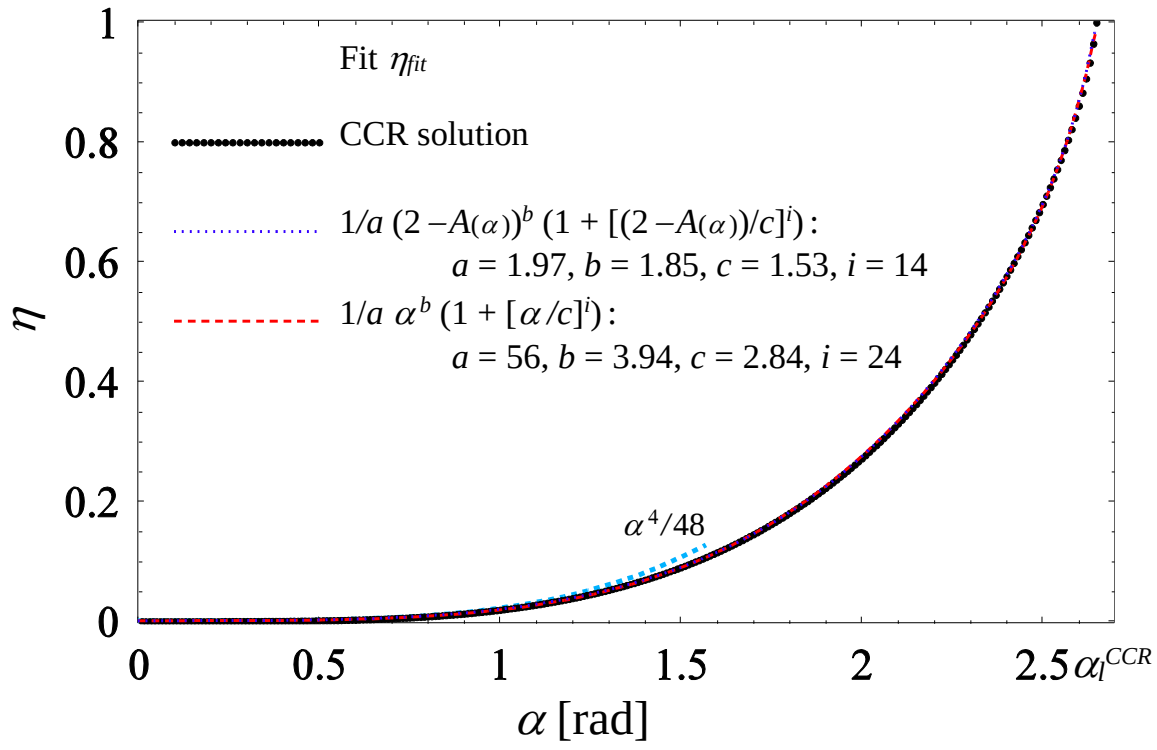

Figure 14: CCR solution. Fit η_{fit} of η as a function of α.

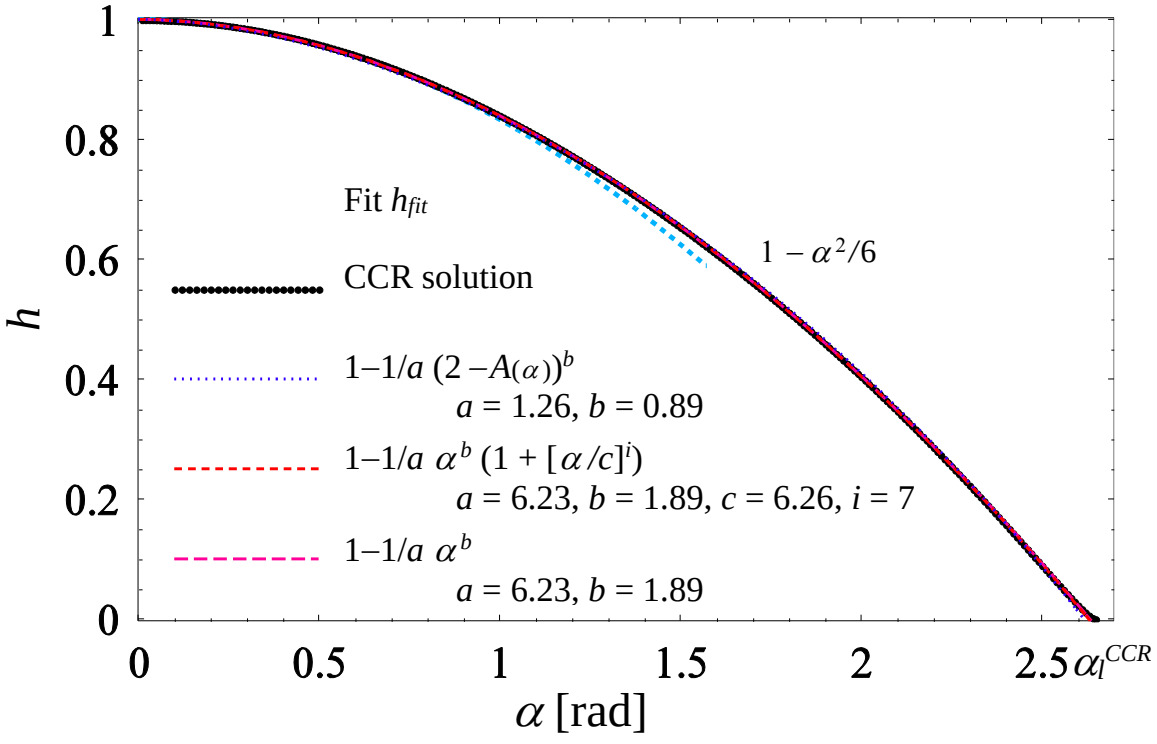

Figure 15: CCR solution. Fit h_{fit} of h as a function of α.

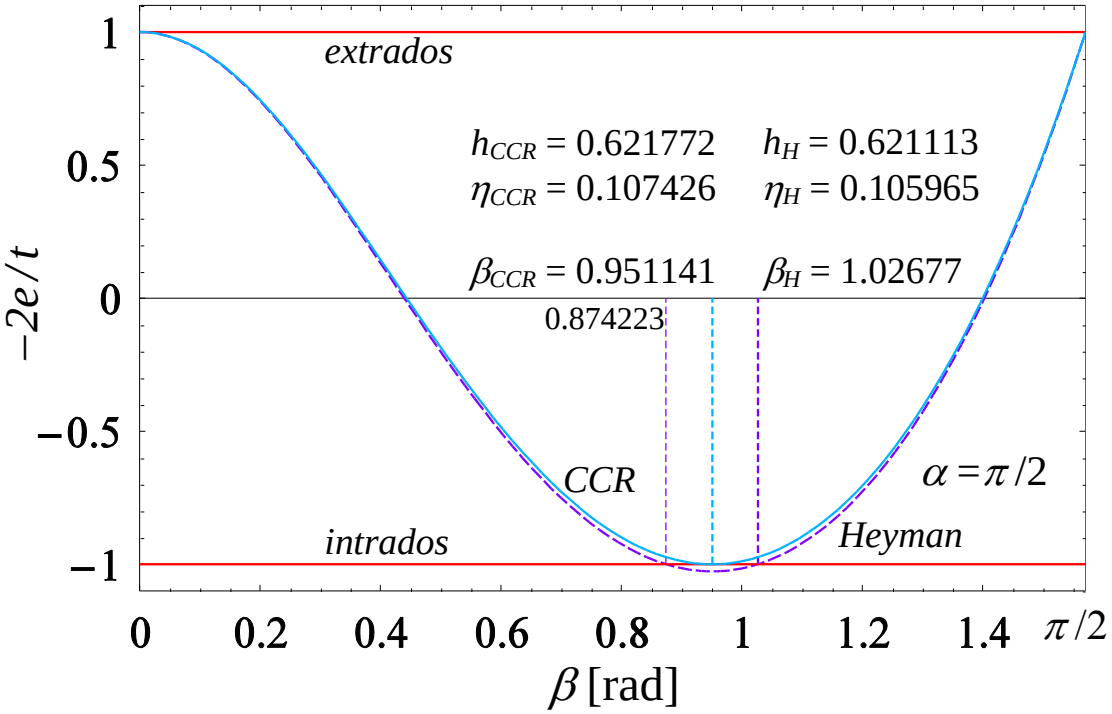

Figure 16: Plot of the eccentricity of the line of thrust for CCR (line tangent to the intrados) and Heyman solutions (line going out of the arch thickness), $\alpha = \pi/2$.

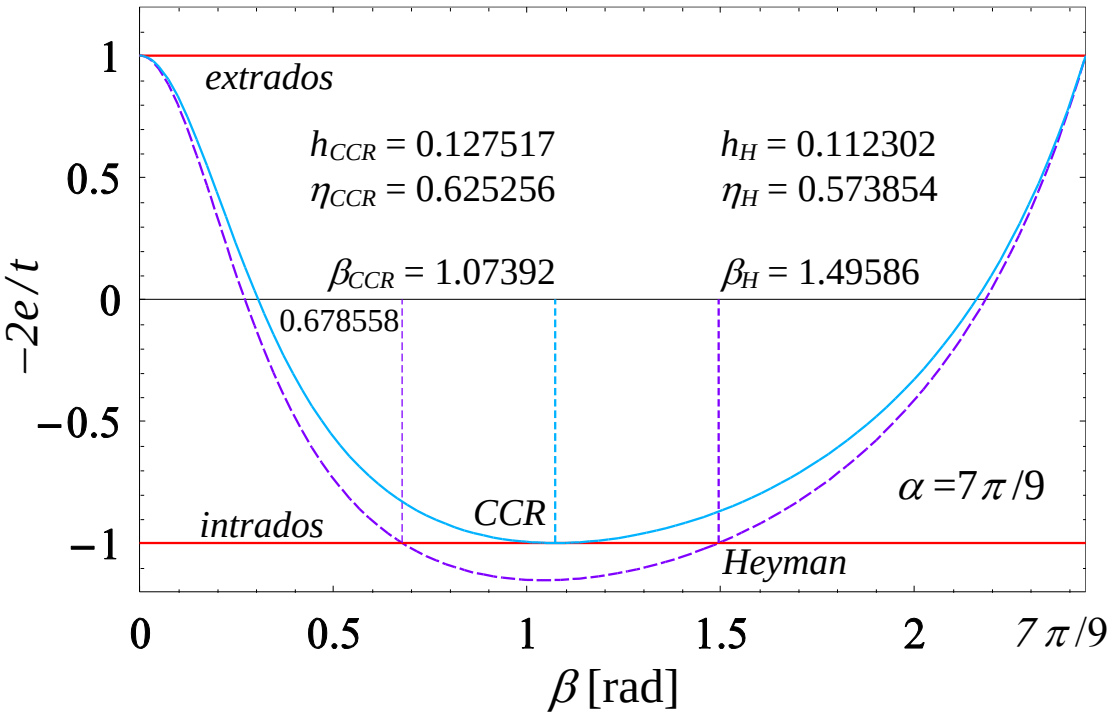

Figure 17: Plot of the eccentricity of the line of thrust for CCR (line tangent to the intrados) and Heyman solutions (line going out of the arch thickness), $\alpha = 7\pi/9$.

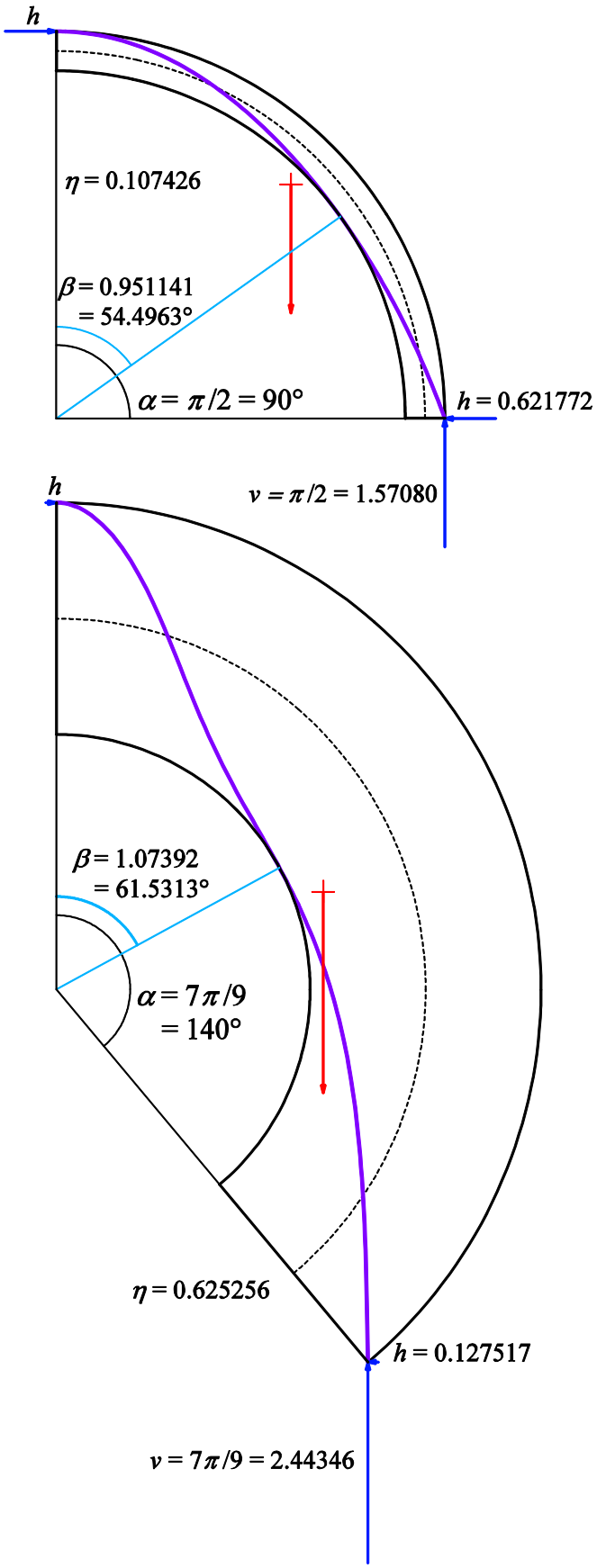

Figure 18: Analytical plots of the line of thrust for CCR solution, for $\alpha = \pi / 2 = 90°$ ($A = \pi / 2$) and $\alpha = 7\ \pi / 9 = 140°$ ($A = 0.889347$).

Figures – Part III

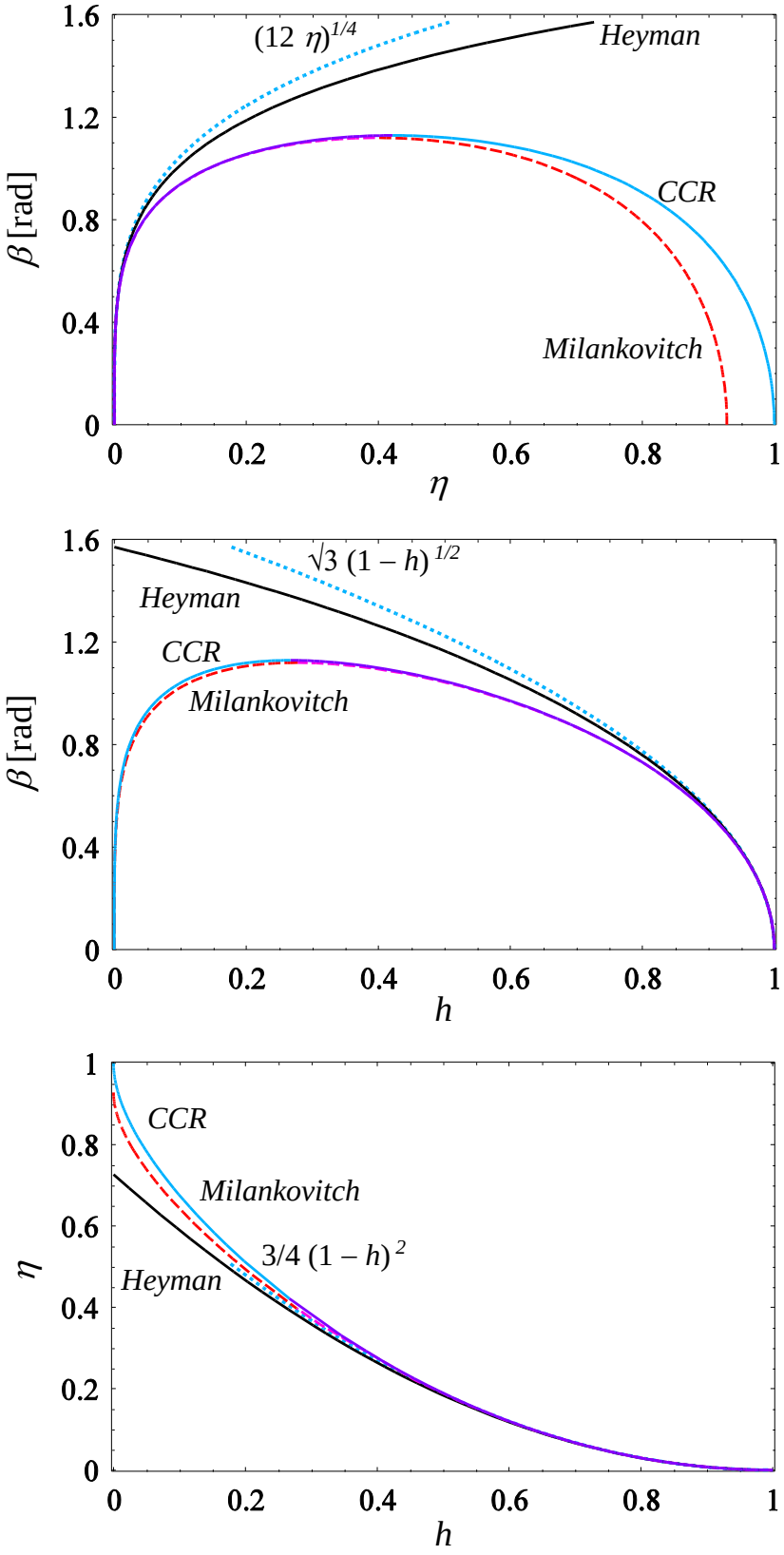

Figure 19: Comparison between Heyman, CCR and Milankovitch solutions in terms of the solution couples (β,η), (β,h), (η,h).

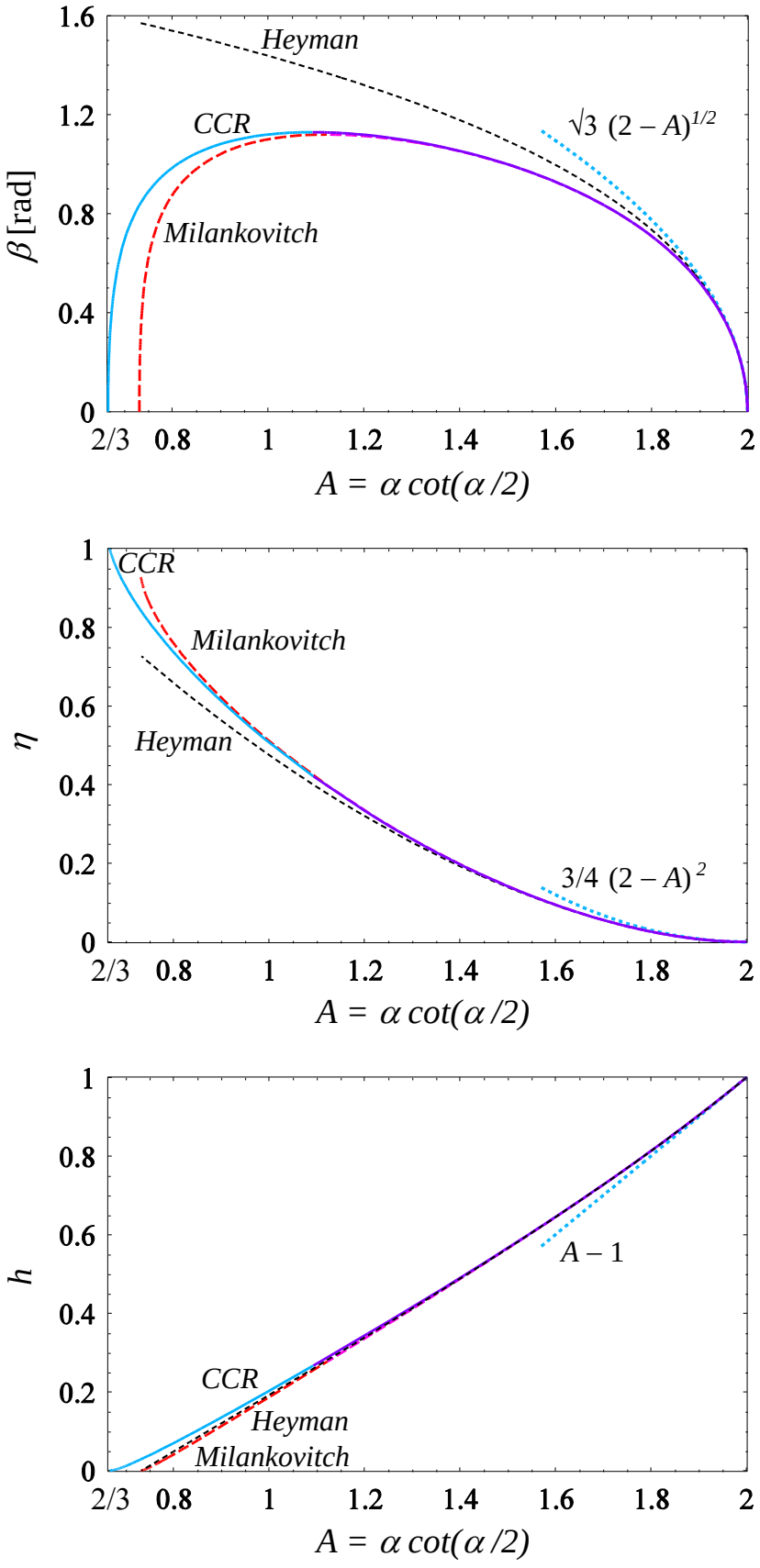

Figure 20: Comparison between Heyman, CCR and Milankovitch solutions in terms of A.

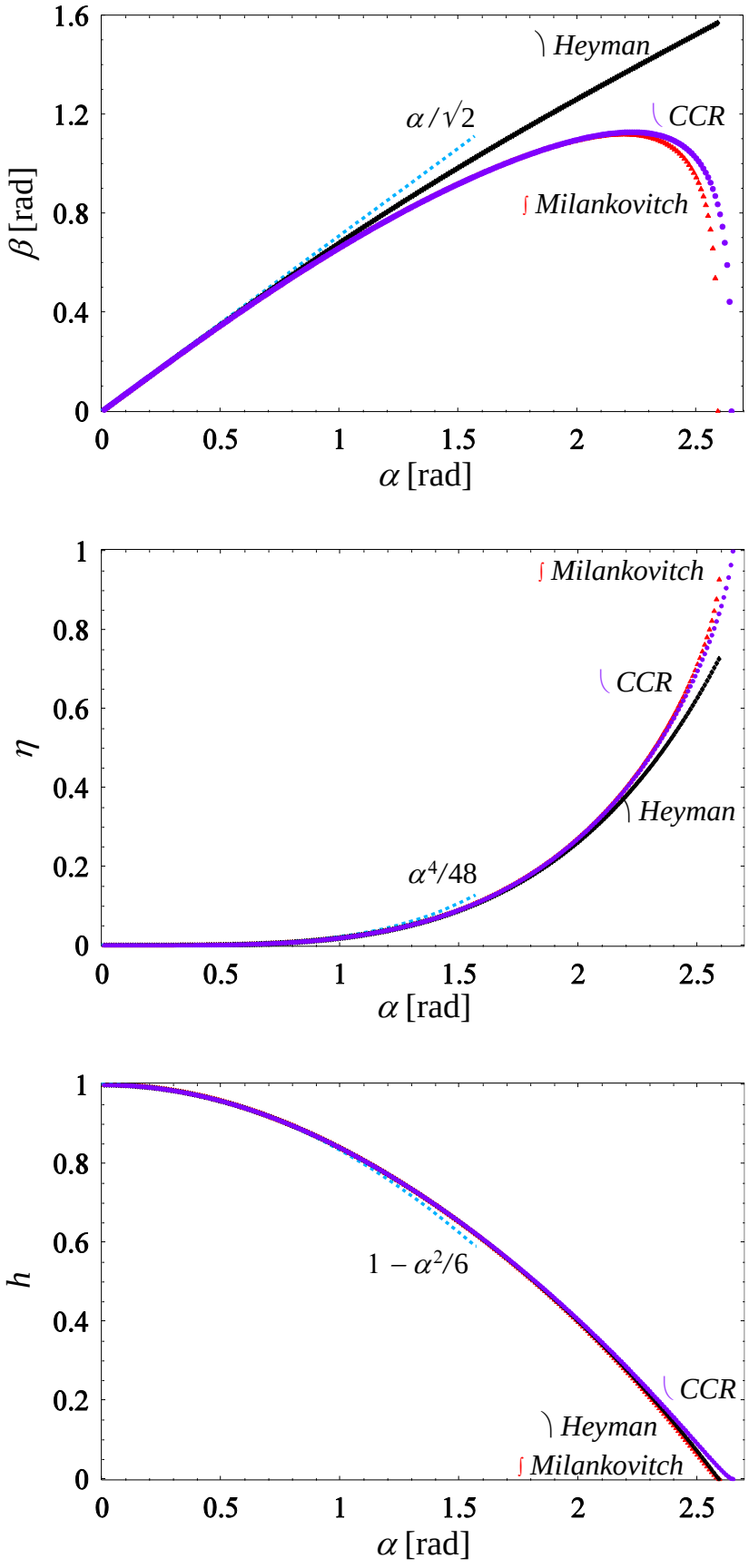

Figure 21: Comparison between Heyman, CCR and Milankovitch solutions in terms of α.

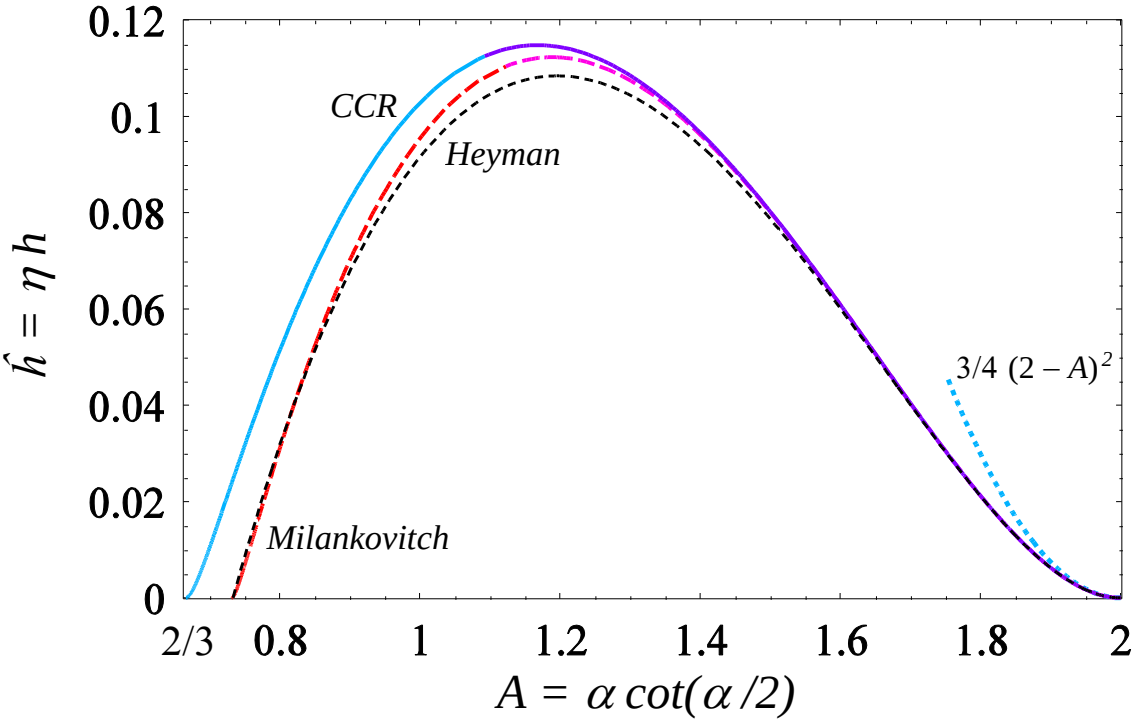

Figure 22: Comparison between Heyman, CCR and Milankovitch solutions for the horizontal non-dimensional thrust $\hat{h} = \eta\, h$ in terms of A.

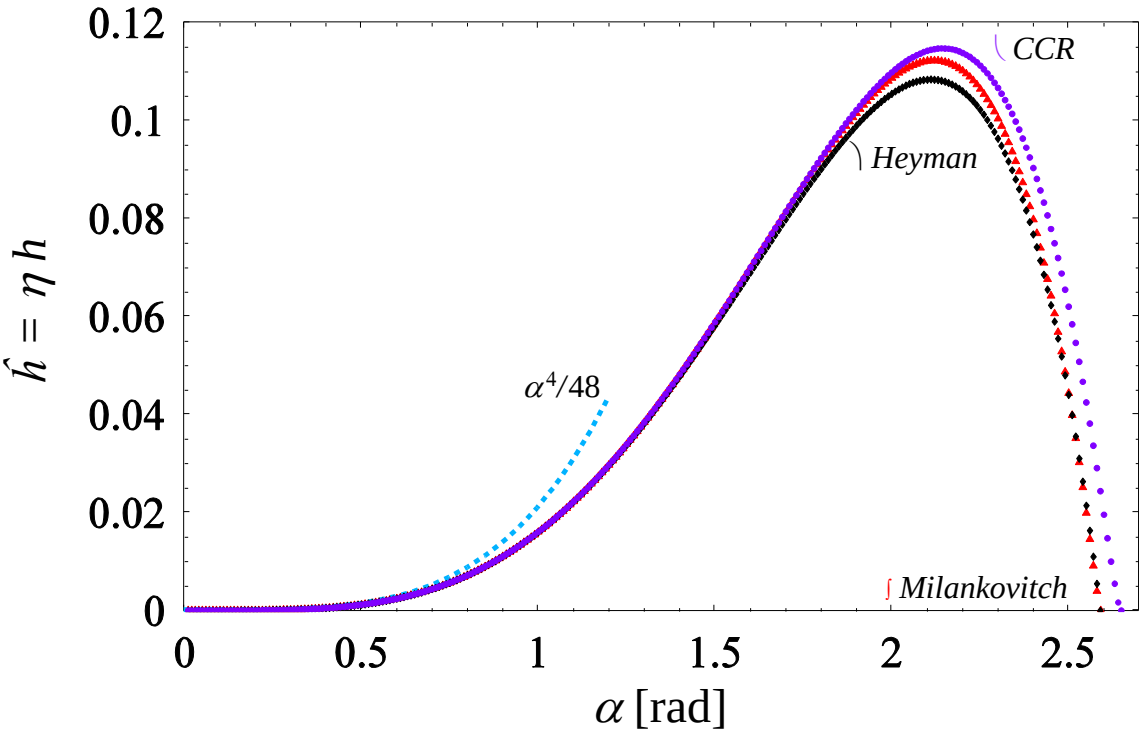

Figure 23: Comparison between Heyman, CCR and Milankovitch solutions for the horizontal non-dimensional thrust $\hat{h} = \eta\, h$ in terms of α.

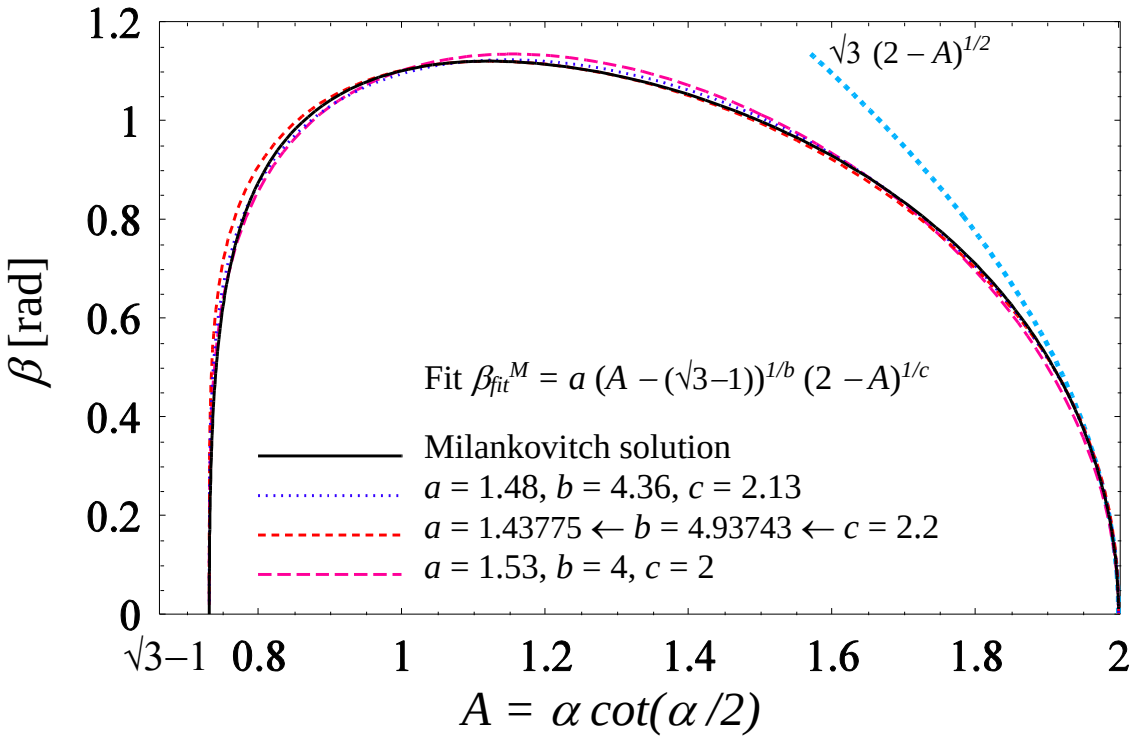

Figure 24: Milankovitch solution. Fit $\beta_{fit}^{M}=a(A-(\sqrt{3}-1))^{1/b}(2-A)^{1/c}$ of β as a function of A.

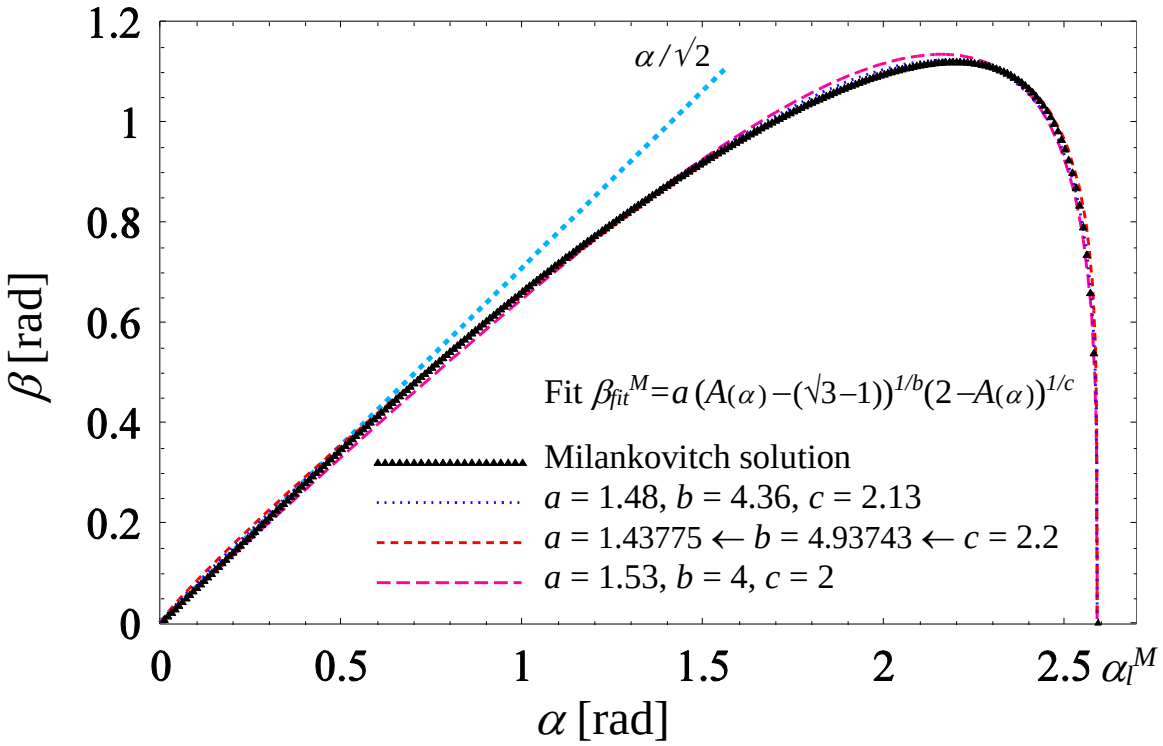

Figure 25: Milankovitch solution. Fit $\beta_{fit}^{M} = a\,(A(\alpha)-(\sqrt{3}-1))^{1/b}\,(2-A(\alpha))^{1/c}$ of β as a function of α.

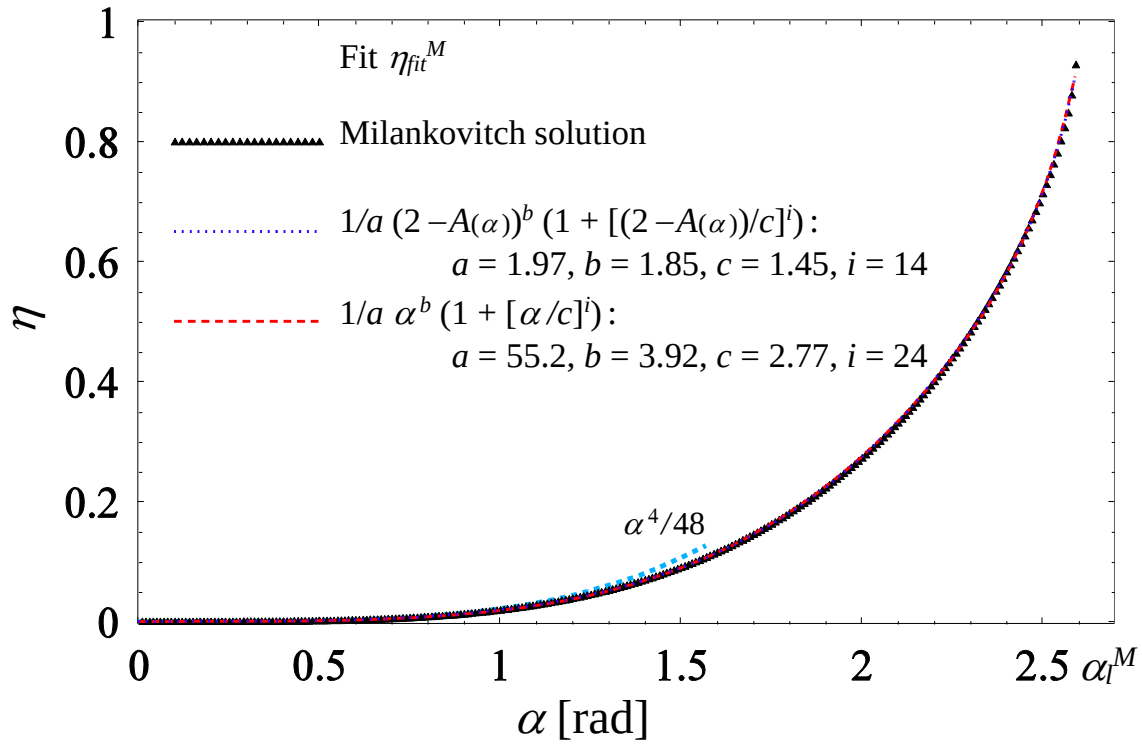

Figure 26: Milankovitch solution. Fit η_{fit}^M of η as a function of α.

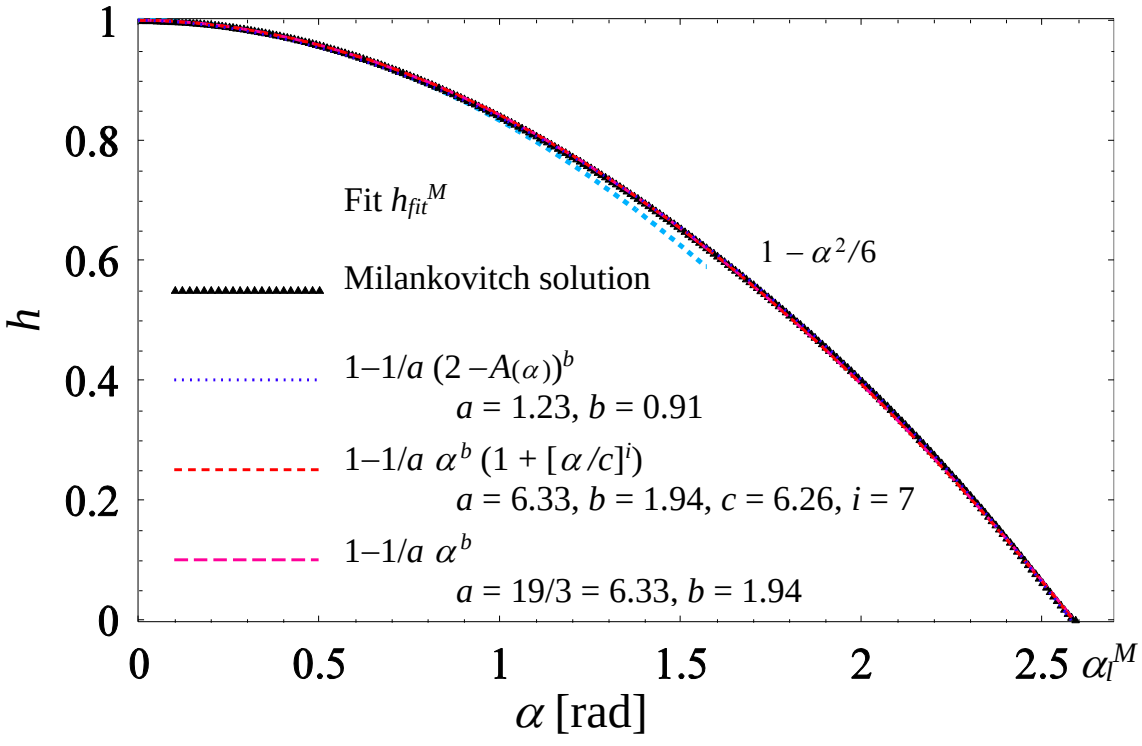

Figure 27: Milankovitch solution. Fit h_{fit}^M of h as a function of α.